Micro-scale Preconcentrators for Vapor-Phase Air Contaminants: Optimizing the Design and Operating Conditions for Integration with Micro-scale Gas Chromatographic Instrumentation

by

Thitiporn Sukaew

A dissertation submitted in partial fulfillment
of the requirements for the degree of
Doctor of Philosophy
(Environmental Health Sciences)
in the University of Michigan
2013

Doctoral Committee:

Professor Edward T. Zellers, Chair

Professor Stuart A. Batterman

Assistant Professor Joseph T. Dvonch

Assistant Professor Anastasios John Hart

2013

Dedication

To My Family

Acknowledgements

First, I would like to thank Professor Ted Zellers for his mentoring as an academic advisor and for giving me an opportunity to work in this exciting area. I benefited a lot from his experience, insight, and scientific expertise. I am grateful to him for training me in every aspect to become a scholar. In addition to Dr. Zellers, I would like to thank my dissertation committee members, Dr. Stuart Batter, Dr. Tim Dvonch and Dr. John Hart for their time, advice and to help me get through several milestones of my PhD candidacy.

I would like to thank my parents, brother, twin sister and other family members for their love and support. Thank you for having faith in me, and to help me come this far.

I would like to give a special thank to Zellers lab members: Judy Zhong, Gustavo Serrano, Lindsay Wright, Will Collin, Sun Kyu Kim, Jonathan Bryant, Kee Scholten for their friendship and advice (both research and non-research stuff). I also would like to thanks WIMS staffs: Robert Gordenker, Katharine Beach and Brendan Casey for technical support, μPCF design and fabrication.

I am especially thankful to all good friends I have made in Ann Arbor for their encouragement, friendship and to help me get through some difficulty periods: Ploy Charoenphol, Radaphat Chongthammakun, Leela Ruckthong, Panchika Prangkio, Monthian Setkit, Dhitirojana family, Pui Chong, Palm Panlada, Parn Chanikarn and many more TSA members; my fellow EHS friends: Siying Huang, Summer Hitchens, Gamola Fortenberry, Huda

Elasaad and Cathy Sotelo. Thank you again for making it easier when life gets hard. I will always remember a good time we shared here.

I would like to acknowledge the Royal Thai governments for providing me a financial support for 6 years. I also would like to acknowledge the WIMS2 center, which is sponsored by the Engineering Research Centers Program of the National Science Foundation under award number ERC-9986866 and the U.S. Department of Defense, ESTCP Grant No. ES-200702, through a subcontract from Integrated Science and Technology.

Table of Contents

List of Figures

List of Tables

Chapter 1

Introduction

1.1 Dissertation Overview

The broad goal of this research is to improve the design and operation of in-line preconcentrators used in field-portable gas chromatographic (GC) instrumentation for the determination of toxic organic vapors at low concentrations encountered in residential and workplace environments. A primary focus is placed on characterizing microfabricated preconcentrators that are designed for integration with microfabricated GC (μGC) instruments for *in situ* environmental analysis.

This research was performed in collaboration with faculty, staff and students affiliated with the Center for Wireless Integrated MicroSensing and Systems (WIMS2) at the University of Michigan [1]. WIMS2 focuses on the design, fabrication, and breadth of applications for microsensors and systems through research, education, and interactions with industry. Our group's research relates to the Environmental Sensors and Subsystems Thrust, which focuses on the development of μGC systems targeted at a rapid analysis of vapor mixtures with sub-part-per-billion detection limit. This research employs microfabricated devices with greater

portability, lower power consumption, and faster response times than those used in conventional GC systems. The applications of the μGC described here are aimed at homeland security, environmental air monitoring, biomarker studies, and medical surveillance [1-5]. These applications require the detection of targeted vapors at concentrations in the parts-per-billion (ppb) to parts-per-trillion (ppt) range, lower than the limits of the detection (LOD) of sensor arrays employed as detectors, thus requiring a preconcentration step. The microfabricated preconcentrator/focuser (μPCF) not only reduces the LOD of the system, but when designed and operated properly, it also provides a focused injection pulse to improve the chromatographic resolution of targets from interferences. This research addresses the lack of information on this topic in the literature. Devices suitable for use with μGC instrumentation were characterized in the context of known models to assess whether they adhere to the performance predicted by such models for single-vapor challenges and binary-mixture challenges. Studies employ commercially available graphitized carbons and carbon nanotubes synthesized in-house whose use in such applications has been the subject of surprisingly few reports. These fundamental studies were complemented by an applied study related to the development of a preconcentrator-focuser (PCF) module (integrating conventional and microfabricated components) for a specific μGC application: monitoring vapor intrusion of trichloroethylene (TCE) into homes situated above contaminated grounwater.

In this chapter, we present background knowledge relevant to the research in this dissertation, including factors related to the preconcentration process and the performance of the preconcentrator. The discussion about different μPCF designs, including the advantages and disadvantages of operating μPCFs on the basis of equilibrium-based preconcentration versus exhaustive preconcentration are discussed prior to an examination of factors that influence

preconcentrator operation and design. A discussion of different μPCFs reported in the literature. The modified Wheeler model, relating thermodynamic and kinetic factors to the design and operation of μPCFs for single vapors, and its extension to binary mixtures are discussed. The properties of adsorbent materials, both commercially available and carbon nanotubes are discussed, including a discussion on the adsorbent material selection used in the μPCF. The last part of this Chapter is devoted to the discussion of vapor intrusion of TCE and the factors affecting the development of the multi-stage PCF module developed for the ppt-concentration level of TCE in this application.

1.2 Background and Significance

1.2.1 Micro-Scale Gas Chromatographs

Field-portable gas chromatographs (GC) designed for on-site determination of multiple volatile organic compounds (VOCs) have been commercially available for nearly 40 years, and the first microfabricated gas chromatograph (μGC) was reported about 30 years ago [6]. Since then, numerous efforts have been made to reduce size and power requirements and to improve the sensitivity, selectivity, and reliability of measurements obtained with such instruments. Prominent among these efforts are those by WIMS2 Center [2-5,7-17].

The layout diagram of the analytical subsystem of one representative WIMS2 μGC is shown in Figure 1-1. The main components of that μGC are: a microfabricated preconcentrator/focuser (μPCF), which serves as both a preconcentrator and an injector; dual, series-coupled, microfabricated separation columns; and a detector consisting of an integrated array of chemiresistor microsensors that employ thiolate monolayer-protected gold nanoparticles

(MPN) as the interface layers. The operation of the μGC involves a sequence of steps: an air sample is drawn through the μPCF; the captured VOCs are thermally desorbed with backflushing to inject the mixture onto the head of the first separation microcolumn; and mixture components are separated then detected. This sequence produces a series of chromatograms; the response pattern generated from the sensor array for each vapor is combined with its chromatographic retention time to identify the vapor while the average peak area is used for quantification.

Although efforts by other research groups to develop μGC components are also noteworthy [18-25], relatively few have developed complete microsystems [22-25]. Most applications of the μGC require the determination of targeted compounds at concentrations in the ppb- or sub-range, which is lower than the limits of detection (LOD) of most microsensor arrays for typical analyte vapors; hence the need for preconcentration prior to analysis. The research and development effort described in this dissertation is concerned exclusively with the devices and subsystems used for preconcentration, whereby the VOCs in a large volume of air are captured and desorbed into a smaller volume to increase the concentration.

1.2.2 Preconcentration Process

Preconcentration is defined by the International Union of Pure and Applied Chemistry (IUPAC) as "an operation (process) as a result of which the ratio of the concentration or the amount of microcomponents (trace constituents) and macrocomponents (matrix) increases." [26]. In practice, a preconcentrator is packed with a certain kind of adsorbent used for capturing VOCs from a large volume of ambient air, and the VOCs collected in the device are thermally desorbed into the separation column in a much smaller volume [26-29]. The desorption of captured VOCs

into a small volume creates the preconcentration factor, which can effectively increase sensitivity and reduce the LOD of the detector by increasing the analyte mass presence at the sensor array.

By reducing the sample volume, the process also reduces matrix effects, facilitates the calibration, and thereby increases the accuracy of the results [26,28].

The preconcentration process can be described by the following equation;

$$C_f = \frac{C_i f_r S_i}{S_r} \tag{1.1}$$

Where C_i is the concentration of targeted analytes in the initial sample size S_i. C_f is the concentration in the preconcentrated sample size S_f, and f_r represents the chemical recovery of targeted analytes in the preconcentration step. The ratio of *Si/Sf* is called the preconcentration factor, and C_f must be high enough for accurate determination of targeted analytes. This equation can be used to calculate the required sample size needed to meet the LOD of the system [26, 28].

Since the typical concentration of contaminants found in the field is lower than the LOD of the detector employed in the WIMS2 μGC, a preconcentrator is considered an essential component of the μGC. Preconcentration can be selective, effectively reducing the number of interferences and simplifying the chromatography required to separate the target analyte(s) [3,4]. A preconcentrator can be single-stage or multi-stage. For direct-reading instrumentation, it should ideally serve as a thermal injector that provides a focused injection band to the separation column to maximize chromatographic resolution of the mixture components [8,9,30-33]. Zellers et al. coined the term ‘preconcentrator/focuser’ to highlight the dual function of such devices, as well as the tradeoffs required for optimizing performance.

1.2.3 Preconcentration Methods

Preconcentration of organic vapors can be achieved via several methods: absorption in a suitable solution, cryofocusing, chemisorption or on-tube derivatization and adsorption on solid at ambient temperature. [26, 27, 34-37].

1.2.3.1 Absorption in a suitable solution

Preconcentration of vapor phase analytes can be achieved via absorption into a solution. This method provides the possibility of using reaction with an absorption medium to convert targeted compounds into less volatile or more stable compounds, for example the preconcentration of aldehydes, organic acids, and isocyanates [26]. This method is also suitable for sampling moderately volatile compounds and sampling in high humidity atmospheres. However, the risk of losing targeted compounds due to evaporation and stripping or dilution by the sample gas stream passing through the absorption medium limit its use for preconcentrating highly volatile compounds. Also the requirement to use a train of bubblers (with specific requirements for shape and size depending on the targeted analyte) in this method limits the usefulness of this method in the field or as a personal monitor [26].

1.2.3.2 Cryofocusing

Cryofocusing, or cold trapping, can be used to preconcentrate vapors by the employment of a cooled preconcentration device. Preconcentration can be achieved by passing an air sample through a sampling tube that is cooled to a sufficiently low temperature. For example, in open tubular devices, the tube can be empty or packed with a simple inert substance such as glass bead or quartz wool. All compounds in the sample stream, including those that are very volatile, can be trapped with this method [26, 34]. A temperature gradient, or the use of liquid cryogen such as CO_2 or N_2, can be employed to cool the vapors to a sufficiently low temperature [26,34]. In the

modification employing a sorbent, the trap does not need to be cooled so far below ambient temperature. In general, a trap filled with a liquid or solid sorbent or a chromatographic phase coated on a support are cooled to temperatures ranging from 0 to -80 ^{o}C [26]. Sequential trapping can be used to eliminate at least some of the disadvantages and limitations of the method. To liberate the preconcentrated components, the cooling agent is removed and the trap is rapidly heated to the desired temperature. In this way, selective trapping or subsequent fractional distillation can be achieved. However, several factors make it inappropriate to integrate such a device for field study. These factors include the cost of operation, problems with ice blockage, the risk of losing the high boiling compounds from aerosol formation (leading to difficulty recovering preconcentrated samples of high molecular weight molecules), interference in subsequent analysis by the entrapment of water, and the poor retention of ultra-volatile analytes [26,34].

1.2.3.3 Chemisorption and Derivatization

The process of chemisorption implies that the target analyte reacts when it comes into contact with the substrate forming a specific derivative that facilitates or enhances measurement. Common examples include color indicator tubes (used extensively in the workplace for screening air quality) and various monitors that use silica gel substrates, impregnated with dinitrophenylhydrazine to derivitize formaldehyde prior to analysis with high-performance liquid chromatography (HPLC) and UV [26,34]. Since chemisorption involves the formation of a chemical bond between adsorbate and adsorbent, the reverse of this process requires a high-input energy method to break the covalent bond, such as a very high thermal desorption energy or the employment of a chemical solvent for derivitization [26,34]. This limitation precludes the use of this method in the field.

1.2.3.4 Adsorption on solids

This preconcentration method involves packing the sampling device with adsorbent granules. The preconcentration can be achieved by either an absorption or adsorption method, in which the intermolecular force involved in this study includes physisorption which relies on the Van der Waals force for sorption. With this weak intermolecular bond, reversal of the process can be achieved with low energy, and thermal desorption at an optimal temperature can be used to release the adsorbed vapors [26,27,35-40]. The simplicity and low energy required to reverse this preconcentration process make it a favored method in the design of automated instruments for the field. This preconcentration method is simple and allows the use of mixed packing or sequential selective packing. Additionally, selective preconcentration can be achieved by selection of suitable adsorbent [3,4,17,33,41].

This method has several limitations, for example the competition for available adsorption sites could result in the loss of components of low molecular weight [26,35]. Chemical reaction of preconcentrated compounds with functional groups on the adsorbent material is also possible [26,27,35,36,37]. The high (non-optimal) sampling flow rate contributes significantly to the loss of sample from breakthrough, especially in the case of complex mixture sampling (water vapor (humidity) in the air can compete for the available adsorption site, depending on the type of material used. [26,35,37]. The method used to reverse the preconcentration also needs to be optimized for complete desorption, especially for high molecular weight compounds [26,27,35, 37].

Since compounds trapped on a solid sorbent must be released as quantitatively as possible before determination, solvent extraction or thermal desorption can be used for this

purpose. One example of a solvent used for sample extraction is carbon disulfide (used mainly for compounds trapped on charcoal) [26,37]. Diethyl ether, acetonitile, methanol, n-hexane, ethyl acetate, chloroform, toluene, n-pentane, benzene, or a mixture of solvents, such as methanol-water, acetone-water, or propanol-water have also been used [26, 37]. The use of a solvent for desorption has several disadvantages, such as a decrease in sensitivity of the analytical method, depending on the volume of solvent and size of aliquot used. The solvent peak could also interfere with the chromatographic separation of the sample compounds. Solvent toxicity must also be considered [26,37].

Thermal desorption is the method of choice for automation analysis, including the instrument designed for directly reading field measurements, because the entire amount of preconcentrated analyte can be recovered with optimal temperature [26]. This method is suitable for analysis with gas chromatography because the thermal desorption sample is directly injected into the separation column, without the additional extraction step required in the solvent extraction method [26,37]. The elimination of this additional step contributes to the higher sensitivity of this methods compare to the solvent extraction method [37]. However, the desorption temperature needs to be optimized to avoid sample degradation or sorbent degradation [26,37].

To obtain complete desorption or high desorption efficiency, in the desorption step the trap should be heated to the required temperature (based on the thermal sensitivity of the sorbent and the preconcentrated compounds) as quickly as possible (preferably in a few seconds, or at most a few minutes), and the carrier-gas flow rate should be minimized [42, 43]. Flushing the adsorbent bed with a high desorption flow rate decreases the time between desorption and separation of the column, however, an increase in the flow rate can also broaden the injection

plug once it is injected into the column [42]. This is the case when the flow rate is higher than the optimal linear velocity flow through the column as determined by the Golay equation, which decreases separation resolution and can also effectively dilute the injected VOCs [42,43].

1.2.4 Dynamic adsorption in Packed Beds in Packed Beds

Adsorption refers to the physical interaction between a molecule of gas or liquid and a solid surface. The adsorption process on a solid sorbent is represented by various schemes. The scheme for a single microporous carbon granule is shown in cross-section in Figure 1-2 [26]. The air-vapor mixture is shown flowing across the granule. As the vapor diffuses into the pores, it migrates to the carbon surface and condenses in the pores. The pores continue to fill until some maximum value is achieved, depending on the prevailing conditions. There is a high degree of pore filling at high concentrations of relatively non-volatile solvent vapors [26]. The dynamic adsorption process of vapor in the adsorbent bed is presented at a macroscopic scale in Figure 1-3 [44]. At the beginning of the adsorption process, when the vapor travels through the clean adsorbent bed, the vapor concentration decreases rapidly to zero and this concentration profile continues until the steady condition is achieved (curve 3). This concentration profile is generally termed the adsorption wave (wave front) [26,44,45]. An alternative view of the distribution of vapor concentration at a given point in the sorbent bed as a function of bed depth is shown in Figure 1-4 [26], diagrammatically by shading, and also in graphical form. Figure 1-4a shows the first layer of the sorbent bed adsorbing the first fraction of vapor, where C_i represents the incident concentration, the process that takes place similarly to frontal chromatography, and equilibrium is established between the adsorption and desorption processes [26]. For a well-designed adsorbent bed where the adsorbent bed is long enough, a saturation zone is established

behind the adsorption zone. This process continues until the first layer of the sorbent is completely saturated and the immediate layer is partially saturated as shown in Figure 1-4b. As the length of a saturation zone increases from zero to a maximum, this concentration profile moves with a constant shape through the end of the adsorbent bed, where breakthrough occurs as the adsorption zone reaches the outlet of the bed. It is important to point out that breakthrough occurs when there is unused carbon (virgin carbon) available, as shown in Figure 1-4b. Figure 1-4c shows the sorbent bed almost completely saturated at 50% breakthrough. Breakthrough occurs at a concentration (C_b) as shown by curve 5 in Figure 1-3 [26]. The adsorption zone moves out of the bed in a constant pattern until the bed is saturated. The vapor concentration in this region is equivalent to the vapor capacity as defined by the adsorption isotherm for the sorbent/gas system at the same challenge concentration [26,44,45]

Adsorption efficiency, the ratio of the amount of adsorbate retained on the bed to the amount of adsorbate required to fully saturate the bed, depends on the distribution of adsorbate across the bed. Under ideal conditions of mass transfer, the adsorbate front in the bed remains sharp and the sample stream can be completely depleted of vapor until the sorbent bed is fully saturated. In practice, however, while under non-ideal mass-transfer conditions, breakthrough occurs before the bed is fully saturated (as described previously) and the sorbent has to be discarded before it is [26,44-46]. Figure 1-5 shows the theoretical breakthrough curve as a function of time. Typically, only 2% of the incident solvent vapor has penetrated the sorbent trap at 10% breakthrough [26].

At the breakthrough state, the vapor concentration distribution in the bed is illustrated in Figure 1-6 [44]. The saturation zone (ds) represents condition at the equilibrium state, where the concentration distribution in this region is similar to the challenge concentration. The adsorption

zone (dz) represents where there are available adsorption sites and thus where the adsorption process can occur. The vapor concentration is observed to decrease in this region. The adsorption zone refers to the region where there are unused adsorption sites (where the adsorption process can occur) and the concentration of vapor is continuously declining in this region. The breakthrough curve, which shows vapor concentration in the effluent as a function of time, is a mirror image of the adsorption wave, and it provides information on the vapor distribution in the adsorbent bed. In a well-designed adsorbent bed, efficient adsorption occurs when the beds are distinguished by a sharp, narrow wavefront and dz<<ds [44].

1.2.5 Adsorbent Material Classification

Adsorbent material is classified into 4 different groups based on its interaction with four different groups of chemical compounds. The results of this classification reflect the degree of nonspecificity as a function of the material used, impurities present, and the surface treatment that has been done to remove those impurities [26,27,37].

Examples of the classes of VOCs that can be used to test the degree of nonspecificity of solid sorbents are:

Group A: n-Alkanes, Spherical symmetrical shells, σ bonds

Group B: Aromatic, halogenated hydrocarbons and ketones, Electro density concentrated on bonds/links, π bonds

Group C: Organometallics, Positive charges (+) on peripheral links

Group D: Primary alcohols, amines, and carboxylic acids, Concentrated electron densities, Positive charges (+) on adjacent links

Adsorbents can be classified into three classes based on the analysis of the adsorption isotherm they give with these groups of organic chemicals [27]. Table 1-1 lists some of the commonly used adsorbents used for the collection of VOCs in air and emission samples together with their most important features. The adsorbent classification in this method can be used to identify the degree of nonspecificity. Additional information regarding adsorbent material can be found in a technical report by Supelco [39], a supplier of commercial adsorbents.

Beyond conventional adsorbent material, the goal of this study also includes the search for new adsorbent material with the potential to improve the performance of μPCF. One of the novel adsorbent materials that we are interested in is Carbon nanotubes.

Carbon nanotubes (CNTs) are the one-dimensional analogues of zero-dimensional fullerene molecules. Conceptually, a nanotube is a micrometer-scale graphene sheet rolled into a cylinder of nanoscale diameter and capped with a spherical fullerene [47,48]. CNTs have attracted special attention because of their unique properties, such as electrical conductivity, optical conductivity, and mechanism strength. Combining a nanoscale diameter with a micro- to centimeter length produces CNT structures of exceptional aspect ratio [48-50]. With their unique chemical and physical properties, CNTs are an ideal candidate for widespread applications such as drug delivery and energy conversion, catalyst supports, optical devices, molecular (memory) switches, quantum computing, biomedical uses, and environmental remediation [48-50]. The adsorption property of CNTs has been studied for its potential environmental applications: for use as a superior adsorbent, for removal of organic pollutants, metals, fluoride, and radionuclide AM(III). These studies focused on the adsorption of organic vapors and metals [49-51]. As sorbents, we rely on bulk properties of carbon nanomaterials; size, surface area, molecular specificity, and hydrophobicity [50]. General features of organic chemical adsorption on CNTs

are similar to the adsorption on the conventional adsorbent material, and classical isotherm models such as Freundlich, Langmuir, BET and Polanyi-Manes models can be used to describe the adsorption of organic vapors on CNTs [49,50]. With their high surface area, high thermal stability, and high thermal conductivity, CNTs are a good candidate for use in both aqueous and air phase adsorptive vapor preconcentrators [48-60], and their performance has been proven in several approaches, such as CNTs packed in a column [55,56], self-assembly CNTs on steel tubing or microfabricated devices [59,60], and CNTs dispersed and subsequently retained on a filter [58,60].

In terms of microfabricated preconcentrator (μPCF) design, the ability of CNTs to be grown and patterned inside microfabricated devices directly supports their selection as an adsorbent material in the μPCF. This method would avoid the aggregation and loss of available adsorption surface, and exploit their nanoscale characteristics. Chapter 4 presents results from the preliminary breakthrough testing that has been done to investigate the dynamic adsorption capacity of CNTs packed in cPCF and then grown inside the μPCF cavity.

1.2.6 Adsorbent Material Selection

The adsorbent chosen for use in the μPCFs must meet criteria that assure the accurate determination of VOCs, and also allow the complete desorption of a sample with the lowest temperature possible, in order to minimize the power used by this portable device. Other factors that affect the decision of adsorbent materials to be used in the μPCF include dynamic adsorption capacity (retention volume), desorption peak width, temperature stability, low affinity for water vapor, high mechanical and thermal stability. An inert surface is also important to minimize

artifact formation, especially when air is used as a carrier gas during the thermal desorption [26,27,29,35,37].

Several factors that affect the performance of the adsorbent bed must be considered in adsorbent material selection including:

1. The chemical nature and specific surface area of the adsorbent (in m^2/g)

The surface properties, the presence of the functional groups on the adsorbent surface, and the porosity of the adsorbent affect the adsorption capacity of the adsorbent [26,27]. The presence of pores affects the entropy of the adsorption process because gas and vapors diffusing through pores are subjected to much stronger lateral interactions than those deposited over a flat surface. Depending on the size and volume of the pores, adsorbed molecules can be assembled so closely to one to another that a thick film of liquid can be formed inside the cavity. Material characterized by comparable size and distribution of pores exhibits a linear increase in retention of n-alkanes with surface area [27].

2. Temperature and flow rate at which sampling is performed

Because adsorption is an exothermic process, the sampling temperature has to be considered carefully. The effect of increasing sampling temperature is to reduce the adsorption capacity of adsorbent material [26,27]. The effect of the sampling flow rate (or dynamic process) is to reduce the equilibrium adsorption capacity of the adsorbent. The modified Wheeler model describes the effect of these parameters on the dynamic adsorption capacity of the adsorbent bed and is detailed below [61-62].

3. The concentration and composition of the air sample

Vapor concentration and the presence of covapors affect the adsorption capacity of the adsorbent. Even though the increase in the vapor concentration would result in the increase in the equilibrium adsorption capacity in case that the concentration in the linear region of the isotherm [26,27,38]. Beyond this concentration region, the increase vapor concentration would reduce the equilibrium adsorption capacity dramatically. The effect of covapor (or even high humidity air) is to reduce the equilibrium adsorption capacity of the targeted vapor. Stronger vapors are retained on the adsorbent material and would reduce the breakthrough volume of the other vapors in the mixture [26,27,63,64]. This effect is clear in the case of activated carbon which has a functional group presence on the adsorbent surface, when the air mixture is complex (100-200 components) and has very polar constituents, such as free acids present in large amounts [26,27]. Since they are strongly retained by the adsorbent surface, they can dramatically reduce the capacity of nonpolar and moderately polar components eluted before them. The formation of thick water layers over the adsorbent surface also could occur at the adsorption partition of vapor [26,27,35,37]. Graphitized carbon blacks meet these criteria and have therefore been the material of choice for integration in WIMS2 μGC [3-5,7,41].

Graphitized carbon blacks are made out of soot in an inert atmosphere at a temperature of about 2700 ^{o}C. Graphitized carbon blacks (pre-trated soot at 3000 ^{o}C), are classified as thermal graphitized carbon blacks [26,27,37-39]. The degree of graphitization is determined by the starting material and the manufacturing process. The graphitization process can be followed by a heat treatment with hydrogen at 1000 ^{o}C to remove any remaining polar groups from the surface of the adsorbent. Washing with acid, such as perchloric acid or phosphoric acid, removes basic carbonium complexes and sulfides from the surface. The higher the degree of graphitization, the lower the specific surface area of the material, which varies between 5 and 250 m^2/g for

commercial materials [39]. Following these processes, the material is classified as a non-polar adsorbent with a physically and chemically homogeneous surface. The preconcentration process takes place on the basal planes of the graphite crystallites and is caused by non-specific interaction (dispersion, induction) [38,39]. Besides the molecular size, the shape and degree of polarization determines the adsorption strength, for example, n-butane has a higher breakthrough volume than iso-butane due to the higher number of contacts with the surface. Graphitized carbon blacks are commonly used in ambient air analysis, as a multiple trap. Due to their high hydrophobicity, graphitized carbon blacks could be used for the sampling of VOCs in an extremely humid atmosphere without using additional drying agents [26,37].

1.2.7 Preconcentrator Classification

Preconcentrators can be classified into two groups. The first group relies on equilibrium-based preconcentration, in which the vapor concentration on/in the adsorbent, or in a sorbent film, is at equilibrium with the air sample. In this approach, the captured analyte mass is independent of the sample volume (beyond some minimum), but is directly dependent on the vapor concentration in the sample air [65-67]. In the equilibrium sorption technique, a steady flow of enriched sample gas is generated by pumping a volume of air sample through the preconcentrator. Sampling continues until the sorbent phase is in equilibrium with the gas phase (that is, until the saturation has occurred). In this case, sampling is continued beyond the breakthrough point, and the partition coefficient is used to quantify the preconcentrated sample [65]. The second type of preconcentrator employs *exhaustive trapping* and is designed to capture all the analytes from a given sample volume [30,31]. This design allows for a range of sample volumes, but will have a finite capacity beyond which partial (and, eventually complete)

breakthrough will occur and quantitative analysis will be compromised. In addition, due to the use of larger adsorbent masses, devices designed for exhaustive preconcentration are typically larger, require more power to heat, and provide broader injection bands. The miniature (i.e., conventional packed capillary) [30,31] and microfabricated preconcentrators [8,9,41,68] developed by Zellers et al. over the past 15 years employ exhaustive trapping (Figure 1-7).

1.2.7.1 Equilibrium Based Preconcentrators

The guide in adsorbent selection for this type of preconcentrator is different from the exhaustive preconcentrator, in that sample saturation is required in order to allow the rapid equilibration of the entire bed of sorption material in a reasonably short time, while simultaneously allowing quantitative desorption of the trapped components at a mild temperature [65]. Moreover, to produce a stable desorption profile, the sorbent bed has to be homogeneous and the concentration of the solutes has to be fairly stable within the sampling time [34,65]. Other disadvantages arising from the use of solid adsorbents include the competitive nature of the adsorption process, the large water vapor effect, and the influence of residual active sites on the adsorbent surface [34,66,67]. An example of a conventional equilibrium-based preconcentrator is the solid-phase microextraction (SPME) fiber, which is typically applied to headspace sampling of VOCs [66,67]. SPME is fundamentally different from sorbent trapping. Whereas the aim of solid sorbent sampling is complete selective retention of organic vapors from a flow of air, SPME relies instead on the partitioning of organic components between a liquid- or gas-phase sample matrix and a thin layer of solid or liquid sorbent (stationary phase) [34,65]. Typically, SPME devices are composed of a fiber or small cylinder covered in a thin coating of non-polar sorbent which is introduced directly into the liquid- or gas-phase sample. Analytes

partition between the sample and sorbent coatings until equilibrium is reached. Generally speaking, the lower the analyte volatility, the higher the partition coefficient, meaning higher boiling compounds are retained more effectively [34,66,67]. Provided analyte concentrations remain stable throughout sampling, the analyte concentration in the sorbent coating after equilibrium is reached will be constant and will be representative of the concentration of that compound in the sample. At the end of the sampling period, the SPME device is removed from the sample, then washed, dried, and analyzed using liquid extraction or thermal desorption in combination with GC/MS [66,67] SPME has limited utility in an exposure monitoring application for several reasons. SPME cannot be used for grab sampling because it takes time to establish the various equilibria. It is also unsuitable for time-weighted average (TWA) monitoring of the variable vapor concentrations observed in most real atmospheres[34]. Results might indicate much lower or higher levels than the true average due to the timing of significant concentration fluctuations during the monitoring period [34].

Most microfabricated preconcentrators reported in the literature operate on the principle of equilibrium partitioning – they are essentially microhotplates with adsorbent thin films applied to the surface. For example the device by Tian et al is coated by an amorphous and porous carbon film [69]. The device by Kim and Mitra is coated with a thin-film polymeric layer of commercially available gas chromatography stationary phase, OV17 (50% polymethyl-50% phenyl-phase) deposited above the heater in the channel [70]. The device by Martin et al is in a flow through plate configuration; analyte is both collected and desorbed perpendicular to the collection surface. With sorbent material deposited on the plates as a polymer, this approach lends itself well to stacking the devices one atop the next for enhancing both collection efficiency and breadth of analytes captured [71]. The device by Manginell et al. is called a smart

preconcentrator (SPC) that determines when it has collected sufficient analyte for analysis by a downstream chemical microsystem. The SPC is coated with an adsorbent; sol gels and DKAP which are selective toward organophosphate compounds. The frequency of operation varies inversely with the mass of collected analyte [72].

Some other equilibrium based preconcentrator employed commercial adsorbent material such as what reported by Davis et al. that tested with Carbosieve, Carbotrap, Carboxen 569, Carboxen 1000 and Tenax GR. Tested vapor: ~ 21 ppm of m-xylene. Carboxen 1000 was chosen to show the decrease in limit of detection of m-xylene by more than two orders of magnitude, from 13.5 ppm to 61.8 ppb [73].

The device by Voiculescu is based on a perforated flow through microhotplate structure that is coated with the sorbent layer to maximize vapor trapping efficiency. Adsorbent material: HCSA2 polymer, a hyperbranched polycarbosilane functionalized with hexafluoroispropanol (HFIP) pendant groups. The HFIP pendant groups are strongly hydrogen-bondacidic and function to target hydrogen-phosphonate ester or nitroaromatic species [18]. Lewis et al. [23] reports three examples of equilibrium based micropreconcentrator reported in this paper. Microhotplate planar preconcentrators which is the heated area of the preconcentrator is fabricated from a free-standing silicon-nitride (Si2N3) membrane coated with the microporous hydrophobic surfactant-templated sol-gel layer. The analyte flow was directed parallel to the device. The other device is designed for the air flow directed perpendicular to the device. The device is classified as the three-dimensional (3D) hotplate could provide large adsorbent capacity and a large heating surface capable of uniform heating surface capable of uniform heating of adsorbent materials. The device is coated with nanoporous carbon, sol gels, and commercial packing material and tested with DMMP. No preconcentration factor reported: only reported that

the 3D device takes more than 20 minutes to saturate, compare to the planar device reported earlier that take only 2 minutes to saturate.

The device reported by Alfeeli et al is a microthermal preconcentrator (μTPC) device with high-aspect-ratio 3D structures (240 um) [74]. The μTPC has on-chip thermal desorption capability and comprises more than 3500 micropillars with dimemsions of 27 μm x 115 μm x 240 μm. The device was coated with a uniform polymer adsorbent film (PDMS, Tenax TA) using a high coverage coating method based on the principle of inkjet printing technology and heated with off-board high-performance ceramic heater. The device by Wong et al. is classified as a preconcentrator chip employing μSPME array coated with in-situ-synthesized carbon adsorbent film: ~ 2 mg of coated cellulose film which was converted into a porous film via pyrolysis at 600^{o} C [75].

Since competitive adsorption is likely to affect the uptake of mixture components, the use of such devices for quantitative analysis of components of complex mixtures is tenuous. Thus, in such devices an emphasis is placed on rapid, low-power desorption rather than high capacity and quantitative capture. With these purpose, the devices are designed for the smallest dimensions possible. The quantity of adsorbent materials packed (or coated) in the microdevices is limited and impart a very low equilibrium adsorption capacity. Most of the studies only present the fabrication process and demonstrate adsorption performance without attempt to evaluate an effect of flow rate, vapor concentration, or adsorbent mass on the adsorption capacity of the preconcentrator.

1.2.7.2 Exhaustive Preconcentrators

In general, microfabricated devices reported in this category are devices fabricated with silicon technology that consists of micro-scale cavity that can be packed with commercially

available adsorbent material. For example, the device reported by Tian et al, which is the single stage μPCF packed with Carbopack X [8], and the multi-stage μPCF packed with Carbopack B, Carbopack X and Carboxen 1000 [9]. Several designs of the latest generation of WIMS2 μPCF (Figure 7) are open cavity devices that can be packed with any adsorbent material of choice, depends on the target application. The device reported by Dow et al. [76] is packed with Carboxen 1000. The device reported by Gràcia et al. [77] is packed with 400 μg of Carbopack X. The device reported by Camara et al. is a microchannel in "straight" and "zigzag" design ("V" shaped structures), packed with 0.69-1.85 mg carbon nanopowder (Sigma-Aldrich) [78]. The devices by Rydosz et al. is packed with Carboxen -1003 and Carboxen-1018 [79].

Like other preconcentrator/focuser devices, the development of devices reported in this categories also targeted at the design to achieve the low power consumption device, to promote efficient desorption and to yield chromatogram with sharp injection bandwidth. By definition, an exhaustive preconcentration device is required to be able to capture targeted vapor in the sample stream without breakthrough. Therefore it is important to ensure that the adsorbent materials packed in the devices have enough capacity for targeted vapors at specific sampling conditions. However, most studies only described the device's fabrication process, the desorption performance, its ability to concentrate the specific vapor at arbitrary concentration without the prove of quantitative capture of target analyte despite a limited quantity of adsorbent mass packed in the devices.

Among all reported exhaustive micro-scale preconcentrators, only the work of Lu et al [30, 31] considered the tradeoff between capacities and desorption efficiency for small adsorbent bed (i.e., < 15 mg of total adsorbent bed). The studies prove that a multi-stage adsorbent beds consists of different surface area adsorbent materials is required to capture a complex set of

vapor mixtures. A microscale-cPCF packed with different mass of Carbopack X (specific surface area = 250 m^2/g), Carbopack B (specific surface area = 100 m^2/g) and Carboxen 1000 (specific surface area = 1,200 m^2/g) to create a 3-stage preconcentrator for generalized VOC trapping is capable of efficiently trap and desorb complex VOC mixtures spanning a 10^4-fold range of vapor pressure with preconcentrator factor greater than 5600 [30]. The results are extended by Tian [8, 9] and Chan [68] to support the fabrication of single- and multi-stage preconcentrators.

As mentioned in an earlier section, the preconcentration in trace analysis is defined by IUPAC as "an operational (process) as a result of which the ratio of the concentration or the amount of microcomponents (trace constituents) and macrocomponents (matrix) increases" [26]. The preconcentration factor is defined as the ratio of sample volume to desorption volume, and this parameter reflects the degree of preconcentration. The PF calculated by IUPAC would provide useful information since it links between sample volumes required to reach sensitivity limit of detector at specific targeted condition. It provides information of the device is capable of preconcentrating the targeted vapor at background concentration to the desired concentration (ex. to reach limit of detection of detectors).

By PF definition, it should be able to use this parameter to compare the performance of μPCF devices, however the different in operational methods between equilibrium based and exhaustive devices prohibit the use of this approach for μPCF performance comparison. Since the PF definition defined by IUPAC assumes mass balance between preconcentration process; sample captured and desorption. An operation of equilibrium based preconcentrator which allow vapor to breakthrough during the sampling process violates this assumption. In most of the equilibrium based μPCF studies, the preconcentration factors are reported as the ratio of peak

area with and without adsorbent material. Therefore, it is not suitable to compare adsorption performance across these devices with the term PF and concentration factor.

1.2.8 The Modified Wheeler model

The Wheeler model was first developed to describe the saturation of a catalytic bed by a poison [61]. Jonas modified this equation to use it to predict the adsorpiton of VOCs on actived carbon beds [62]. It relates factors affecting the μPCF design and operation to the breakthrough time (t_b) or breakthrough volume (V_b) of the adsorbent under a continuous vapor challenge.

It is the model commonly use in the selecting and using an organic vapor air-purifying respirator cartridge. The model is used to predict breakthrough time or service life. This parameter is determined by the equilibrium sorbent bed capacity and the kinetic transfer of air contaminant(s) to the sorbent bed, and it is determined by the vapor the cartridge is used against, the vapor concentration, the cartridge design, its contents, the user's breathing rate, the environmental conditions, and the allowable penetration [80]. The applicability of the model has been demonstrated , i.e. one can use this equation to extrapolate single laboratory breakthroughs by varying the independent variables of the equation (amount of adsorbent, flow rate, inlet and breakthrough concentrations) in various experimental conditions [80-83].

The most common form of the equation is given in Eq. (1.2) and Eq. (1.3):

$$V_b = \frac{W_e W_b}{C_o}\left[1 - \frac{1}{k_v \tau}\ln\left(\frac{C_o}{C_x}\right)\right] \tag{1.2}$$

$$t_b = \frac{\rho_b W_e}{C_o}\left[\tau - \frac{1}{k_v}\ln\left(\frac{C_o}{C_x}\right)\right] \tag{1.3}$$

where V_b is in liters, t_b is in minutes, W_e is the (kinetic) adsorption capacity (adsorbate mass/adsorbent mass), W_b is the packed-bed mass (g), $\tau = W_b/(\rho_b Q)$ is the bed residence time (min), ρ_b is the adsorbent bed density, Q is the volumetric flow rate (cm3/min), k_v is the kinetic rate constant (min^{-1}), C_o is the inlet concentration (g/cm^3), and C_x is the outlet concentration (g/cm^3)

The first term contains the absolute (versus relative) equilibrium capacity, $W_e W_b$, of the bed in equilibrium with vapor at C_o. This term represents the breakthrough time if the transfer kinetics were infinitely fast, i.e. k_v is infinitely large. The quantity $W_e W_b/C_o$ is the volume of air, V_t, containing the vapor at C_o that is required to achieve thermodynamic equilibrium of the vapor between the air and the adsorbent. Since the adsorption efficiency, $1-[\ln(C_o/C_x)/k_v\tau]$ is generally≤ 1, Vb is generally $\leq$ Vb. The quantity $\ln(C_o/C_x)/k_v\tau$ represents the fractional unused bed capacity [30,61,62]. The apparent decrease in V_b as C_o increases is partially offset by an increase in W_e with C_o which is often assumed to be proportional at low concentrations. The second part, containing k_v, which describes the shape of the concentration front moving through the adsorbent bed. Higher flow rates lead to increased k_v values, and provided k_v is constant, a steep, s-shaped front will result. If the rate coefficient changes as the front moves through the bed, a skewed asymmetric curve will result [46,84].

For this approach at constant C_x/C_o, C_o, W_e, k_v and ρ_b, this second term can be considered a constant. Adsorption capacity, W_e, can be obtained from the slope, $S = W_e/C_o Q$, of plots of breakthrough time, t_b, versus bed weight, W_b, when the experimental values of C_o and Q are known. The linearity of such plots has been demonstrated, confirming the validity of this approach. This also confirms the "constant pattern assumption," fundamental to the derivation of

the breakthrough curve equations, which says that the adsorption wavefront form quickly in the sorbent bed and moves at a constant shape and rate through it [83].

In general, the air sampling at high flow rate to reduce sampling duration is preferred in order to shorten the instrumental cycle. However, this would lead to the decrease in τ and in the efficiency of adsorption, causing a decrease in dynamic capaity of the adorbent [44,80,83]. For a higher sampling flow rate approaching τ_c, the breakthrough volume decreases sharply with increasing flow rate, and sampling flow rate at this region should be avoided. In the lower flow rate range, the bed become more efficient and breakthorugh volume become less dependent on flow rate. Therefore the operational sampling flow rate should be optimize to allow the shortest sampling time possible, but without the risk of sample loss from breakthrough.

In order to use the Wheeler model in a predictive manner, W_e and k_v need to be determined independently. Alternative ways of determining W_e include gravimetric analysis (e.g., via thermogravimetric analysis) and the use of the so-called Dubinin-Radushkevich (D/R) model [85-88]. The D/R model is presented in its linearized form in Eq. (1.4):

$$\ln W_e = \ln(V_o \rho_L) - \left[\left(\frac{RT}{\beta E_o} \right) \ln \left(\frac{p_{sat}}{p} \right) \right]^2 \qquad (1.4)$$

where V_o is the micropore volume (mL/g), ρ_L is the density of the adsorbate in its liquid form (g/mL), R is the ideal gas constant, T is temperature (K), β is an affinity coefficient, E_o is the so-called characteristic energy (kJ/mole), p is the partial pressure of the compound to which the adsorbent is exposed, and p_{sat} is its saturation vapor pressure at the temperature of the test. A plot of ln (W_e/ρ_L), which is an expression for the amount of vapor uptake in terms of its condensed volume versus$\ln^2 (p_{sat}/p)$, which is inversely related to the vapor concentration, permits estimates

of E_o and V_o from the slope and y-intercept, respectively (note: values of β can be derived from published polarizability data).

1.2.9 Adsorption rate coefficient, k_v parameter

It is generally recognized that the removal of a gas from air by a porous adsorbent may involve one or more of a following steps: (1) diffusion (mass transfer) of the gas from the gross surface of the granule; (2) diffusion of the molecules of gas into (or along the surface of) the large pores of the adsorbing particle; (3) adsorption of the molecules on the interior surface of the granule; (4) chemical reaction between the adsorbed gas and the adsorbent or adsorbed oxygen, water, or impregnant [26,45]. The relative importance of each of these four steps may vary widely with the particular conditions under which the removal is taking place. Mass transfer is influenced strongly by the flow rate of the gas stream, by the diffusion coefficient of the gas, and by the particle size of the adsorbent, but is relatively unaffected by temperature [89-93].

Such factors as the particle size, the structural characteristics of the pores, certain diffusion properties of the system, and the rate of reaction at the internal surface determine the important of diffusion in the pores. Factors influence the speed of adsorption at the interface is the nature and extent of the surface as well as on the activation energy for the adsorption of the particular gas under consideration [45]. Even though there is no theoretical models of k_v is known, empirical models have been developed that express k_v as a function of linear velocity, v_L (cm/sec) and particle diameter, d_p (cm). In the review by Wood [46], only the Wood/Stampfer [92] and Lodewyckx/Vansant models [93] showed positive correlations with experimental rate coefficients for a wide variety of chemical vapor. The Lodewyckx equation includes carbon granule diameter as a parameter, but was developed for only 0.1% breakthrough. The Wood

Equations do not include granule diameter, but take into account observed breakthrough curve asymmetery (skew) to allow estimating rate coefficients at a range of breakthrough fractions [46, 93]. The Lodewyckx and Wood-Stampfer Adsorption Rate Coefficient Models are the only ones found to predict the trend of experimental rate coefficients with vapor type. They both include vapor parameters (molar polarizability and affinity coefficients, respectively) and air flow velocity parameter.

The empirical Lodewyckx/Vansant equation for rate coefficients was based on k_v calculating using a rearranged Eq. (1.5) with experimental times for 0.1% breakthrough and independently calculated adsorption capacities *We*. The results includes affinity coefficients β, which is a function of the chemical:

$$k_v = 48\beta^{0.33} v_L^{0.75} d_p^{-1.5} \quad \text{min}^{-1} \tag{1.5}$$

It has the advantage of also including average carbon granule diameter (d_p in centimeters) and linear flow velocity as parameters.

The study by Wood and Lodewyckx [94], employed the above equation to predict the adsorption rate coefficient. The results of 776 experimentally derived 0.1 % adsorption rate coefficients from the four sources showed good overall accuracy, but not overall precision using this model. Since the deviations of the experimental data could be attributed to the experimental variations, which can easily introduce errors into the calculate of rate coefficient from the breakthrough times, the author suggested that the adsorption rate is predicted to be a function of the molar equilibrium adsorption capacity. Therefore, the equation developed by Lodewyckx/Vansant was extended to include the parameter of equilibrium molar capacity to an adjustable power.

$$k_v = a\beta^{0.33} v_L^{0.75} d_p^{-1.5} \left(\frac{W_e}{MW} \right)^n \quad \text{min}^{-1} \tag{1.6}$$

for gravimetric capacities W_e (g/g carbon) and molecular weights MW. The 776 experimental, skew-extrapolated, 0.1% rate coefficients were best fit in this equation. The overall correlation coefficient, and the overall accuracy were improved. The value is essentially 800 within the uncertainties involved, so that

$$k_{v0.1\%} = 800\,\beta^{0.33} v_L^{0.75} d_p^{-1.5} \left(\frac{W_e}{MW} \right)^{0.5} \quad \text{min}^{-1} \tag{1.7}$$

or

$$k_{v0.1\%} = 13.3\beta^{0.33} v_L^{0.75} d_p^{-1.5} \left(\frac{W_e}{MW} \right)^{0.5} \quad \text{sec}^{-1} \tag{1.8}$$

Where β is the affinity coefficient of the Dubinin Radushkevich Isotherm model (given as a ratio of the molar polarizability of the analyte to the molar polarizability of the reference compound, benzene.

This new adsorption rate coefficient expression provides an improved average description of experimentally derived rate coefficients for a wide variety of vapors or gases and conditions. However, this equation valid only for 0.1% breakthrough fraction, however, the authors applied average skew parameters and functions to this equation and successfully estimate adsorption rate coefficient at 1% breakthrough fraction. Therefore, adjustments for breakthrough fraction extend the usefulness of this equation.

1.2.10 Binary Mixtures

Very few studies have looked at the effect of co-vapors on the dynamic adsorption capacity of packed adsorbent beds [46, 95-101]. Since most real atmospheres contain mixtures of

many contaminants in varying quantities and proportions, it is important to investigate the effect of these co-contaminants on the capacity for the targeted vapor. Common observations for the kinetics of adsorption of mixtures onto sorbents include the displacement of already adsorbed compounds by compounds with stronger affinity to the adsorbent. The weakly adsorbed vapor (vapor 1) moves through the sorbent bed more rapidly than the more strongly adsorbed vapor (vapor 2). Displacement of vapor 1 from the adsorbent can cause "roll up" or "overshoot", in which the concentration of vapor 1 downstream of the adsorption wavefront of vapor 2 can exceed the concentration of vapor 1 entering the bed [46,63].

There have been a few studies in which the effect of the second vapor on the values of W_e and k_v of the first vapor have been explored. Most of these studies rely on performing linear regression with the Wheeler model to determine W_e and k_v for both the single vapor and binary vapor analysis [97-101]. Wood provides a review of these methods with analysis of their accuracy [46,95]. The molar proportionality method (MPM) is one of these, and we have chosen to use it to model W_e for binary mixtures in this study. This simple model assumes that the amounts adsorbed from a vapor mixture are equal to the component vapor-phase mole fractions multiplied by the mass that would have been adsorbed from a pure vapor at the same partial pressure (or concentration), W_e for a vapor in a mixture therefore decrease with decreased mole fraction of the vapor in air. Implicit is the assumption that the different components do not interact except to "deny" adsorption to one another. This assumes a limited number of adsorption sites or surface area can be covered (the Langmuir isotherm assumption). The model has been applied with accurate determination of V_b for large-scale adsorbent beds. The detail of the model and its performance is described in Chapter 4.

The approach to be used for the determination of k_v in this study will also based on the review by Wood, who found that the effect of mixture components on k_v differs depending on the breakthrough order [96]. He developed a set of operational rules of thumb. The vapor that breaks through first showed no difference between k_v in mixture and k_v for single vapor. That is, the rate of adsorption of the first vapor moving through the bed is unaffected by the presence of co-interferences. Vapors that breakthrough later demonstrated an average 15% decrease in k_v, (mixture k_v:single k_v = 0.85). In the case of vapors with similar breakthrough volumes, the 15% decrease is to be applied to both vapors. The applicability of these rules to miniature preconcentrators using non-microporous adsorbents has not been tested, and none of the published studies has examined the adsorption of mixtures over a range of flow rates.

Among the studies performed on miniature preconcentrators, none of them has addressed the modeling of binary mixtures. In this dissertation, we investigated this topic, including the aforementioned approaches to modeling W_e and k_v, and the performance of Wheeler model for describing t_b for the components of binary vapor mixtures.

1.2.11 Designing a PCF Module for TCE from Vapor Intrusion

Vapor intrusion (VI) is a term used to describe indoor air contamination arising from the migration of volatile organic compounds (VOC) into residences or office buildings from surrounding contaminated ground water or soil. The problem is generally associated with improper waste disposal or leakage of storage tanks, and can take many years to develop. Due to its volatility, persistence, widespread use as a degreasing solvent, and improper disposal practices historically, trichloroethylene (TCE) is a common VI contaminant that has been identified in more than 1,500 hazardous waste sites around the U. S. [102].

In considering the adaptation and deployment of a μGC for the assessment of TCE contamination from VI in homes, it became apparent that the air sample volume required to achieve the sub-ppb detection limits demanded by this application would exceed the capacity of the μPCF devices we have used in previous μGC prototypes. Thus, a high-volume sampler was required upstream from the μGC. It was also apparent from samples collected and analyzed by standard methods at some of the anticipated field-testing sites under consideration that a number of semi-volatile organic compounds (SVOCs) were present in the air, which would tend to adsorb to surfaces or only partially desorb from the μPCF at normal desorption temperatures. Thus, a means of precluding such compounds from entering the system was needed.

In response to these requirements, we have developed a multi-stage preconcentrator-focuser (PCF) module consisting of a pre-trap, sampler, and microfabricated focuser (μF) to facilitate the deployment of one of our μGC prototypes (SPIRON) for TCE determinations in VI-impacted residences. The layout of the instrument is shown in Figure 1-8. The detail of the development is described in Chapter 5.

1.2.12 Summary

The broad goal of this dissertation is to improve the design of miniaturized and microfabricated vapor preconcentrator devices used to capture, focus, and thermally inject analytes in microfabricated gas chromatographic analyzers for the determination of toxic vapors encountered in workplace or residential environments. Fundamental and applied laboratory studies were performed to address the key design and operating variables affecting the performance of such devices. The primary performance metrics are the dynamic vapor

adsorption capacity associated with the preconcentration function and the desorption rate and efficiency associated with the injection function. Micromachined-Si devices with different-sized cavities, glass caps, fluidic inlet and outlet ports, and integrated heaters are to be packed with commercial granular adsorbent materials or with carbon nanotubes (CNTs) grown *in situ*. Devices were challenged with individual vapors at different flow rates and concentrations. Devices of a more conventional, capillary design packed with the same quantities of adsorbents will be tested in parallel for comparison. The effect of covapor was performed in the small adsorbent bed. Data was interpreted in the context of the well-known modified Wheeler equation, which relates the breakthrough time, t_b, to the important design and operating parameters of such devices, in particular, the bed residence time, τ, the kinetic rate constant, k_v, and the equilibrium adsorption capacity, W_e. The models will be used to explore the effects of changes in adsorbent bed design, material properties, challenge vapor, and operating conditions on t_b. The application of the Wheeler model was extended to study t_b for binary organic vapor mixtures. The development of a microfabricated preconcentrator/focuser for a portable µGC prototype that has upstream pre-trap and high-volume sampler devices has been explored for the specific problem of quantifying trichloroethylene (TCE) in homes at risk of vapor intrusion from contaminated soil and groundwater.

Table 1-1. The Most Commonly Used Adsorbents for Volatile Organic Compounds (VOCs) [27]

Commercial name	MDT[a] (°C)	SA[b] m^2/g_1	Porosity [c]	Type [d]	Hydrophobicity [e]	Class [f]
Carboxen 1000	400	1200	MIP	CMS	L	III
Carbosieve S III	400	840	MIP	CMS	L	III
Chromosorb 106	250	750	P	SP	H	III
Porapak Q	250	550	P	EVD-DVB-CP	H	III
Carbograph 5	>400	520	MAP	GCB	H	I
Carboxen 569	400	390	MIP	CMS	M	III
Chromosorb 102	250	350	P	S-DVB-CP	H	III
Porapak S	300	350	P	PVP	H	III
Carbotrap X	>400	260	MAP	GCB	H	I
Carbotrap	>400	100	MAP	GCB	H	I
Carbopack B	>400	100	MAP	GCB	H	I
Tenax TA	350	35	P	PDPPO	H	III
Tenax GR	350	35	P	PDPPO+ GCB	H	I
Carbotrap C	>400	12	MAP	GCB	H	I
Carbopack C	>400	12	MAP	GCB	H	I
Carbopack F	>400	5	NONP	GCB	H	I
Glass Beads	400	<1	NONP	Silicate	H	II

[a]MDT = maximum desorption temperature.
[b]SA = specific surface area.
[c]MIP = microporous (mean pore diameter 1–10 nm); P = porous (mean pore diameter 20–100 nm); MAP = mesoporous (or macroporous) (mean pore diameter 100–300 nm); NONP = nonporous (mean pore diameter > 300 nm).
[d]CMS = carbon molecular sieve; EVB-DVB-CP = ethylvinylbenzene-divinylbenzene copolymer; GCB = graphitized carbon black; PDPPO = poly(2,6-diphenyl-*p*-phenylene oxide); PVP = polyvinylpiridine; S-DVB-CP = styrene-divinylbenzene copolymer; SP = polystyrene polymer.
[e]H = high; M = medium; L = low.
[f]Classification according to Kiselev (see text).

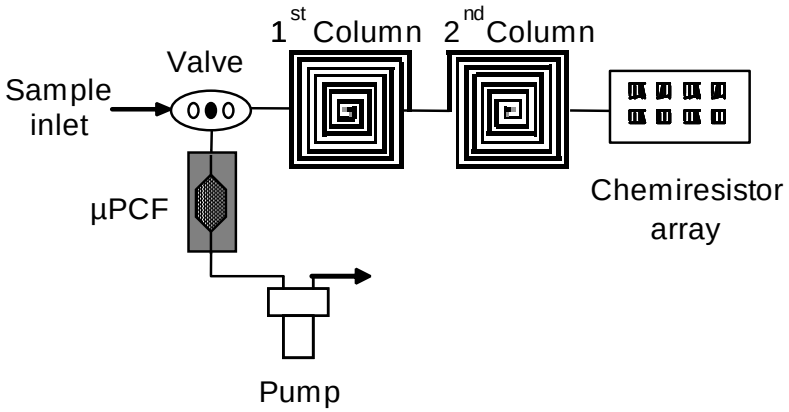

Figure 1-1. Diagram of WIMs μGC, the single-stage μPCF employed in the system can be replaced with dual or three-stage μPCF depends on the characteristic of targeted compounds.

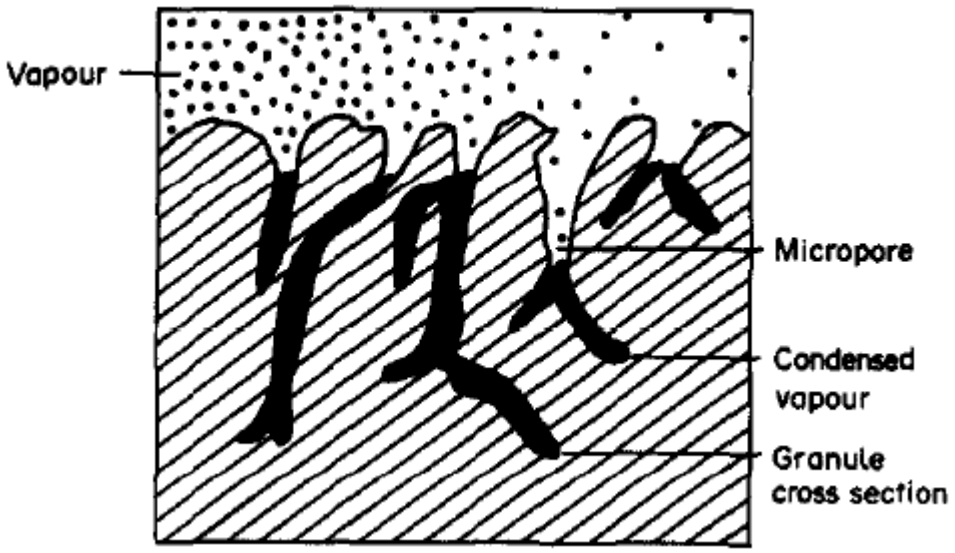

Figure 1-2. The adsorption process in microporous adsorbent material [26].

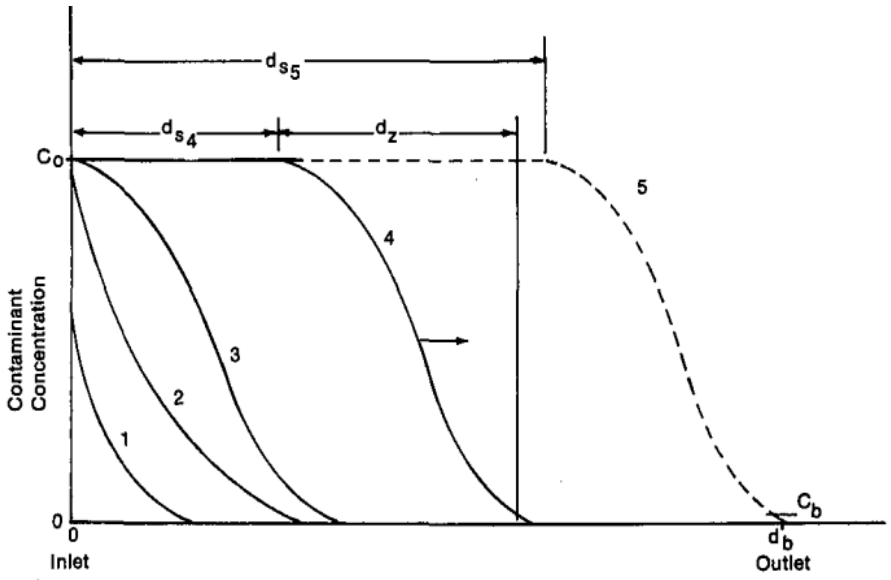

Figure 1-3. Dynamic adsorption process of vapor in the adsorbent bed is presented in the macroscopic scale [44].

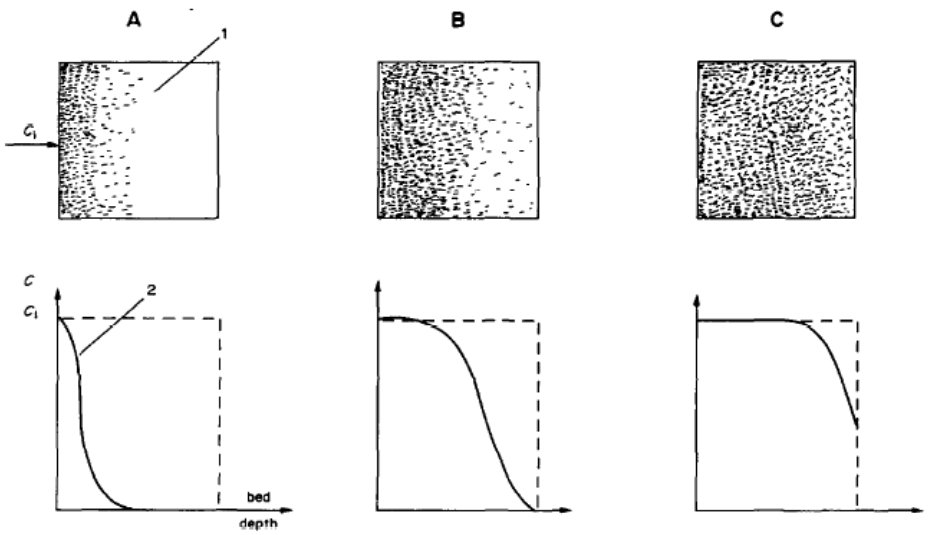

Figure 1-4. Cartridge loading patterns and migration of the adsorption front through the sorbent trap as a function of time: 1-organic vapor cartridge; 2-adsorption front [26].

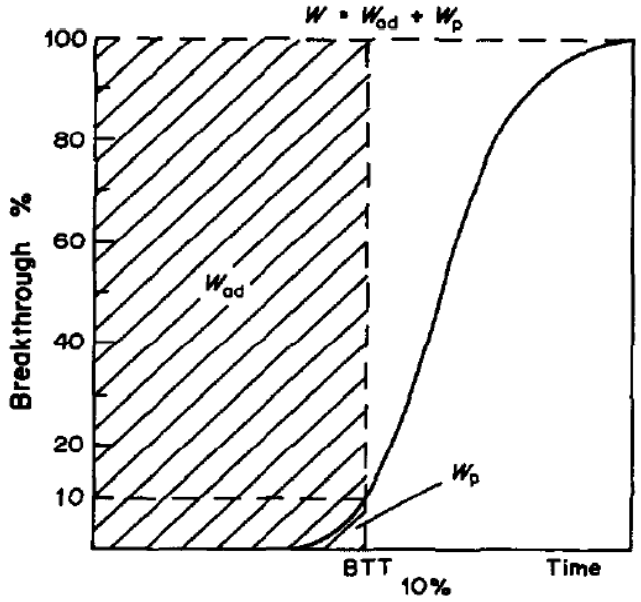

Figure 1-5. Percentage breakthrough as a function of time: Wad-amount of vapor being adsorbed; Wp=amount which passes through the cartridge unadsorbed, W-amount of vapour which contacts the adsorbent in time [26].

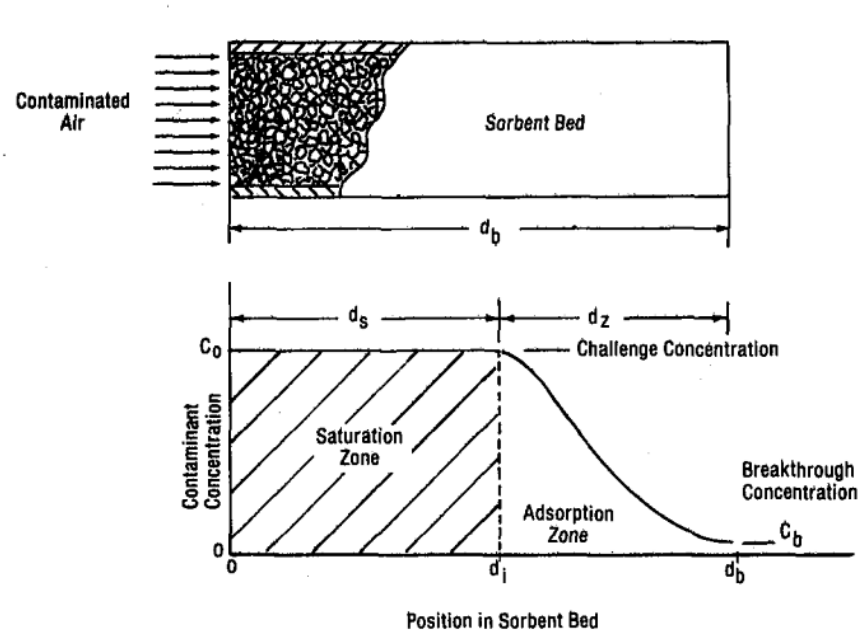

Figure 1-6. Concentration profile in adsorbent bed at the breakthrough time [44].

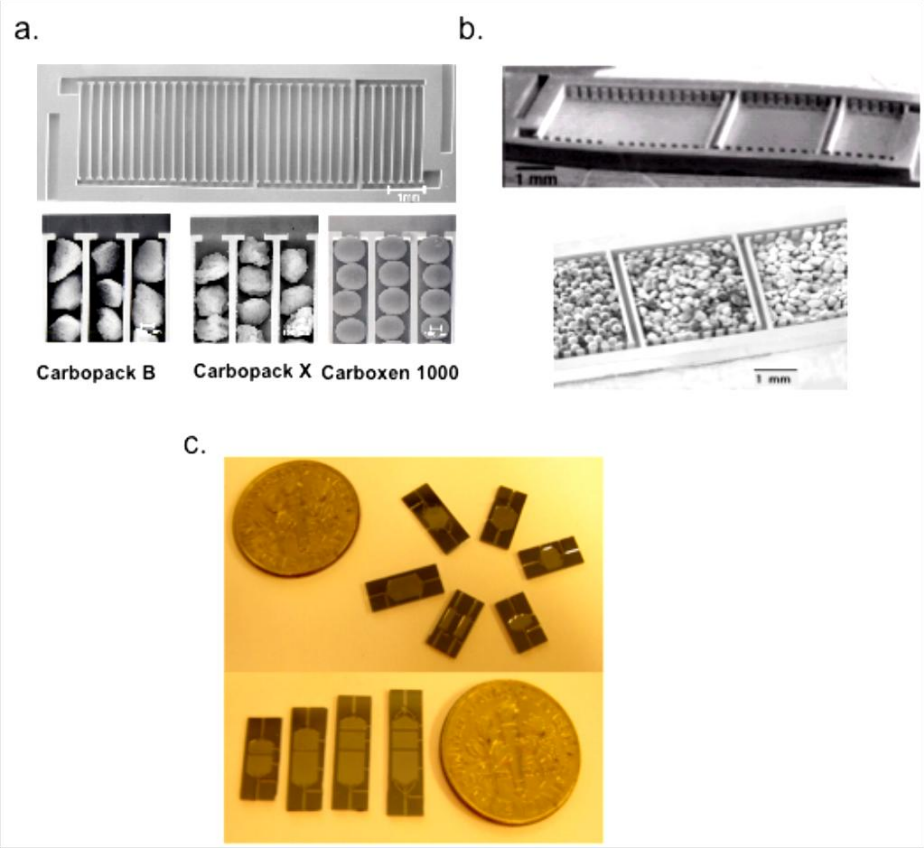

Figure 1-7. Pictures of WIMs μPCFs. Figure 1-7a and 1-7b show first and second generation of WIMS2 μPCF. The current version of WIMs μPCF is shown in Figure 1-7c, they are available in different sizes and shapes. The larger devices can be packed with more adsorbent to obtain higher capacity, but with wider injection-plug width obtained.

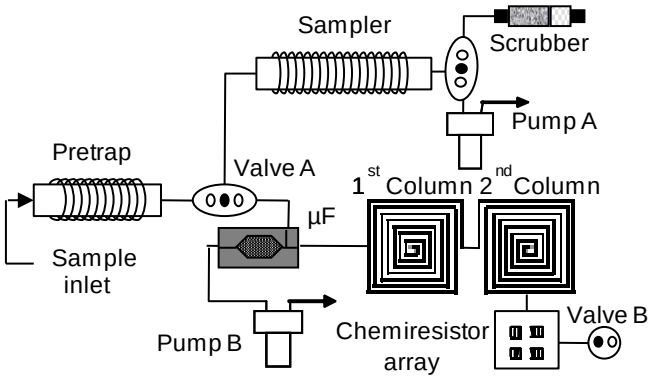

Figure 1-8. SPIRON concept diagram [41].

References

1. Center for Wireless Integrated MicroSensing and Systems (WIMS2) website: http://www.wims2.org, accessed December 2012
2. J. H. Seo, S. K. Kim, E.T. Zellers, and K. Kurabayashi, *Lab Chip*., 2012, 12, 717.
3. S. K. Kim, D. R. Burris, H. Chang, J. Bryant-Genevier, and E. T. Zellers, *Environ Sci Technol*, 2012, 46, 6065.
4. S. K. Kim, D. R. Burris, H. Chang, J. Bryant-Genevier, and E. T. Zellers, *Environ Sci Technol*, 2012, 46, 6073.
5. G. Serrano, H. Chang, L. K. Amos, and E.T. Zellers, Proc. Transducers'11, Beijing, China, 2011, 1654.
6. S. C. Terry, J. H. Jerman, and J. B. Angell, *IEEE Trans*, Electron Dev., 1979, 26, 1880.
7. C. J. Lu, W. H. Steinecker, W. C. Tian, M. Agah, J. M. Potkay, M. C. Oborny, J. Nichols, H. Chan, J. Driscoll, R. D. Sacks, S. W. Pang, K. D. Wise, and E. T. Zellers, *Lab Chip*, 2005, 5, 1123.
8. W.C. Tian, S. W. Pang, C. J. Lu, and E. T. Zellers, *J. Microelectromech. Sys.*, 2003, 12, 264.
9. W. C. Tian, H. K. L. Chan, C. J. Lu, S. W. Pang, and E. T. Zellers, *J. Microelectromech. Sys.*, 2005, 14, 498.
10. J. A. Potkay, J.A.; Lambertus, G.R.; Sacks, R.D.; Wise, K.D.; *J. Microelectromech. Sys.*, 2007, 16, 1071.
11. M. Agah, G.R. Lambertus, R. Sacks and K.Wise, *J. Microelectromech. Sys.*, 2006, 15, 1371.
12. S.K. Kim, H. Chang, E.T. Zellers, *Proc. 15th International Conference on Solid-State Sensors, Actuators, and Microsystems; Transducers '09,* Denver, CO, 2009, pp. 128.
13. F. I. Bohrer, E. Covington, Ç. Kurdak, and E. T. Zellers, *Proc. 15th International Conference on Solid-State Sensors, Actuators, and Microsystems; Transducers '09*, Denver, CO, 2009, pp. 148.
14. G. Serrano, S. Reidy, and E. T. Zellers, *Sens. Actuators. B*, 2009, 141, 217.
15. S.-J. Kim, S. M. Reidy, B. P. Block, K. D. Wise, E. T. Zellers, and K. Kurabayashi, *Lab Chip*, 2010, 10, 1647.
16. H. Chang, S. K. Kim, T. Sukaew, F. Bohrer, and E. T. Zellers, *Proc. Solid-State Sensors, Actuators, and Microsystems Workshop*, Hilton Head, South Carolina, 2010, pp. 278.
17. G. Serrano, T. Sukaew and E.T. Zellers, *J. Chromatogr. A*. accepted for publication, 2012.
18. I. Voiculescu, R. A. McGill, M. E. Zaghloul, D. Mott, J. Stepnowski, S. Stepnowski, H. Summers, V. Nguyen, S. Ross, K. Walsh, and M. Martin, *IEEE Sens. J.*, 2006, 6, 1094. K. Nachef, B. Bourlon, K. Danaie, P. Guieze, E. Donzier, E. Marty, and T. Bourouina, *Proc. IEEE Sensors*, Elancourt, France, 2009, pp. 1081.
19. J. Liu, Y. Sun, D. J. Howard, G. Frye-Mason, A.K. Thompson, S. Ja, S. Wang, M. Bai, H. Taub, M. Almasri and X. Fan, *Anal.Chem*. 2010, 82, 4370.

20. A.D. Radadia, A. Salehi-Khojin, R.I. Masel and M A Shannon, *J. Micromech.Microeng*., 2010, 20, 015002.
21. S. Ali, M. Ashraf-Khorassani, L.T. Taylor and M. Agah, *Sens. Actuator, B.*, 2009, 141, 309.
22. C. Y. Lee, R. Sharma, A. D. Radadia, R. I. Masel, and M. S. Strano, *Angew. Chem*. 2008, 120, 5096.
23. P. R. Lewis, R. P. Manginell, D. R. Adkins, R. J. Kottenstette, D. R. Wheeler, S. S. Sokolowski, D. E. Trudell, J. E. Bymes, M. Okandan, J. M. Bauer, R.G. Manley, and G. C. Frye-Mason, *IEEE Sens. J.*, 2006, 6, 784.
24. S. Zampolli, I. Elmi, F. Mancarella, P. Betti, E. Dalcanale, G. C. Cardinali and M. Severi, *Sens. Actuator, B.*, 2009, 141, 322.
25. B. Kaanta, H. Chen, X. Zhang**,** *Proc. 23th International Conference on Micro Electro Mechanial Systems (MEMS)*, 2010, Wanchai, Hong Kong. 2010, 907.
26. J. Namiesnik, *Talanta*, 1988, 35, 567.
27. Frank R. Burden; Ulrich Foerstner; Ian D. MaKelvie; Alex Guenther: Environmental Monitoring Handbook. Sampling of Atmospheric Volatile Organic Compounds (VOCs) with Sorbent Tubes and Their Analysis by GC-MS, chapter (McGraw-Hill Professional, 2002), AccessEngineering
28. K. Othmer, Encyclopedia of Chemical Technology, 3rd Ed., Vol. 23, p. 310. Wiley, New York, 1983
29. US EPA, *TO-17, Compendium of Methods for the Determination of Toxic Organic Compounds in Ambient Air*, Report No. EPA/625/R-96/010b, US EPA, Washington DC, 2nd edn., 1999
30. C.J. Lu, E.T. Zellers, *Anal. Chem*, 2001, *73*, 3449.
31. C.J. Lu, E.T. Zellers, *Analyst*, 2002, 127, 1061.
32. Feng, and S. Mitra, *J. Microcolumn Separations*, 2000, 12, 267.
33. Q. Zhong, R.A. Veeneman, W.H. Steinecker, C. Jia, S.A. Batterman and E.T. Zellers, *J. Environ. Monit*., 2007,9, 440.
34. Elizabeth Woolfenden, *J. Chromatogr. A*, 2010, 1217, 2674.
35. Elizabeth Woolfenden, *J. Chromatogr. A, 2010, 1217,* 2685.
36. D.K.W. Wang and C.C. Austin, *Anal. Bioanal. Chem*., 2006, 386,1089.
37. K. Dettmer and W. Engewald, *Anal. Biochem*., 2002, 373, 490.
38. Kenneth S.W. Sing, *Carbon*, 1994, 32, 1311
39. J. Brown and B. Shirey, Technical Report for Supelco, T402025, Bellefonte, PA, 2001.
40. R. Yang, Adsorbent: *Fundamentals and Applications*, Wiley Science: Hoboken, New Jersey, 2003.
41. T. Sukaew, H. Chang, G. Serrano, E.T. Zellers, *Analyst.*, 2011, 136, 1664.
42. R.L. Grob, E.F. Barry, Modern Practice of Gas Chromatography, New Jersey: John Wiley & Sons, 2004.
43. J. J. Whiting and R. D. Sacks, *J. Sep. Sci.*, 2006, **29**, 218.
44. M.W. Ackley, Am. *Ind. Hyg. Assoc. J*., 1985, 46, 679.
45. I.M. Klotz, *Chem Rev*, 1946, 39, 241.
46. G.O. Wood, Report LA-UR-00-5268. Los Alamos, NM: Loas Alamos National Laboratory
47. S. Iijima, *Nature*, 1991, 354, 56-58.
48. A. Merkoçi, *Microchim Acta*, 2006, 152, 157.
49. B. Pan and B. Xing, *Environ. Sci. Technol*, 2008, 42, 9007.

50. M. S. Mauter and M. Elimelech, *Environ Sci Technol*, 2008, 42, 5843.
51. M. Valcarcel, S. Cardenas, B.M. Simonet, Y. Moliner-Martinez, and R. Lucena., *TrAC, Trends Anal. Chem.*, 2008, 27, 34.
52. F. Zheng, D. L. Baldwin, L. S. Fifield, N. C. Anheier, Jr., C.L. Aardaht, and J.W. Grate, *Anal. Chem*., 2006, 78, 2442.
53. A. Stafiej, K. Pyrzynska,, *Sep Purif Technol*, 2007, 58, 49.
54. Q. Li., D. –X Yuan, Q. –M Lin, *J. Chromatogr. A*, 2004, 1026, 283.
55. C.M. Hussain, C. Saridara and S. Mitra, *Analyst*, 2008, 133, 1076.
56. C.M. Hussain, C. Saridara and S. Mitra, *J. Chromatogr. A*, 2008, 1185, 161.
57. C. Saridara, S. Ragunath, Y. Pu and S. Mitra, *Anal. Chim. Acta.*, 2010, 677, 50.
58. O. Sae-Khow and S. Mitra, *Anal. Chem.* 2010, 82, 5561.
59. M. Stadermann, A. D. McBrady, B. Dick, V.R. Reid, A. Noy, R.E. Synovec, and O. Bakajin, *Anal. Chem.*, 2006, 78, 5639-5644.
60. C. M. Hussain and S. Mitra, *Anal Bioanal Chem*., 2011, 399, 75.
61. A. Wheeler and A. J. Robell, *J. Catal.*, 1969, 13, 299.
62. L. A. Jonas and W. J. Svirbely, *J. Catal.*,. 1972, 24, 454.
63. N. Vahdat, *Carbon.*, 1997, 35, 1545.
64.. Y. H. Yoon and J. H. Nelson, *Am. Ind.Hyg. J*., 1984, 45, 509.
65. H.P. Tuan and A. Handley, *J. Chromatogr. A,* 1997, 791, 177.
66. G. Ouuand and J. Pawliszyn, *Anal.Bioanal.Chem*., 2003, 366, 1059.
67. M. Jia, J. Koziel, and J. Pawliszyn, *Field Anal Chem Techy*, 2000, 4, 73.
68. H.K.L. Chan, S.W. Pang, R.A. Veeneeman, E.T. Zellers, and M. Takei, *Proc. 2005 Solid-State Sensor and Actuator Conf*.-Transducers-05, Seoul, Korea, 2005, pp. 2901-2904.
69. W.-C. Tian, T. H. Wu, C.-J. Lu, W. R. Chen, H. J. Sheen, *J. Micromech. Microeng.*, 2012, 22, 065014.
70. M. Kim, S. Mitra, *J. Chromatogr. A*, 2003, 996, 1.
71. M. D. Martin, T. J. Roussel, S. Cambron, J. Aebersold, D. Walsh, J. Lin, M. G. O'Toole, and R. Keynton, *Int. J. Ion Mobil*. Spec., 2010, 13, 109.
72. R. P. Manginell, D. R. Adkins, M.W. Moorman, R. Hadizadeh, D. Copic, D.A. Porter, J. M. Anderson, V. M. Hietala, J. R. Bryan, D.R. Wheeler, K. B. Pfeifer, and A. Rumpf, *J. Microelectromech. Syst*., 2008, 17, 1396.
73. C.E. Davis, C.K. Ho, R.C. Hughes, and M.L. Thomas, *Sens. Actuators, B*, 2005, 104, 207.
74. B. Alfeeli, D. Cho, M. Ashraf-Khorassani, L. T. Taylor, and M. Agah, *Sens. Actuators, B*, 2008, 133, 24.
75. M. –Y. Wong, W.-R. Cheng, M.-H. Liu, W.-C. Tian, and C.-J. Lu, , *Talanta*, 2012, 101, 307
76. A. B. A. Dow, W. Lang, *IEEE Sens. J.*, 2012, 12, 2528.
77. I. Gràcia, P. Ivanov, F. Blanco, N. Sabaté, X. Vilanova, X. Correig, L. Fonseca, E. Figueras, J. Santander, and C. Cané, *Sens. Actuators, B*, 2008, 132, 149.
78. E.H.M. Camara, P. Breuil, D. Briand, L. Guillot, C. Pijolat, and N.F. de Rooij, *Sens. Actuators, B*, 2010, 148, 610.
79. A. Rydosz, W. Maziarz, T. Pisarkiewicz, K. Domański, and P. Grabiec, A gas micropreconcentrator for low level acetone measurements, *Microelectron. Reliab.*, 2012, 52, 2640.
80. P. Lodewyckx, G.O. Wood and S.K. Ryu, *Carbon*, 2004, 42, 1351.
81. G.O. Wood, *Carbon*, 1992, 30, 593.

82. O. Busmundrud, *Carbon*, 1993, 31, 279.
83. G.O. Wood, E.S. Moyer., *Am Ind Hyg Assoc J* , 1989, 50, 400.
84. G.O. Wood, *Carbon*, 2002, 40, 1883.
85. A. Gil, P. Grange, *Colloids Surf., A*, 1996, 113, 39.
86. S.G. Chen and R.T. Yang, *Langmuir*, 1994, 10, 4244.
87. C. Nguyen, D.D. Do, *Carbon*, 2001, 39, 1327.
88. M.M. Dubinin, *Chem. Rev*. 1960, 60, 235.
89. L. A. Jonas, Y. B., Tewari, and E. B. Sansone, *Carbon*, 1979, 17, 345.
90. L. A. Jonas and J. A. Rehrmann, , *Carbon* , 1974, 12, 95.
91. J. A. Rehrmann and L. A. Jonas, *Carbon*, 1978, 16, 47.
92. G. O. Wood and J. F. Stampfer, *Carbon*, 1993, 31, 195.
93. P. Lodewyckx and E. F. Vansant, *Am. Ind. Hyg. Assoc. J.* , 2000, 61, 501.
94. G. O. Wood and P. Lodewyckyx, *Am. Ind. Hyg. Assoc. J.* , 2003, 64, 646.
95. G.O. Wood, Carbon, 2002, 40, 231.
96. G.O. Wood, *Carbon*, 2002, 40, 685.
97. C. A. Robbins and P. N. Breysse, *Am. Ind. Hyg. Assoc. J.*, 1996, 57, 717.
98. L. A. Jonas, E. B. Sansone, and T. S. Farris, *Am. Ind. Hyg. Assoc. J.* , 1983, 44, 716.
99. H. J. Cohen, D. E. Briggs, and R. P. Garrison, *Am. Ind. Hyg. Assoc. J., 1991,* 52, 34.
100. L. A. Jonas and E. B. Sansone, *Am. Ind. Hyg. Assoc. J., 1986,* **47**, 509.
101. S. J. Doong and R. T. Yang, *Ind. Eng. Chem. Res., 1988,* **27**, 630.
102. U. S. EPA, Draft Guidance for Evaluating the Vapor Intrusion to Indoor Air Pathway from Groundwater and Soils. Report No. EPA/540/1-89/002, U. S. EPA, Washington DC, 2002

Chapter 2

Evaluating the Dynamic Retention Capacities of Microfabricated Vapor Preconcentrators as a Function of Flow Rate

2.1 Introduction

The limited sensitivity and/or selectivity of most stand-alone microsensors and microsensor arrays preclude their use for quantitative analysis of mixtures of airborne volatile organic compounds (VOC) at the low concentrations required for applications such as monitoring of ambient or indoor air pollutants [1,2], breath analysis for biomedical diagnostics [3], and explosives detection for homeland security [4], where field determinations are of greatest value. Only by integrating such microsensors with upstream devices designed to preconcentrate and separate the components of VOC mixtures prior to detection can microsystems capable of quantitative, trace-level, multi-VOC determinations be realized [5-10].

In conventional applications of adsorbent preconcentrators for environmental VOC sampling, relatively large packed beds (containing tens-to-hundreds of mg of adsorbent material) and relatively low flow rates are employed to minimize the likelihood of breakthrough losses [11-12]. During subsequent analysis, typically by gas chromatography (GC), captured vapors are thermally desorbed and transferred to a smaller adsorbent bed or to a cryogenically cooled trap prior to separation and detection. This focusing step serves to reduce the width of the injected

band, which is necessary for efficient chromatographic separation of the VOC mixture components [13]. Since most microfabricated preconcentrators are implemented without separatedownstream focusers, we prefer the terms "(micro)preconcentrator/injector" or "(micro)preconcentrator/ focuser" (μPCF), which highlight the dual function of such devices, as well as the tradeoffs required for optimizing performance [14-17].

In most reported μPCF devices, small size and low (heating) power are given priority over high capacity, such that, by design, only a fraction of the vapor mass in the sample stream is collected [6,18-25]. Assuming a constant partition (adsorption) coefficient and sufficient residence time for sorption equilibrium to be established, then the mass of vapor retained on the adsorbent will be proportional to the air concentration and quantitative analysis is possible [26-29]. However, the PFs achievable with devices relying on such equilibrium-based sorption are inherently low (i.e., <<100) due to the limited adsorbent mass and low trapping efficiency [19,28]. In fact, the PF, per se, is technically indeterminate because only a fraction of the vapor mass is captured from the sample stream and this fraction can vary with flow rate, sample volume, and the number and nature of competing vapors in the sample (note: the PF is defined as the ratio of volumes in which a given mass of vapor is contained before preconcentration and after desorption [11,30]; since equilibrium-based preconcentrators do not conserve mass, it is not possible to calculate a bonafide PF value).

With careful adjustment of the design and operating conditions of a μPCF it is possible to remove the entire mass of vapor(s) from the sample stream. Provided that subsequent heating is rapid enough to desorb the trapped vapors into a small enough volume, the exhaustive trapping provided by devices of this design can yield much higher PF values than those relying on equilibrium-based sorption, because more mass is being captured per unit volume of sampled air.

Previous efforts in our laboratory to develop miniaturized and microfabricated PCFs for multi-vapor analysis have focused exclusively on devices designed for exhaustive trapping [5,14-17, 31]. Others have also reported on micro-scale devices with similar design features [32-36]. Examples include adsorbent-filled glass or metal capillaries (cPCF) with wrapped-wire heaters [14,15] and adsorbent-filled single- and multi-stage Si μPCFs relying on bulk or membrane heating for desorption [5,16,17,31-36].

In devices designed for exhaustive trapping, the *dynamic retention capacity* is the primary performance criterion [14,37,38]. It is affected by both thermodynamic and kinetic factors. Thus, a certain minimum mass of adsorbent is required, which depends on the adsorbent properties and the nature, number, and concentrations of vapors in the sample stream that are partitioning onto the adsorbent surface [39]. In addition, the rate of mass transfer of the vapor in the sample to the adsorbent surface is important, which depends on the linear velocity, packing density, and microporosity of the adsorbent material [40,41].

The dynamic retention capacity is conveniently determined by continuously drawing a sample of vapor in air through the PCF and monitoring downstream for the appearance of breakthrough. The breakthrough volume, $V_{b\text{-}x}$, or breakthrough time, $t_{b\text{-}x}$, is used as the measure of retention capacity and is defined as the volume or time, respectively, required to observe some pre-determined fraction, x, of the inlet vapor concentration (e.g., 0.1) downstream from the PCF [14,37,38].

The modified Wheeler Model serves as a useful guide for designing cPCF and μPCF devices and assessing their performance [14-16]. This model relates several important design and operating parameters to the $V_{b\text{-}x}$ or $t_{b\text{-}x}$ of a densely-packed bed of granular adsorbent under a continuous vapor challenge:

$$V_{b-x} = \frac{W_e W_b}{C_o}\left[1 - \frac{1}{k_v \tau}\ln\left(\frac{C_o}{C_x}\right)\right] = \frac{W_e W_b}{C_o} - \frac{W_e \rho Q}{C_o k_v}\ln\left(\frac{C_o}{C_x}\right) \quad (2.1)$$

$$t_{b-x} = \frac{\rho W_e}{C_o}\left[\tau - \frac{1}{k_v}\ln\left(\frac{C_o}{C_x}\right)\right] = \frac{W_e W_b}{C_o Q} - \frac{\rho W_e}{C_o k_v}\ln\left(\frac{C_o}{C_x}\right) \quad (2.2)$$

where $V_{b\text{-}x}$ is in liters, $t_{b\text{-}x}$ is in min, W_e is the adsorption capacity (g adsorbate/g adsorbent), W_b is the adsorbent bed mass (g), $\tau = W_b/(\rho Q)$ is the bed residence time (min), ρ is the adsorbent bed density (g/cm^3), Q is the volumetric flow rate (cm^3/min), k_v is the kinetic rate constant (min^{-1}), C_o is the inlet concentration (g/cm^3), and C_x is the outlet concentration (g/cm^3).

Estimates of the true (i.e., thermodynamic) W_e (i.e., $W_{e\text{-}th}$) can be obtained from theoretical adsorption isotherm models or from experimental measurements of equilibrium vapor uptake as a function of concentration [39]. Estimates of the so-called kinetic W_e ($W_{e\text{-}k}$) can be obtained via Eq. (2.1) by measuring $t_{b\text{-}x}$ for a series of devices with different W_b values at a fixed Q or for a single device with fixed W_b tested over a range of Q values; plotting $t_{b\text{-}x}$ vs. either τ or W_b yields a line the slope of which is proportional to $W_{e\text{-}k}$ [14,37,38,40].

The modified Wheeler Model predicts a non-linear decrease in $V_{b\text{-}x}$ and a linear decrease in $t_{b\text{-}x}$ with decreasing τ. The critical bed residence time, $\tau_{c\text{-}x}$, corresponding to the point at which $V_{b\text{-}x}$ (or $t_{b\text{-}x}$) = 0, represents the practical limit to miniaturization of the PCF. That is, for a given value of Q, this defines the minimum volume of the PCF: when $\tau = \tau_{c\text{-}x}$ a fraction, x, of the incoming vapor will breakthrough immediately after sampling commences, and quantitative analysis is compromised. By the same token, for a PCF of a given size, this determines the critical (i.e., maximum) flow rate, $Q_{c\text{-}x}$.

The quantity $W_{e\text{-}k}W_b/C_o$ is the volume of air, $V_{e\text{-}k}$, containing the vapor at C_o that is required to achieve dynamic equilibrium in the distribution of vapor between the air and the entire adsorbent bed. The bed efficiency, $1- \ln(C_o/C_x)/(k_v\tau) = V_{b\text{-}x}/V_{e\text{-}k}$, is always < 1 for finite values of τ, and it reflects the fraction of the adsorbent bed used at specific value of x [14]. Note that the expected decrease in $V_{b\text{-}x}$ as C_o increases is offset by a proportional increase in $W_{e\text{-}k}$ with increasing C_o at low challenge concentrations where sub-monolayer adsorption predominates (i.e., a linear increase in W_e with C_o is assumed in all common isotherm models) [39].

Building upon the work of Lu et al. [14,15] and Tian et al. [16], this article describes a systematic study of the effects of Q and τ on $t_{b\text{-}10}$ and $V_{b\text{-}10}$ for μPCFs designed for exhaustive trapping of VOCs. The vapor concentrations tested were an order of magnitude lower than those tested in these previous studies and, therefore, are more relevant to many potential applications. A commercial graphitized carbon, Carbopack X (C-X), was used, which is a granular, hydrophobic, non-microporous solid commonly employed for environmental VOC sampling applications [12,42]. It is thermally stable in air and it captures and subsequently releases VOCs of low-to-moderate polarity with vapor pressures, p_v, in the range of ~ 3.3 to 13 kPa quite efficiently [14,15]. Representative breakthrough curves for a single test vapor are presented first to illustrate some generic aspects of device performance. Results of preliminary breakthrough testing of the same vapor with μPCFs of different designs and bed sizes are then presented. Next, results of additional testing of the largest μPCF are compared to those obtained from a cPCF containing the same adsorbent mass, and the dynamic retention capacities are considered in the context of the modified Wheeler Model. Three additional vapors tested on one or both devices allow the trends in performance to be assessed. Critical flow rates are estimated and a proposal for a broadly applicable safe sampling flow rate is presented. The range of PF values

achievable with the μPCF, along with the required minimum sampling times, are then presented assuming its incorporation into a GC microsystem (μGC). Finally, the difficulty faced in using the Wheeler Model to *predict* the dynamic retention capacity of such devices is illustrated.

2.2 Experimental

2.2.1 Materials and devices

Benzene (BEN, p_v = 13 kPa), 2-butanone (MEK, p_v = 12 kPa), toluene (TOL, p_v = 4 kPa) and n-heptane (HEP, p_v = 6 kPa) were purchased from Sigma-Aldrich/Fluka (Milwaulkee, WI) or Acros/Fisher (Pittsburgh, PA) in >99% purity and were used as received. Samples of C-X (60/80 mesh, specific surface area = 250 m^2/g) obtained from Supelco (Bellefonte, PA) were sieved and the fractions with nominal diameters in the range of 212-250 μm were isolated and packed in the appropriate device.

Four different μPCF device designs (Figure 2-1, Types A-D) were fabricated from double-polished 4-inch Si wafers. Deep-reactive-ion-etching (DRIE) was used to form a central cavity with opposing, tapered inlet and outlet sections, and a set of pillars (0.15 mm widths and spaces, 0.38 mm height) near the inlet and outlet ports for retaining the adsorbent granules. The devices have cavity volumes ranging from 1.5 to 5 mm^3 and are sealed with an anodically bonded Pyrex plate (0.1 mm thick). A third port etched on the side of the Si cavity is used for filling the chamber of the sealed device with the adsorbent. Inlet and outlet fluidic channels, 0.4 mm (w) × 1.77 mm (l) x 0.38 mm (h), are etched into the μF chip on opposing sides of the cavity, one of which has tee branch that facilitates loading and backflushing of the VOC samples. All three fluidic channels have expansion sections at the edge of the chip that accept the

fused-silica capillaries used for fluidic interconnections. A Ti/Pt resistive temperature device (RTD) was evaporated onto the backside of the Si along with two large Ti/Pt contact pads for applying current to heat the devices during desorption. Electrical connections to a custom printed circuit board are made using Al wire-bonds. Deactivated fused-silica capillaries (0.25-mm i.d., 0.32-mm o.d., Supelco) were inserted in the three fluidic ports and secured with silicone adhesive (Duraseal® 1531, Cotronics, Brooklyn, N.Y). Type A, B, C, and D devices have cavity volumes of 1.4, 2.6, 3.4 and 4.5 μL, respectively (see Figure 2-1). The Type-C design differs from that of the other devices in that it has split inlet and outlet channels, which were designed to explore whether performance might improve by distributing the flow in and out of the cavity. In these Type-C devices, additional sets of pillars were included at all inlets and outlets to the cavity.

2.2.2 Device preparation

To pack the devices with C-X, a low vacuum pressure was applied at the outlet port to draw the adsorbent granules in through the fill port at the side of the cavity, while the capillaries extending from the unused ports were temporarily blocked with septa. The adsorbent was retained in the cavity by the pillars described above. Each device was filled to capacity by visual inspection, with the amount of adsorbent loaded being determined by weighing the device before and after packing. Type A, B, C, and D devices held 0.8, 1.5, 1.9 and 2.3 mg, respectively. After packing, the fill ports were sealed with Duraseal®.

The cPCF was constructed by packing a 5-cm-long section of thin-walled Inconel tubing (1.59-mm o.d., 1.35-mm i.d., cross sectional area = 0.0143 cm^2) with 2.3 ± 0.1 mg of C-X. The

adsorbent was drawn into the device under vacuum and was retained by small pieces of stainless steel mesh and silanized glass wool. The bed occupied a length of ~4 mm and was located within 1-cm of the distal end of the tubing to minimize the downstream dead volume. A thin sleeve of polyimide (Microlumen, Tampa, FL) was placed around the packed section of the tube and a fine-wire type-K thermocouple was held snugly against the tube with another thin polyimide sleeve. A section of varnished Cu wire, used to resistively heat the adsorbent bed following each test, was then coiled tightly around this assembly to create a heated length that extended beyond that of the adsorbent bed.

Packed cPCF and μPCFs were preconditioned by heating under a low flow of N_2 for 4 hr at 300°C. After each experiment, adsorbed VOCs were removed by heating to 275 ºC for 20 min under a flow of N_2.

2.2.3 Breakthrough Testing

The apparatus used to test breakthrough as a function of flow rate is shown in Figure A-1 of the Appendix. Test atmospheres containing ~ 100 ppb of BEN, MEK, TOL, and HEP in N_2 were created in 10-L or 40-L Tedlar® bags by serial dilution. This corresponds to absolute concentrations of 0.32, 0.29, 0.38, and 0.41 mg/m^3, respectively. Breakthrough volumes were determined by drawing the atmosphere through the μPCF or cPCF using a vacuum pump (UN86KTDC, KNF Neuberger, Trenton, NJ). At 1-min intervals an aliquot of the outlet stream was directed onto the column (15-m long, 320 μm i.d. capillary column with a 0.25 μm thick HP-1 stationary phase) of a GC with flame-ionization detector (GC-FID, Model 6890, Agilent Technologies, Palo Alto, CA) via a six-port valve equipped with a 250-μL gas sampling loop.

The flow rate through the device was measured at the inlet using a primary flow standard, and a needle valve placed upstream from the pump was adjusted to achieve the desired flow rate. The column oven temperature was adjusted to give a retention time of less than one minute for all tested compounds. Peak integration was performed using GRAMS 32 (Version 6.0. Thermo-Scientific, Pittsburg, PA). All four vapors were tested with the cPCF. Only benzene and MEK were tested with the Type D μPCF.

Breakthrough curves were generated for a series of Q values from ~15–110 mL/min for the cPCF (corresponding to τ values of ~20–2.7 msec). Due to the high pressure drop across the Type D μPCF, tests were confined to Q values of 10–60 ml/min (corresponding to τ values of ~24–4 msec). All connections were leak checked periodically. Experiments were allowed to continue long enough to extract values of $t_{b\text{-}10}$ and $V_{b\text{-}10}$ at C_x/C_o = 0.1 directly or by (linear) interpolation between the two nearest data points. The flow rate and the challenge concentration were measured before and after every breakthrough determination and were found to vary by < 10 %. The average $t_{b\text{-}10}$ values from duplicate experiments varied by 2-15%, with an average relative standard deviation of < 10%. To confirm the challenge concentrations, the FID was calibrated by analyzing separate serially-diluted test atmospheres prepared in Tedlar bags that spanned the required range of injected masses.

Values of $W_{e\text{-}th}$ for the test vapors with C-X were obtained from thermogravimetric analyzer (TGA) measurements. Adsorption isotherms were generated from mass uptake at discrete concentrations ranging from ~50 - 2,000 ppb created by diluting saturated vapor streams generated with a fritted bubbler with clean, dry air. Vapor concentrations were periodically verified by GC-FID. For this study, the $W_{e\text{-}th}$ values determined at 100 ppb were used. They are 90, 400, and 1500 μg/g for MEK, BEN, and TOL, respectively. Values collected for HEP were

found to be in error and so are not reported.

For the cPCF, which has a constant cross section, τ is simply the ratio of the bed volume to the volumetric flow rate (Q), where the bed volume is the ratio of the bed mass (W_b) to the packed bed density (ρ), both of which were measured directly by weighing the device before and after loading and then measuring the length of the packed bed. Since the cavities in the μPCF devices are tapered at the inlet and outlet, the linear velocity varies continually in these regions at a given Q value, and the value of τ was taken as the volume-weighted average of the triangular and rectangular subsections of the bed at a given Q. Values of ρ were 0.56, 0.57, 0.56 and 0.52 g/ml for type A, B, C, and D μPCF devices, respectively, and 0.47 g/mL for the cPCF.

2.3 Results and discussion

2.3.1 Breakthrough curves

Figure 2-2 shows a set of representative breakthrough curves for benzene and toluene, determined with the Type-D μPCF and the cPCF. The breakthrough curve is the reflection of the corresponding vapor profile moving through the bed, and its characteristic S shape reflects the evolving nature of the vapor-adsorbent interaction over time as the wave front passes through a well-packed bed [38,43]. The first portion of the curve is convex with respect to the time axis, which is indicative of an excess of active adsorption sites and mass transfer kinetics that are pseudo-first-order with respect to the vapor concentration. The final portion of the curve is concave with respect to the time axis, which reflects a depletion of available adsorption sites and mass transfer kinetics that are pseudo-first-order with respect to the number of active sites. The point at which breakthrough occurs at a given challenge flow rate depends primarily on W_e (Eq.

(2.2). The central segment of the breakthrough curve is linear and the slope depends on the rate of mass transfer of vapor on to adsorbent surface, k_v, which increases with the sampling flow rate [37,38].

2.3.2 Performance of different μPCF devices

Initial tests of the Type A-D μPCF devices were performed with BEN at flow rates in the range of 5-60 mL/min. The breakthrough curves for these two devices are presented in Figures A-2a and b in the Appendix. The Type-A device showed immediate breakthrough at 5, 10, and 25 mL/min, and although the Type C device gave a $t_{b\text{-}10}$ value of ~9 min at 10 mL/min, flow rates ≥ 20 mL/min led to nearly immediate breakthrough (i.e., $t_{b\text{-}10}$ < 2 min). The Type A and C μPCFs show some degree of retention, but the shapes of the breakthrough curves indicate that the type of adsorption wave front expected in a properly functioning adsorbent bed is not established. For the former device this is likely due to the values of τ starting to approach the 'characteristic removal time' whereby the wave front occupies a significant fraction of the adsorbent bed immediately after exposure commences [40]. For the latter device it is more likely due to channeling through specific pathways in the bed, enhanced by the split inlet/outlet design. The Type B device gave S-shaped breakthrough curves and $t_{b\text{-}10}$ values that decreased from 25 to 3.5 min as Q increased from 20 to 60 ml/min, respectively. The Type D device gave the highest dynamic capacity of all the μPCF devices, with $t_{b\text{-}10}$ values ranging from 90-11 min for Q values of 15-60 mL/min, respectively. This device was chosen for further testing.

Three identical Type-D devices were loaded with similar quantities of C-X and challenged with BEN at several flow rates within the range of 15-60 ml/min. Two of the devices

gave consistent results when plotting $t_{b\text{-}10}$ versus τ, whereas the third device gave anomalously low $t_{b\text{-}10}$ values. Inspection of the latter device showed that the adsorbent bed had void spaces indicating that some of the C-X had been lost either to rupture of the particles (note: C-X is known to be friable/brittle) or to inefficient sieving of the irregularly shaped C-X particles loaded into this device. Since the two other devices gave similar values of $t_{b\text{-}10}$, the data from these were combined in subsequent analyses.

Figure 2-3 summarizes the performance of the μPCF devices. Figure 2-3a shows that $t_{b\text{-}10}$ varies inversely with Q for all four devices, but the dependence is very weak for Type A and C devices. To the extent that these devices conform to the behavior expected from the modified Wheeler model, the differences in τ should reconcile the observed differences in $t_{b\text{-}10}$ as a function of Q. Figure 2-3b shows that this is approximately the case for the Type B and D devices; the dependence of $t_{b\text{-}10}$ on τ for both devices can be described by a single line with positive slope and a regression $r^2 = 0.96$. The x-axis intercept, τ_c, is 2.3 msec, which corresponds to Q_c values of ~60 and ~100 mL/min for the Type B and D devices, respectively. Differences between the two devices can be ascribed to the inherent 5-10% error in specifying W_b and ρ due to the small quantities of adsorbent used. The $t_{b\text{-}10}$ values for the Type A and Type C devices fall below the regression line and show virtually no dependence on τ, indicating that they do not adhere to the modified Wheeler Model for the reasons stated above.

Figure 2-3c presents the plots of $V_{b\text{-}10}$ vs. τ. The dashed curves represent the fits to the modified Wheeler model for each device type (from Figure 2-3b regressions, lumping all other variables into the regression coefficients). The data appear more scattered vertically than in Figure 2-3b because each value of $t_{b\text{-}10}$ is effectively amplified by Q at each point. As shown, $V_{b\text{-}10}$ is more sharply dependent on τ at smaller τ values. As τ increases $V_{b\text{-}10}$ should asymptotically

approach a limiting value equal to $V_{e\text{-}k}$ (=$W_{e\text{-}k}W_b/C_o$), which is the first term on the right hand side of Eq. (2.1).

These plots illustrate the tradeoff, in effect, among (sampling) time, device size, and capacity. For longer values of τ, the efficiency of the adsorbent bed is higher, $V_{b\text{-}10}$ is less dependent on flow rate, the capacity is greater, but it takes longer to collect a sample. Regardless, smaller devices have smaller lower capacity due to their values of V_e. In most practical circumstances, one would like to operate at the highest possible flow rate to shorten the analytical duty cycle. The curves in Figure 2-3c (and Figure 2-3b) illustrate that the ultimate limit is defined by τ_c which defines Q_c for a given device, but also that up to a value of ~2.5τ_c small changes in Q lead to large changes in $V_{b\text{-}10}$, which is undesirable. We return to this topic further below.

2.3.3 Comparison of μPCF and cPCF Performance with Several VOCs

Figure 2-4 shows the dependence of $t_{b\text{-}10}$ on τ for the test vapors on the Type D μPCF and/or the cPCF. As shown for BEN and MEK, the two devices have comparable performance: the $t_{b\text{-}10}$ values for both vapors vary in direct proportion to τ ($r^2 > 0.95$), consistent with Eq. (2.2), and the slopes differ by 2 and 25 % for MEK and BEN, respectively. The modified Wheeler Model implicitly assumes a bed diameter that is many times that of the adsorbent granule diameter, such that the impact of voids and channeling along the walls is minimized [43]. In these devices, the ratio of bed diameter (or maximum width) to granule diameter is only ~6 for the cPCF and ~14 at the widest point for the μPCF (~1.6 with respect to the height of the cavity). Thus, even small shifts in the adsorbent in the bed can have significant effects on the flow path.

The slopes for MEK are not significantly different at the 95% confidence level, whereas those for BEN are significantly different (p = 0.05).

The slopes of the lines in Figure 2-4 reveal that for any given value of τ (or Q) the $t_{b\text{-}10}$ values differ by as much as 50-fold (HEP:MEK). By reference to Eq. (2), the slopes among the different vapors are proportional to $W_{e\text{-}k}/C_o$ and independent of k_v. Estimates of $W_{e\text{-}k}$ derived from these slopes are presented in Table 2-1 and span a 75-fold range (recall that the absolute challenge concentrations differed among the vapors). Curiously, $W_{e\text{-}k}$ for HEP is higher than that for TOL despite the former having a higher value of p_v. This is accordant with the ability of alkanes to pack more tightly than planar aromatic compounds on carbon-based adsorbent surfaces [44]. Note that the $W_{e\text{-}k}$ values are 1.3-3.7 times smaller than the corresponding $W_{e\text{-}th}$ values, and the $W_{e\text{-}th}$:$W_{e\text{-}k}$ ratio, which reflects the fraction of the total possible adsorption capacity being used under the test conditions, decreases with increasing W_e value. The implications of this divergence in $W_{e\text{-}th}$ *and* $W_{e\text{-}k}$ on using the Wheeler model to predict μPCF performance are discussed below.

The x-axis intercepts in Figure 2-4 yield the values of τ_c, which are listed, along with the corresponding Q_c values, in Table 2-2. The τ_c values for MEK for the two devices were very close, so the average is presented. As shown, higher Q_c values are obtained for the vapors with higher values of $W_{e\text{-}k}$, though no clear functional relationship between these variables could be found on the basis of this small data set.

2.3.4 General guideline for limiting the flow rate; projected PF values

Figure 2-5a presents plots of $V_{b\text{-}10}$ vs. τ for all four vapors with the reference cPCF device. The values of $V_{b\text{-}10}$ were determined from the corresponding values of $t_{b\text{-}10}$ by multiplying

by Q, and the curves in Figure 2-5a were derived similarly using the regressions from Figure 2-4. These plots illustrate the influence of $W_{e\text{-}k}$ on $V_{b\text{-}10}$, and the associated influence of τ (or Q) on performance. As shown, vapors with higher affinity for the adsorbent exhibit larger $V_{b\text{-}10}$ values at a given τ, they maintain higher values of $V_{b\text{-}10}$ as τ decreases, and they approach larger values of $V_{e\text{-}k}$ as τ increases.

To compare the cPCF and μPCF performance data collectively, Figure 2-5b plots the bed efficiency (i.e., $V_{b\text{-}10}/V_{e\text{-}k}$) as a function of τ for all six vapor-device combinations. Normalizing the regression-derived $V_{b\text{-}10}$ value to its effective maximum value for each vapor-device combination reveals the rate at which the latter value is approached. For TOL and HEP, which have the highest $W_{e\text{-}k}$ values, > 90% efficiency is maintained down to a τ value of 7 msec, whereas for MEK and BEN the efficiency is already < 60% at this value of τ. Furthermore, the approach to maximum efficiency is more gradual for MEK and BEN. Regardless, for τ values less than ~ 2.5 τ_c the rate of change in efficiency increases dramatically, and in this regime a small increase in Q leads to a large decrease in $V_{b\text{-}10}$ (i.e., capacity).

With a goal of developing a general guideline for stipulating maximum operating flow rates of μPCF devices, on the basis of these data we suggest imposing a cut-off value at 60% efficiency. Although somewhat arbitrary, this represents a reasonable tradeoff between flow rate (i.e., sampling time) and capacity, and corresponds to the point at which the vapors at the lower end of the retention range start to lose efficiency at a higher rate. The value of τ associated with this efficiency cut-off is considered the minimum safe value, τ_{safe}, and the corresponding safe (i.e., maximum recommended) flow rate is therefore designated Q_{safe}. The ratios of τ_c to τ_{safe} range from 0.39-0.43, averaging ~ 0.4. Multiplying Q_c by this factor yields the value of Q_{safe} for each vapor. The values of these parameters for all vapors are listed in Table 2-2.

The range of Q_{safe} values among the six vapor-devices is 28 to 120 mL/min and the corresponding range of sample volumes is 0.11 to 5.8 L (i.e., the values of $V_{b\text{-}10}$ corresponding to these values of Q_{safe}). Assuming an injection band width of, say, 3 sec upon subsequent thermal desorption into a microcolumn at a flow rate of, say, 3 mL/min [5,13,14,45], the resulting PF values span from 730 to 39,000. This, then represents a practical limit to the extent of preconcentration achievable with cPCF or μPCF devices of this size designed and operated to provide exhaustive preconcentration. These are remarkable high values. Although the range of PF values would vary with the adsorbent material and vapors under consideration, less retentive adsorbents would not give as high $V_{b\text{-}10}$ values and less volatile vapors would not yield such narrow injection bands. Thus, this range is probably fairly representative of what one would expect for a single-stage μPCF of similar dimensions, packed with an adsorbent at a similar density. It must be emphasized, however, that while the PF value of 730 could be achieved within a 4-min sampling period, the highest PF value (i.e., 39,000) would require 48 min. The latter time period may be suitable for some applications, but would not be for those requiring shorter analytical duty cycles in which case a high-volume sampler would be required upstream of the μPCF [8-10,45,46].

2.3.5 Device modeling

In order to use Eqs. (2.1) or (2.2) for predicting the performance of a cPCF or μPCF, independent determinations of the variables W_e and k_v are required for each vapor. The former ostensibly could be estimated from theoretical models or determined as a function of vapor concentration by gravimetric methods [38]. However, as shown here, the resulting values of $W_{e\text{-}th}$ are of limited value because they overestimate the effective value of W_e (i.e., $W_{e\text{-}k}$) to an extent

that is vapor specific; 1.3- to 3.7-fold in this study. Since $t_{b\text{-}10}$ and $V_{b\text{-}10}$ are both directly proportional to $W_{e\text{-}k}$, the magnitudes of these errors translate directly to errors in predicted performance. Deriving $W_{e\text{-}k}$ values directly would require running breakthrough tests at a series of flow rates or bed masses, effectively obviating any predictive capability.

Since there is no theoretical expression for k_v, it must be derived empirically by correlation with relevant variables. Published models derived from breakthrough tests of vapors through large air-purifying respirator cartridges packed with (microporous) activated carbon portray k_v as a function of linear velocity, v_L, as well as other variables, including particle diameter, W_e, the affinity coefficient (β) from the Dubinin-Radushkevich isotherm equation, and molecular weight [41,47]. The best of these models was only able to show modest correlations of experimentally derived k_v values with such variables (e.g., $r^2 = 0.86$ on the basis of > 700 values) [41].

Eq. (2.2) predicts a plot of $t_{b\text{-}x}$ vs. $ln(C_o/C_x)$ to be linear for values of x less than ~0.2, where the assumption of pseudo-first-order rate of adsorption is valid. Values of k_v can be determined from the slopes of such plots by substituting in values of $W_{e\text{-}k}$ and ρ. We performed such analyses for x values ranging from 0.05-0.20. Regression analysis gave r^2 values > 0.94 in all cases; a few representative plots are presented in Figure A-3 (Appendix). Due to the rapid breakthrough of MEK, it was only possible to gather such data at lower flow rates for this vapor.

Figure 2-6 shows the relationship between k_v and v_L for all vapors and devices over a range of v_L values from 8-120 cm/sec. The best fit was obtained with a power-law model, $k_v = 7.2 v_L^{1.3}$ ($r^2 = 0.86$). The use of other predictor variables, such as MW, β, and $W_{e\text{-}k}$ did not improve the correlation. The resulting average absolute error in k_v was quite high for MEK (i.e., 85%) but reasonably low for the remaining vapors (i.e., 20, 23, and 20% for BEN, TOL, and

HEP, respectively); notwithstanding the consistent negative bias for BEN with the μPCF. Thus, reasonably accurate values of k_v could be obtained for most vapors. Given the form of Eq. (2.2), the fractional errors in $t_{b\text{-}10}$ are smaller than the fractional errors in k_v and they diminish with increasing flow rate (decreasing τ). However, since a value of $W_{e\text{-}k}$ is required to evaluate k_v, as stated above, the practical value of this approach is lost without an independent estimate of $W_{e\text{-}k}$.

2.4 Conclusions

This study has confirmed that the modified Wheeler Model provides a useful framework for assessing the effect of flow rate on the performance of miniaturized and microfabricated PCF devices designed to provide exhaustive trapping of VOCs [14,16]. Within the context of this model, the bed residence time is a particularly useful parameter for comparing and reconciling performance among different devices and VOCs.

As shown, the bed residence time must be maintained above a critical value to avoid immediate breakthrough, which would negatively bias any subsequent quantitative analysis. This has direct implications for the sizes and operating flow rates of such devices. It was also shown, however, that the critical bed residence time varies inversely with the vapor adsorption capacity of the adsorbent (i.e., $W_{e\text{-}k}$). The VOCs examined here spanned the range of $W_{e\text{-}k}$ values for which the adsorbent examined here (i.e., C-X) would be recommended. Although vapors with higher $W_{e\text{-}k}$ values could conceivably be sampled at higher flow rates, the desorption efficiency is also a key performance factor and vapors with exceedingly high $W_{e\text{-}k}$ values (on any particular adsorbent) would likely give rise to broader desorption bands or incomplete desorption; the ensuing degradation of chromatographic resolution and/or detectability by

downstream microsystem components could undermine the higher dynamic retention capacity obtained.

In recognition of the sharp dependence of the breakthrough volume on bed residence time near the critical point, where small changes in flow rate can greatly impact the resulting breakthrough volume, we have proposed a generalized guideline for determining a safe (i.e, maximum) flow rate that strikes a reasonable balance between sampling frequency and retention capacity.

This study also showed that there is a limit to μPCF miniaturization, below which it is not possible to operate the device at reasonable flow rates without suffering early breakthrough. On the other hand, by operating well above this limit the projected preconcentration factors were shown to be remarkably high, though contingent upon time and $W_{e\text{-}k}$. The tradeoff of time and sensitivity enhancement precludes the use of stand-alone microsystems for applications requiring high-speed, quantitative determinations of trace-level VOCs.

Two limitations of the Wheeler Model became apparent in this study. First, despite its utility for interpreting performance and guiding design and operating conditions, it is not possible to use this model in a predictive manner for untested vapors. This constraint arises from the inability to specify $W_{e\text{-}k}$ *apriori* arising from its dependence on idiosyncratic aspects of device implementation, despite being able to model k_v values with reasonably high accuracy. Second, the Wheeler Model is applicable only to single-vapor exposures. Where multiple vapors are present and competing for adsorption sites on the adsorbent material, adjustments must be made to account for the effect on dynamic retention. On-going work is examining this issue for several binary mixtures. Results will be presented in a subsequent report.

Table 2-1. Equilibrium adsorption capacities and equilibrium volumes of tested vapors.

Vapor	$W_{e\text{-}th}$ [a] (µg/g)	$W_{e\text{-}k}$ [b] (µg/g)	$V_{e\text{-}k}$ [c] (mL)	$W_{e\text{-}th}/W_{e\text{-}k}$
MEK	90	24[d]	190[d]	3.7
Benzene (µPCF)	410	190	1700	1.7
Benzene (cPCF)	410	250	1300	2.1
Toluene	1500	1200	6900	1.3
Heptane	NA	1800	9500	NA

[a] from TGA; [b] from Eq. (2) using data presented in Figure 4; [c] from Eq. (1) using $W_{e\text{-}k}$, [e]Average of cPCF and µPCF, standard deviations are 0.83 µg/g and 6.3 mL for $W_{e\text{-}k}$ and $V_{e\text{-}k}$, respectively.

Table 2-2. Critical and "safe" values of τ and Q.

vapor	τ_c [a] (msec)	τ_{safe} [b] (msec)	τ_c / τ_{safe}	Q_c [c] (mL/min)	Q_{safe} [d] (mL/min)
MEK	3.8[e]	9.2[e]	0.41[e]	71[e]	28[e]
BENZ (µPCF)	2.7	7.4	0.36	90	36
BENZ (cPCF)	3.0	6.9	0.43	100	40
TOL	1.0	2.3	0.43	290	120
HEP	1.1	2.6	0.42	260	100

[a] intercept of plots in Figure 2-4; [b] value corresponding to 60% bed efficiency; [c] bed volume/τ_c ; [d] 0.4(Q_c); [e]Avg. of cPCF and µPCF values, relative standard deviations of τ_c and Q_c are are 2.5% and 18%, respectively.

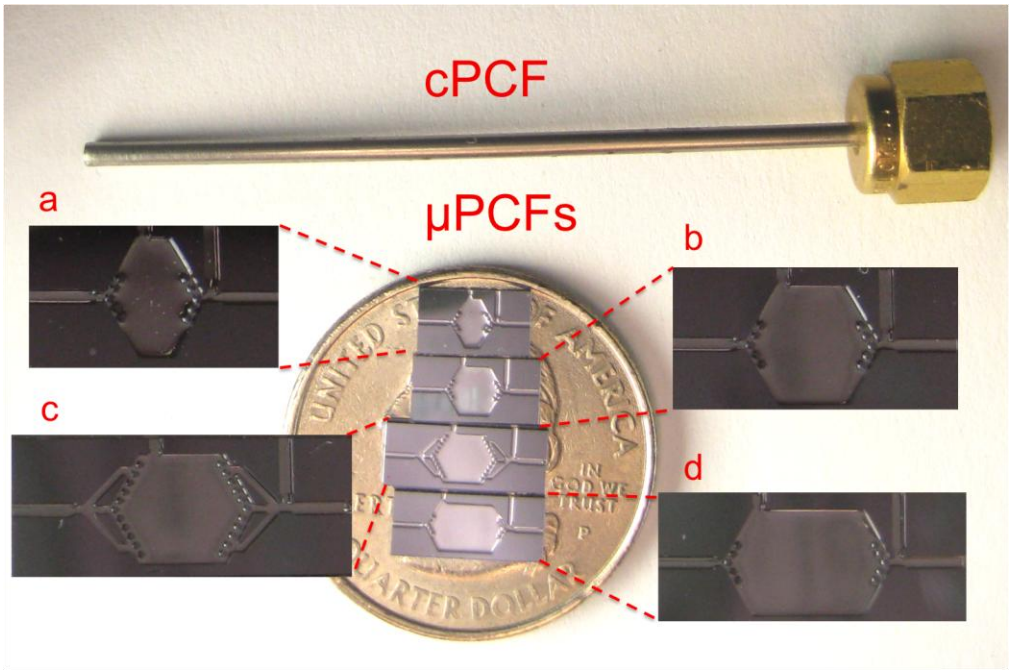

Figure 2-1. Photographs of the cPCF and the Type A, B, C, and D μPCFs on a U.S. quarter. Enlargements reveal the adsorbent-retention pillars within the cavities and inlet/outlet channels on the μPCF chips.

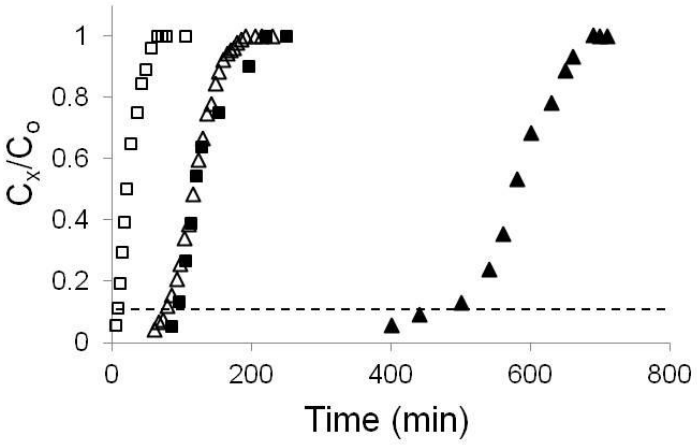

Figure 2-2. Representative breakthrough curves for toluene (triangles) and benzene (rectangles) with cPCF at 20 mL/min (filled symbols) and Type-D μPCF at 50 mL/min (open symbols). The dashed line at $C_x/C_o = 0.1$ corresponds to $t_{b\text{-}10}$.

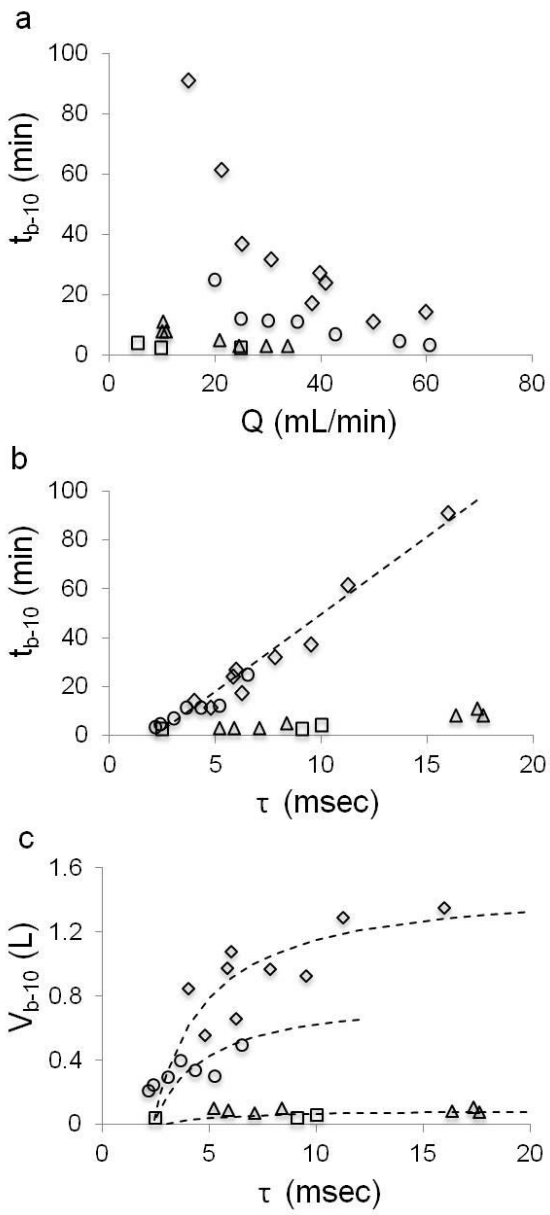

Figure 2-3. Dynamic retention capacity of benzene as a function of Q and □ for Type A (rectangles), Type B (circles), Type C (triangles), and Type D (diamonds) μPCF devices: a) t_{b-10} as a function of Q; b) t_{b-10} as a function of τ (best-fit regression line for Type B and D devices is shown); and c) V_{b-10} as a function of τ (best-fit regression curves for all devices are shown).

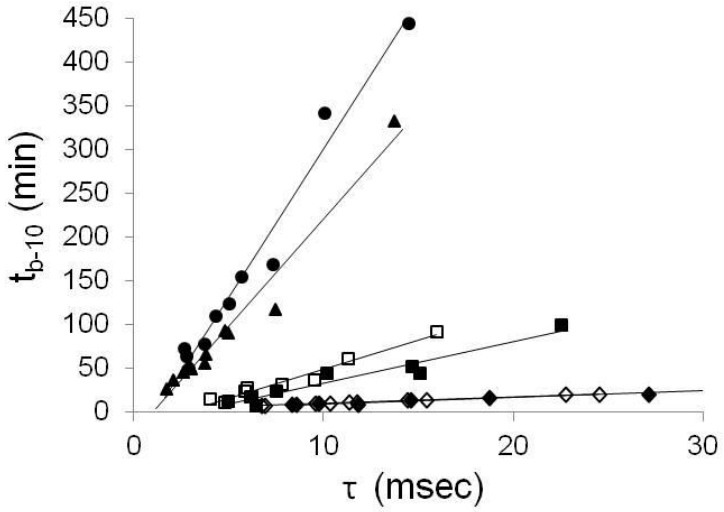

Figure 2-4. Plots of t_{b-10} as a function of τ for MEK (diamonds), BEN (rectangles), TOL (triangles) and HEP (circles); filled symbols are for cPCF and open symbols are for µPCF (MEK and BEN only). Best-fit regression lines are shown (r^2 range: 0.93-0.99).

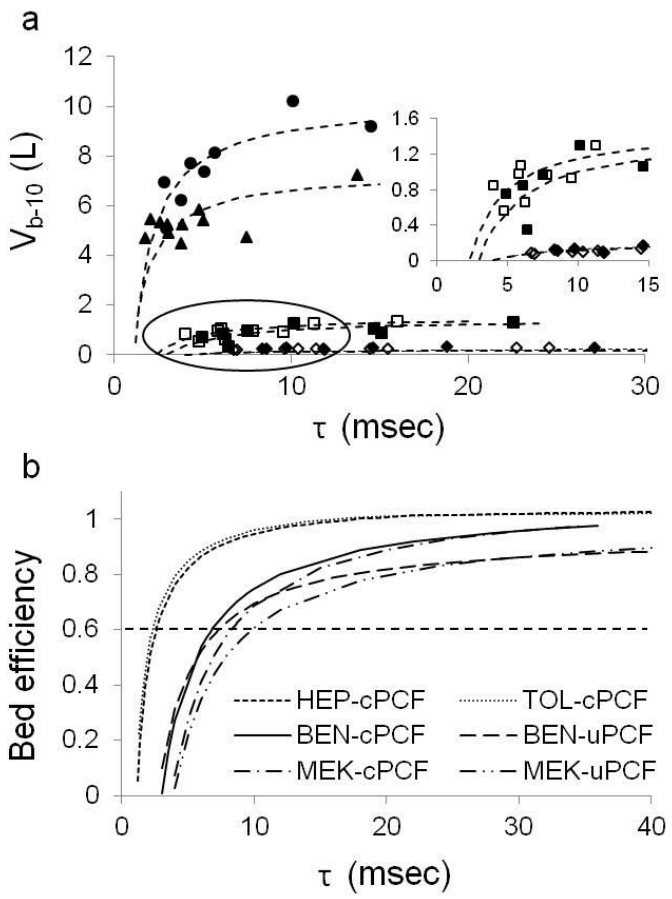

Figure 2-5. a) Plots of V_{b-10} as a function of τ for MEK (diamonds), BEN (rectangles), TOL (triangles) and HEP (circle); filled symbols are for cPCF and open symbols are for µPCF (MEK and BEN only). Best-fit regression curves are shown and the inset shows an expanded view of the circled region for MEK and BEN. b) Plots of bed efficiency (V_{b-10}/V_{e-k}) as a function of τ; the dashed horizontal line shows the value of bed efficiency (0.6) used to determine Q_{safe} (Table 2).

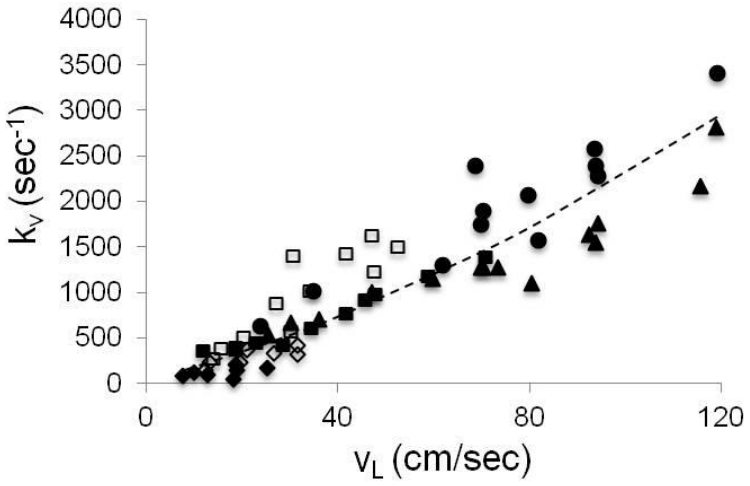

Figure 2-6. Plot of experimentally derived values of k_v vs. linear velocity for MEK (diamonds), BEN (rectangles), TOL (triangles) and HEP (circles); filled symbols are for cPCF and open symbols are for µPCF (MEK and BEN only); best-fit regression curve is shown assuming a power-law model ($r^2 = 0.86$; see text).

References

1. J. Namieśnik, T. Górecki, B. Kozdroń-Zabiega, and J. Łukasiak, *Build. Environ*., 1992, 27, 339.
2. C.-Y Peng and S. Batterman, *J. Environ. Monit.*, 2000, 2, 313.
3. M.E. O'Hara, T.H. Clutton-Brock, S. Green, S. O'Hehir, and C. A. Mayhew, *Int. J. Mass Spectrom.*, 2009, 281, 92.
4. M. Joshi, K. Rigsby, and J.R. Almirall, *Forensic Sci. Int*., 2011, 208, 29.
5. C. J. Lu, W. H. Steinecker, W. C. Tian, M.C. Oborny, J. M. Nichols, M. Agah, J. A. Potkay, H. K. L. Chan, J. Driscoll, R. D. Sacks, S. W. Pang, K. D. Wise, and E. T. Zellers, *Lab Chip*, 2005, *5*, 1123.
6. P.R. Lewis, P. Manginell, D.R. Adkins, R.J. Kottenstette, D.R. Wheeler, S.S. Sokolowski, D.E. Trudell, J.E. Byrnes, M. Okandan, and J.M. Bauer, *IEEE Sens. J*., 2006, *6*, 784.
7. S. Zampolli, I. Elmi, F. Mancarella, P. Betti, E. Dalcanale, G.C. Cardinali, and M. Severi, *Sens. Actuators, B.*, 2009, 141, 322.
8. S. K. Kim, H. Chang, and E. T. Zellers, *Anal. Chem.*, 2011, 83, 7198.
9. S. K. Kim, D. R. Burris, H. Chang, J. Bryant-Genevier, and E. T. Zellers, *Environ. Sci. Technol.*, 2012, 46, 6065.
10. S. K. Kim, D. R. Burris, J. Bryant-Genevier, K. A. Gorder, E. M. Dettenmaier, and E. T. Zellers, *Environ. Sci. Technol*., 2012, 46, 6073.
11. J. Namiesnik, *Talanta*., 1988, *35*, 567.
12. US EPA, *TO-17, Compendium of Methods for the Determination of Toxic Organic Compounds in Ambient Air*, Report No. EPA/625/R-96/010b, US EPA, Washington DC, 2nd edn., 1999.
13. J. J. Whiting and R.D. Sacks, *J. Sep. Sci*., 2006, 29, 218.
14. C. J. Lu and E. T. Zellers, *Anal. Chem*., 2001, 73, 3449.
15. C. J. Lu and E. T. Zellers, *Analyst*, 2002, 127, 1061.
16. W.-C. Tian, S.W. Pang, C.J. Lu, and E.T. Zellers, *J. Microelectromech. Syst*., 2003, 12, 264.
17. W.-C. Tian, H. K. L. Chan, C. J. Lu, S.W. Pang, and E.T. Zellers, *J. Microelectromech. Syst*., 2005, 14, 498.
18. W.-C. Tian, T.H. Wu, C. J. Lu, W. R. Chen, and H. J. Sheen, *J. Micromech. Microeng*., 2012, 22, 065014.
19. M. Kim and S. Mitra, *J. Chromatogr. A*., 2003, 996, 1.
20. M. D. Martin, T. J. Roussel, S. Cambron, J. Aebersold, D. Walsh, J. Lin, M. G. O'Toole, and R. Keynton, *Int. J. Ion Mobil. Spec*., 2010, 13, 109.
21. R. P. Manginell, D. R. Adkins, M. W. Moorman, R. Hadizadeh, D. Copic, D. A. Porter, J. M. Anderson, V. M. Hietala, J. R. Bryan, D. R. Wheeler, K. B. Pfeifer, and A. Rumpf, *J. Microelectromech. Syst*., 2008, 17, 1396.
22. C. E. Davis, C. K. Ho, R. C. Hughes, and M. L. Thomas, *Sens. Actuators, B.*, 2005, 104, 207.
23. I. Voiculescu, R. A. McGill, M. E. Zaghloul, D. Mott, J. Stepnowski, S. Stepnowski, H. Summers, V. Nguyen, S. Ross, K. Walsh, and M. Martin, *IEEE Sens. J*., 2006, 6, 1094.
24. B. Alfeeli, D. Cho, M. Ashraf-Khorassani, L.T. Taylor, and M. Agah, *Sens. Actuators, B.*, 2008, 133, 24.
25. M.-Y. Wong, W.-R. Cheng, M.-H. Liu, W.-C. Tian, and C.J. Lu, *Talanta*, 2012, 101, 307.

26. M. Urbanowicz, B. Zabiegata, and J. Namiesnik, *Anal. Bioanal. Chem*., 2011, 399, 277.
27. C. Duan, Z. Shen, D. Wu, and Y. Guan, *TrAC, Trends Anal. Chem*., 2011, 30, 1568.
28. H. P. Tuan, H. G. Janssen, and C. A. Cramers, *J. Chromatogr. A*., 1997, 791, 177.
29. J. Pawliszyn, *J. Chromat. Sci*., 2000, 38, 270.
30. B. McDuffie, Trace and residue analysis, in Kirk-Othmer Encyclopedia of Chemical Technology, 3rd Ed., Vol. 23, Wiley, NY, 1983, p. 322.
31. H. K. L. Chan, S. W. Pang, R. A. Veeneman, and E. T. Zellers, M. Takei, Microfabricated preconcentrator for quantitative analysis of low concentration volatile organic compounds. Technical Digest, Solid-State Sensor and Actuator Conf., Transducers '05, Seoul, Korea, 2005, pp. 2091-2094.
32. A. B. A. Dow and W. Lang, *IEEE Sens. J*., 2012, 12, 2528.
33. A.M. Ruiz, I. Gràcia, N. Sabaté, P. Ivanov, A. Sánchez, M. Duch, M. Gerbolés, A. Moreno, and C. Cané, *Sens. Actuator, A*, 2007, 135, 192.
34. I. Gràcia, P. Ivanov, F. Blanco, N. Sabaté, X. Vilanova, X. Correig, L. Fonseca, E. Figueras, J. Santander, and C. Cané, *Sens. Actuators B*., 2008, 132, 149.
35. E. H. M. Camara, P. Breuil, D. Briand, L. Guillot, C. Pijolat, and N.F. de Rooij, *Sens. Actuators B*, 2012, 148, 610.
36. A. Rydosz, W. Maziarz, T. Pisarkiewicz, K. Domański, and P. Grabiec, *Microelectron. Reliab.*, 2012, 52, 2640.
37. P. Lodewyckx, G.O. Wood, and S. Ryu, *Carbon*., 2004, 42, 1351.
38. G.O. Wood and E.S. Moyer, *Am. Ind. Hyg. Assoc. J*., 1989, 50, 400.
39. G.O. Wood and E.S. Moyer, *Am. Ind. Hyg. Assoc. J*., 1991, 52, 235.
40. M.W. Ackley, *Am. Ind. Hyg. Assoc. J.*, 1985, 46, 679.
41. G.O. Wood and P. Lodewyckyx, *Am. Ind. Hyg. Assoc. J*., 2003, 64, 646.
42. J. Brown and B. Shirey, A tool for selecting an adsorbents for thermal desorption applications, available at http://www.sigmaaldrich.com/analytical-chromatography/air-monitoring/learning-center/td-tube-selector.html, accessed December, 2012.
43. L.A. Jonas and W. Svirbely, *J. Catal.*, 1972, 24, 446.
44. F. Rouquerol, J. Rouquerol, and K. Sing, Adsorption by powders and porous solids. London: Academic Press, 1999.
45. T. Sukaew, H. Chang, G. Serrano, and E.T. Zellers, *Analyst*., 2011, 136, 1664.
46. G. Serrano, T. Sukaew, and E. T. Zellers, *J. Chromatogr. A*. accepted for publication, 2012.
47. P. Lodewyckx and E.F. Vansant, *Am. Ind. Hyg. Assoc. J*., 2000, 61, 501.

Chapter 3

Approaches to Modeling Breakthrough Times of Binary Vapor Mixture Components for a Miniature Preconcentrator Packed Carbopack X

3.1 Introduction

Significant advances have been made over the past decade in the development of field-portable instrumentation capable of monitoring multiple volatile organic compounds (VOCs). Prominent among these are Fourier-transform infrared spectrophotometers [1] and gas chromatographs (GC) with spectrometric detectors [2-5]. Also intriguing are the advances made recently in GC microsystems (μGC) the core components of which are microfabricated from Si and typically comprise a micropreconcentrator/focuser (μPCF), one or more separation microcolumns, and a microsensor or microsensor array [6-12]. Since many applications require the determination of compounds at concentrations in the low or sub-parts-per-billion (ppb) concentration range [13-15], which are below the limits of detection (LOD) of most portable or μGC detectors, the preconcentrator is of critical importance.

Preconcentrators can be single- or multi-stage, depending on the required speed of analysis, the volatility range of the (target) analytes, and the sample volume required to achieve

the desired LODs. Recent reports have appeared on hybrid PCF modules that use a high-volume preconcentrator containing tens-of-milligrams of adsorbent to rapidly capture VOCs from a large sample and then transfer all or part of VOCs to a smaller, possibly microfabricated, focuser containing just a few mg of adsorbent [16,17]. These studies serve to illustrate that small PCFs often lack the capacity or cannot be operated at high enough flow rates to be useful in stand-alone configurations for high-speed, trace-level VOC analyses. This point was also highlighted by the work in Chapter 2. Regardless of whether they are used alone or as focusers downstream from high-volume preconcentrators, such devices must serve two functions: as VOC traps and as (typically thermal) injectors. For the former function, quantitative capture is the most important performance criterion, while for the latter function, narrow-band injection is most important since it determines the preconcentration factor and can also have great impact on the chromatographic resolution of the VOC mixture components achievable with the downstream column. The term 'preconcentrator/focuser' was coined [18] to highlight the dual function of such devices [18].

The miniature and microfabricated PCFs reported by Zellers et al. exemplify devices designed and operated to provide quantitative (i.e., exhaustive) capture and efficient thermal desorption of multi-VOC mixtures; suitable for integration into portable GC or μGC systems for environmental monitoring [18-22]. Other groups has also reported on PCF devices designed for quantitative VOC analysis [23-27]; however, many of these studies fail to rationalize their design features or operating conditions, document the efficiency of trapping or desorption, report preconcentration factors, or examine the effects of interferences (i.e., co-vapors).

Those studies that have examined interferences [8,18,19,16,17] have been empirical, accounting for the competition for adsorption sites on the PCF adsorbent by merely including sufficient adsorbent to insure sufficient capacity for the targeted VOCs under the conditions anticipated in whatever application is being explored. Although modeling studies have been reported [28-30], none has systematically explored the influence of co-vapors on the dynamic retention capacity of the PCF for VOCs.

In Chapter 2, we explored the performance of small capillary PCFs (cPCFs) and μPCFs packed with the graphtized carbon, Carbopack X (C-X), challenged with individual VOCs and showed that there is a limit to the flow rate that can be employed beyond which immediate breakthrough would be observed. The goal of this study is to extend the results obtained in Chapter 2 to investigate the effect of sampling flow rate on dynamic adsorption capacity of VOCs in binary mixtures. Toward that end, breakthrough data were collected with three pairs of VOCs for a miniature capillary PCF (cPCF) at each of several flow rates. Experimental values of the kinetic adsorption capacity, $W_{e\text{-}k}$, and the kinetic rate coefficient, k_v, were derived using the modified Wheeler Model. These were compared to modeled values of $W_{e\text{-}k}$ and k_v and the accuracy with which binary VOC mixture breakthrough times could be determined was assessed.

3.2 Modeling Approach

The modified Wheeler equation relates several design and operating parameters to the dynamic retention capacity of an adsorbent bed. It has been used as a guide for miniature preconcentrator design and operation [18,31]. In the modified Wheeler Model, the dynamic retention capacity can be expressed in terms of the breakthrough volume or the breakthrough

time, $t_{b\text{-}x}$, at some specified fractional breakthrough, x,. Eq. (3.1) shows the model in terms of the latter.

$$t_{b-x} = \frac{\rho W_e}{C_o}\left[\tau - \frac{1}{k_v}1\left(\frac{C_o}{C_x}\right)\right] = \frac{W_e W_b}{C_o Q} - \frac{\rho W_e}{C_o k_v}1\left(\frac{C}{C}\right. \qquad (3.1)$$

where $t_{b\text{-}x}$ is in minutes, W_e is the adsorption capacity (adsorbate mass/adsorbent mass), W_b is the packed-bed mass (g), $\tau = W_b/(\rho Q)$ is the bed residence time (min), ρ is the adsorbent bed density, Q is the volumetric flow rate (cm^3/min), k_v is the kinetic rate constant (min^{-1}), C_o is the inlet concentration (g/cm^3), and C_x is the outlet concentration (g/cm^3) [18,32].

A plot of the $t_{b\text{-}10}$ and bed residence time (τ) of all vapors yield straight line, the slope of which is used to determine $W_{e\text{-}k}$ and the x-intercept of which represent the critical bed residence time (τ_c) or the limit in sampling flow rate which correspond to the point where immediate breakthrough occur. The τ_c values increase with vapor with higher $W_{e\text{-}k}$, and this reflect the higher tolerance in sampling flow rate of vapor with high affinity to Carbopack X. The main finding from single vapor study is that the W_e parameter is the main parameter that dictates the performance of the microscale preconcentrator.

Common observations for the adsorption of mixtures onto sorbents include the displacement of already adsorbed compounds with co-interferences with stronger affinity to the adsorbent [33,34]. In this case, the more weakly adsorbed vapor of a pair is the one whose ratio of capacity to concentration is the smallest. The weakly adsorbed compound 1 may be replaced by the more strongly adsorbed compound 2, and consequently it travel faster in the adsorption bed, this displacement effect can cause “roll up” in which concentration of vapor 1 downstream of the adsorption wavefront of vapor 2 can exceed the concentration of vapor 1 entering the bed [33].

There have been a few studies in which the effect of a second vapor on the values of t_b,

W_e and k_v of the first vapor has been explored. Most of these studies rely on linear regression with the Wheeler model to determine W_e and k_v for both the single vapor and binary vapor analysis. For binary mixtures, the measured breakthrough time (of the mixture) is plotted against the adsorbent mass to determine W_e and k_v for the mixture from the slope and x-intercept respectively [35,36].

In order to extend the applicability of the modified Wheeler model to binary mixtures, W_e and k_v for each vapor in the mixture must be determined. Various methods have been proposed to determine W_e for the components of mixtures [37]. Among these, the molar proportionality method (MPM) [35-39] is the simplest and most accessible. It assumes that the amounts adsorbed from a vapor mixture are equal to the component vapor-phase mole fractions multiplied by the mass that would have been adsorbed from a pure vapor at the same partial pressure (or concentration). W_e for a vapor in a mixture therefore decrease with decreased mole fraction of the vapor in air. Implicit is the assumption that the different components do not interact except to "deny" adsorption to one another. This assumes a limited number of adsorption sites or surface area can be covered (the Langmuir isotherm assumption). For a binary vapor mixture, the total amount adsorbed by the mixture (g/g), $W_{e(t)}$ can be estimated from the following equation:

$$W_{e(t)} = \chi_1 W_{e(1)} + \chi_2 W_{e(2)} \tag{3.2}$$

where χ_1 and χ_2 are the gas phase mole fractions of component 1 and 2 and $W_{e(1)}$ and $W_{e(2)}$ are the amounts (g/g) adsorbed by single vapor 1 and 2, respectively.

$$\chi_i = \frac{(p / p_{sat})_i}{\sum (p / p_{sat})_i} \tag{3.3}$$

Where p is the partial pressure of the targeted analyte and p_{sat} is the saturation vapor pressure.

There are very few studies concerning the rate of mass transfer of vapor mixture onto adsorbent bed. The investigation of the effect of co-contaminants to the k_v of targeted compounds in this study was established based on the review article by Wood [40]. Wood review the mixture breakthrough data from six different authors and nine different studies, the data were collected mostly on respiratory cartridge, with data from these studies and his independently collected data, he reached the conclusion that the effect of covapor on k_v differs depending on the breakthrough order. Vapor that breakthrough first showed no difference between k_v in mixture and k_v for single vapor. As the rate of adsorption of the first vapor moving through the bed is unaffected by the presence of co-interferences, the ratio of k_v in mixture/k_v single vapor ratios at similar vapor concentrations equal to 1.07 (sd 0.21). Vapors that breakthrough later demonstrated an average 15% decrease in k_v, mixture k_v:single k_v = 0.85 (sd 0.24). However, this observation only applies to the vapors with sufficiently different breakthrough time, in the case of vapors with similar breakthrough time, the 15% decrease is to be applied to both vapors. These correction factors will be apply to the k_v determined from breakthrough curve of single vapor.

The vapor displacement observed in mixture study suggested that there are different adsorption mechanism throughout the adsorbent bed. In some part, there is single-component adsorption, and there is simultaneous adsorption and desorption of different vapors. The study found that the k_v for the more weakly adsorb compound (methylene chloride) was close to those observed for methylene chloride alone, and there was a significantly reduction of k_v of stronger adsorbed compounds (benzene) [35]. Additional study supports the effect of second vapor on the k_v parameter of vapor in the mixture, with the effect on k_v based on the boiling point of second breakthrough vapor [35,38]. The results from some studies found no statistical different between

k_v of vapors in mixture from the one obtain from single vapor, with experimental rate coefficient obtained from 1% breakthrough time vs. bed weight [35,36] or intercept of 1% breakthrough time vs. bed residence time for benzene/toluene mixture [35,39]. In these studies, k_v parameter were extracted from the intercept of linearlized Wheeler equation, in this case the extracted k_v parameter was assumed to be constant over a range of sampling flow rate, which is contrast to the k_v parameter derived from this study.

Vahdat investigated effect of the concentration effect of binary mixture. As the concentration of covapor increases, breakthrough time of the two components in binary mixture decrease. However, at very low concentrations of covapor, the effect of this vapor on the adsorption behavior of the targeted vapor is negligible [33].

Other authors report the underestimation of $t_{b\text{-}10}$ from using MPM model and the Wheeler model when testing the large scale adsorbent bed [35]. An error range was reported by Jonas et al. to be -10 to +20 individual deviations from $W_{e\text{-}k}$ of carbon tetrachloride obtained from slope of plots of 1% breakthrough times vs. carbon bed weights. Robbins and Breysse [38] used the model to predict the $W_{e\text{-}k}$ of p-xylene and pyrrole in the presence of o-dichlorobenzene, p-dichlorobenzene, p-fluorotoluene, and toluene as covapors. Average $W_{e\text{-}k}$ deviations from experimental values ranged from 0 to –35% for p-xylene and from –13 to +32% for pyrrole. Cohen et al. [39] applied MPM to predict their binary mixture data for carbon tetrachloride/n-hexane and carbon tetrachloride/pyridine, the author reports deviations of predicted adsorption capacities from kinetic W_e values obtained from plots of 10% breakthrough times vs. bed residence times were –39% for carbon tetrachloride and +3% for n-hexane in one mixture and –12% for carbon tetrachloride and –39% for pyridine in another [35,39].

Equations describe relationship of k_v vs. v_L for single vapors in Chapter 2 were developed specifically for each vapors tested in Chapter 2. The values of k_v vs. v_L were fit to a power regressionof the form $k_v = m v_L^n$. These equations are listed in Table 3-1 These equation were used along with the correction factors reported by Wood et al. were used to obtain the k_v values of binary mixture at different operational flow rate.

3.3. Single vapor analysis

Breakthrough curves were generated for a series of Q values from ~15-110 mL/min for the cPCF, τ values of ~20–2.7 msec for each of the individual vapors in separate test series. Similar relationships between $t_{b\text{-}10}$ and τ were observed for all four individual. As single vapor we found breakthrough time at constant flow rate for MEK<benzene<toluene< heptane.

The values of k_v for each vapor in binary mixture at specific flow rate was derived from the slopes of plots of $t_{b\text{-}x}$ vs. $ln(C_o/C_x)$, which are predicted by Eq. 1 to be linear over a limited range of fractional breakthrough values (i.e., x < 20%), where the assumption of pseudo first-order rate of adsorption is valid. The results show nonlinear increase in k_v parameters of all vapors with v_L. Experimental k_v values of MEK ranges from ~ 80-200 sec^{-1} over a range of v_L equal to 8-25 cm/sec, k_v values for benzene range from 360-1,400 sec^{-1} at v_L ranges from 12-71 cm/sec, k_v values for toluene ranges from 530-2300 sec^{-1} at v_L ranges from 26-120 cm/sec and k_v values for heptanes ranges from 630-2400 (sec^{-1}) at v_L ranges from 24-130 cm/sec. There was minimal contribution of vapor characteristics to k_v parameters. At constant v_L, k_v values range from MEK<benzene<toluene< heptane, which track an increase in $W_{e\text{-}k}$. This trend agreement with the literature that report the contribution of $W_{e\text{-}k}$ to k_v parameter [41].

3.4 Binary Mixture Components

Vapors of MEK, benzene, toluene and heptanes were tested in various binary combinations. To investigate the effect of covapor on the targeted compounds, four vapors, 2-butanone (MEK, $W_{e\text{-}k\text{-}MEK}$= 25 μg/g), Benzene (BEN, $W_{e\text{-}k\text{-}BEN}$= 190 μg/g), toluene (TOL, $W_{e\text{-}k\text{-}TOL}$= 1200 μg/g) and n-heptane (HEP, $W_{e\text{-}k\text{-}HEP}$= 1800 μg/g) were paired based on its $W_{e\text{-}k}$ at 100 ppb concentration. The $W_{e\text{-}k}$ parameter was used to represent the affinity level of each vapor to Carbopack X [33]. To represent different degree of competition on Carbopack X, the first vapor pair, MEK and benzene as a covapor ($W_{e\text{-}k\text{-}benzene}/W_{e\text{-}k\text{-}MEK}$ = 7.6), represents the condition where the targeted vapor is minimally retained on the Carbopack X. MEK is a polar compound, so its $W_{e\text{-}k}$ is very small compare to benzene which has similar vapor pressure. The mixture of benzene and heptane ($W_{e\text{-}k\text{-}HEP}/W_{e\text{-}k\text{-}BEN}$ = 9.5), represents the condition of a mix between vapor with medium affinity to Carbopack X (benzene) and covapor with high affinity to Carbopack X (heptanes). The last vapor pair, toluene and heptanes ($W_{e\text{-}k\text{-}HEP}/W_{e\text{-}k\text{-}TOL}$ = 1.5), represents the condition where both vapors have high affinity to Carbopack X. For this discussion, the first name in the vapor pair refers to the targeted vapor for the discussion in the mixture, for example MEK/BEN means MEK with benzene as the covapor.

3.5 Experimental

3.5.1 Devices and Materials

Chemicals were purchased from Sigma-Aldrich/Fluka (Milwaulkee, WI) or Acros/Fisher (Pittsburgh, PA) in >99% purity and were used as received. The cPCF was constructed by packing a 5-cm-long section of thin-walled Inconel tubing (1.59-mm o.d., 1.35-mm i.d., cross sectional area = 0.0143 cm^2) with 2.2 mg of C-X that had been passed through sieves to isolate

the fraction with nominal diameters in the range of 212-250 mm (surface area= 240 m^2/g, Supelco, Bellefonte, PA). The adsorbent was drawn into the tubing under vacuum and was retained in place by small pieces of stainless steel mesh and silanized glass wool. The bed occupied a length of ~4 mm and was located within 1-cm of the distal end of the tubing to minimize the downstream dead volume. A thin sleeve of polyimide (Microlumen, Tampa, FL) was placed around the packed section of the tube and a fine-wire type-K thermocouple was held snugly against the tube with another thin polyimide sleeve. A section of varnished Cu wire, used to resistively heat the adsorbent bed following each test, was then coiled tightly around this assembly to create a heated length that extended beyond that of the adsorbent bed.

3.5.2 Breakthrough Testing

Test atmospheres containing ~ 100 ppb of MEK, benzene, toluene and heptanes in binary mixture of MEK/BEN, BEN/HEP and HEP/TOL in extra dry nitrogen were created in 10-L or 40-L Tedlar bags by serial dilution. This corresponds to absolute concentrations of 0.32, 0.29, 0.38, and 0.41 mg/m^3 for MEK, benzene, toluene and heptanes, respectively. Values of $t_{b\text{-}10}$ were determined by drawing the atmosphere through the PCF using a vacuum pump (UN86KTDC, KNF Neuberger, Trenton, NJ). At 1-min intervals an aliquot of the outlet stream was directed into a GC with flame-ionization detector (GC-FID, Model 6890, Agilent Technologies, Palo Alto, CA) via a six-port valve equipped with a 250-mL gas sampling loop. The separation was performed with 15 m long, 320 μm i.d. capillary column with a 0.25 μm thick HP-1 stationary phase (19091Z-411, Agilent Technologies). The flow rate through the test devices was measured at the outlet, using a primary flow standard, and a needle valve placed upstream from the pump was adjusted to achieve the desired flow rate. The column oven temperature was adjusted to give

a retention time of less than one minute for all tested compounds. Peak integration was performed at the conclusion of each experiment using GRAMS32 (Version 6.0. Thermo-Scientific, Pittsburg, PA).

Duplicate breakthrough curves (C_x/C_o vs. time) were generated for a series of Q and ranging from 10-140 mL/min. Values of $t_{b\text{-}10}$ were determined at C_x/C_o = 0.1 directly or by (linear) interpolation between the two nearest data points. The flow rate was measured at the end of every breakthrough experiment with Dry-Cal and the challenge concentration was measured prior to and at the end of every breakthrough determination. To confirm the concentration of tested compounds, the FID was calibrated by analyzing separate serially-diluted test atmospheres prepared in Tedlar bags that spanned the required range of injected mass. The packed cPCF devices were preconditioned by heating under N_2 for four hours at 300°C. Subsequently, after each experiment the adsorbent was regenerated under a flow of N_2 of ~ 40-60 mL/min by heating the device under test to 250-300 ºC for 20- min to desorb the vapor.

3.6 Results and Discussions

3.6.1 Breakthrough Curve Characteristics of Vapors in Binary Mixture

Examples of breakthrough curves for components of binary mixtures are shown in Figure 3-1. The breakthrough curve is a reflection of the corresponding vapor front profile moving through the bed [32]. When examining the shapes of the breakthrough curves, breakthrough of vapor in binary mixtures are similar to what observed from large scale adsorbent bed [33-35]. In theory, the more weakly adsorbed vapor would move through the adsorbent bed more rapidly than the stronger adsorb vapor in the vapor pair. The breakthrough curves of individual component in the binary mixture have S-shapes similar to those observed for single vapors. In

addition, there would be some displacement of weaker adsorb vapor in some extent which can cause the roll up effect.

For MEK/BEN, we observed rapid breakthrough for MEK, which exceeds 100% just as benzene begins to breakthrough. This phenomenon is known as roll-up where the later adsorbing vapor displaces the first vapor, causing a temporary increase in the outlet concentration [33]. When benzene was started to breakthrough, the concentration of MEK is actually higher than the initial test concentration by ~15% since it is being displaced by benzene. The same phenomenon was seen with BEN/HEP and TOL/HEP vapor pairs. BEN/HEP and TOL/HEP exceeds the initial challenge concentration by ~20% and ~30% respectively when heptane started to breakthrough at 60 ml/min sampling flow rate. Toluene exhibits a higher roll-up with heptane than benzene with heptane. This is due to the lower W_e for benzene. Benzene has a W_e value ~six times lower than toluene, so that benzene has occupied fewer sites initially, due to its lower W_e value, which leaves less benzene to be displaced by heptane. Heptane and toluene in contrast have closer W_e values and similar breakthrough volumes as single vapors. Therefore, toluene occupies more sites initially, which yields more toluene for heptane to displace, resulting in a larger roll-up. Comparing to the breakthrough curve of single vapor, we found the decrease in $t_{b\text{-}10}$ in almost every case (the breakthrough curves shift to the left). The $t_{b\text{-}10}$ plot extract from breakthrough curves generated at different flow rate were used to extract $W_{e\text{-}k}$ parameters of binary mixture shown in the following sections.

3.6.2 Effect of Co-vapor on Dynamic Retention Capacity

When further examining the effect of co-vapors on breakthrough, $t_{b\text{-}10}$ was examined as a function of τ, as we did with single vapors. With single vapors, the $t_{b\text{-}10}$ of the vapor is directly

proportional to τ, and the general trend stayed the same between single vapors and binary mixtures. The results in this section were in agreement with the effect of flow rate on the $t_{b\text{-}10}$ reported in the literature [33,35]. Experimental $t_{b\text{-}10}$ values of all vapors in binary mixtures were inversely proportional to Q (R^2= 0.95 -0.98), and the values were consistency lower than their observed values as single vapors at constant τ. Figure 3-2 compares the linear plots of $t_{b\text{-}10}$ and τ for single vapor (filled symbol) and for the targeted compound in the binary mixture (open symbol).

Linear regression analysis of $t_{b\text{-}10}$ vs. τ data for each vapor pair yielded the $W_{e\text{-}k}$ parameter shown in Table 3-2. From Table 3-2, we can see the decrease in $W_{e\text{-}k}$ in binary vapor pair in every case despite the presence of the less strongly adsorbed compounds. The results were in agreement with the literature that reported a decrease in the adsorption capacity of the carbon for each component in the mixtures [33,39]. The magnitude of $W_{e\text{-}k}$ reduction is higher in the vapor with lower $W_{e\text{-}k}$ as a single vapor. The results demonstrated an important of the $W_{e\text{-}k}$ parameter that for binary mixtures, the pure adsorbate with the highest capacity for the same concentration is prefertially adsorbed, hence they are less affected by the covapor [33]. If covapor is more strongly adsorbed, the adsorption capacity targeted vapor will be reduce dramatically with the presence of covapor. In contrast, if the targeted vapor is more strongly adsorbed, adding a covapor would have minimal effect on adsorption capacity of adsorbent to target vapor [33]. The percent decrease in $W_{e\text{-}k}$ compare to the value of single vapor of MEK is higher than benzene, the same results observed for all other vapor pairs. Across the vapor pair, the degree of decreasing in $W_{e\text{-}k}$ value of targeted vapor is higher in the presence of the stronger adsorbed vapor. For example, the $W_{e\text{-}k}$ value of benzene decreases 24 and 28 percent in the presence of MEK and heptane respectively. The $W_{e\text{-}k}$ of heptane decreases 19 and 38 percent in the presence of

benzene and toluene respectively.

3.6.3 The Effect of the Covapor on the Kinetic Rate Coefficient

In this study, we found a reduction in k_v value of vapors in almost all vapors pairs, except for TOL/HEP, for which toluene exhibits similar k_v values as single vapor. Figure 3-3 represents the plot of k_v and v_L of each vapor in binary mixture. The decreasing in k_v could be the results from the $W_{e\text{-}k}$ reduction of all vapors in the binary mixtures, see Table 2-2. An in discrepancy between single and binary vapor data is increasing at higher v_L.

There were mix conclusions regarding the k_v parameter in binary mixture. Carbopack X is mesoporous material and external mass transfer governs the rate of mass transfer of vapor onto the adsorbent bed. In this case, there may not be an effect of the displacement and desorption of the covapor, especially at low concentration. Only the in the case that adsorption rate is surface adsorption or pore diffusion limited that the presence of already adsorbed vapor would retard the adsorption of the second vapor which results in a decreasing k_v [37,40].

3.6.4 Modeling Dynamic Retention Capacity of Binary Mixtures

MPM-modeled values of $W_{e\text{-}k2}$ (i.e., $W_{e\text{-}k2m}$) for the vapors in the binary mixtures determined via Eqs. 3.2 and 3.3 are listed in Table 3-2, and the differences between modeled and experimental values are listed in Table 3-3 As shown, the $W_{e\text{-}k2m}$ values are consistently lower than the experimental values underestimates the $W_{e\text{-}k}$ in most vapor pairs. An underestimation of $W_{e\text{-}k}$ could result from a low concentration use in this experiment [39]. At lower challenge concentration, vapor does not completely filled the available sites at this low challenge concentration, therefore there are excess available sites for all vapors in the binary mixture. The

lack of competition for available adsorption sites led to only slightly decrease in $W_{e\text{-}k}$ in the presence of binary mixture.

The deviation of these experimentally determined k_v from the calculated values was high. The data does not follow the observation provided by Wood, since the reduction of k_v values of compounds that breakthrough second or vapors in the pairs that have similar breakthrough time exhibits greater decline than 15%, especially at higher linear velocity. The average absolute error values for each vapor were listed in Table 3-3. An integration of correction factor create more error with the lower k_v values resulted from the correction factor.

$W_{e\text{-}k}$ generated from MPM and calculated k_v values obtained from vapor specific k_v parameters were integrated in the modified Wheeler equation to calculate $t_{b\text{-}10}$ at a range of τ. The performance of the modified Wheeler equation in $t_{b\text{-}10}$ prediction is presented in Table 3-3 along with the error in the $W_{e\text{-}k}$ and k_v estimate as described previously. The results show an underestimation of the model in general, with the magnitude of the error increase at longer bed residence time. Since $W_{e\text{-}k}$ is the main parameter that dictate the modified Wheeler model performance, an underestimation of this parameter leads to an underestimation in $t_{b\text{-}10}$ prediction. Figure 3-2 show experimentally determined $t_{b\text{-}10}$ and its corresponding predicted $t_{b\text{-}10}$ value using the modified Wheeler equation. The underestimation in $t_{b\text{-}10}$ is in agreement with the literature [35]. According to Eq. (3.1), $W_{e\text{-}k}$ should be the main parameter that contributes to the $t_{b\text{-}10}$ error, especially in the case of high k_v parameter value. However, in the binary mixture where the effective $W_{e\text{-}k}$ is reduced for each vapor, the error in k_v prediction would contribute to the $t_{b\text{-}10}$ error more. As shown in Table 3-3, the error in $t_{b\text{-}10}$ prediction is high for vapor with low $W_{e\text{-}k}$, such as MEK in this case. The error in $t_{b\text{-}10}$ prediction for MEK in MEK/BEN vapor pair was as high as 77 percent, despite only 31 percent error in $W_{e\text{-}k2m}$. This could be the results from the

contribution of more than 200% error in k_v estimation. The same explanation would apply to the BEN/MEK data. In other cases, the error in $t_{b\text{-}10}$ prediction of the data is in the same magnitude or lowers than the $W_{e\text{-}k2m}$ prediction error from MPM.

3.7 Conclusions

The study presented a series of data investigated the effect of covapor on the $t_{b\text{-}10}$ of different vapor on Carbopack X. The model that previously published for estimating $W_{e\text{-}k}$ in binary mixture in large scale adsorbent beds was applied to the $W_{e\text{-}k}$ results obtained from single vapor study. The trend observed for single vapor with regards to relationship between $t_{b\text{-}10}$ and τ was maintained for binary mixture. The results confirm an important of $W_{e\text{-}k}$ parameter in $t_{b\text{-}10}$ prediction. Among all vapor pairs tested, an error in $t_{b\text{-}10}$ estimation by the modified Wheeler model track an error in $W_{e\text{-}k}$ values estimation. The better $W_{e\text{-}k}$ estimation led to the better $t_{b\text{-}10}$ prediction performance of the modified Wheeler equation.

The MPM was used to determine $W_{e\text{-}k}$ value for each vapor in the binary mixture, assume the $W_{e\text{-}k}$ of each vapor in the binary mixture is proportional to its mole fraction in the binary mixture. The MPM underestimates the $W_{e\text{-}k}$ values of all vapors in binary mixture. The underestimation of the model come from the fact that the challenge concentration used in this study is in the linear part of the adsorption isotherm, and since the proportionalities theories assume a limited number of moles (adsorption sites or surface area) can be covered (the Langmuir isotherm assumption), the error of the model performance was affected by an excess number of unfilled active sited for binary mixture concentration used in this study. This underestimate $W_{e\text{-}k}$ is therefore lead to the underestimation of the modified Wheeler model.

The concentration of the binary mixture examined in this study resulted in the mole

fraction of ~ 50%, in the more complex mixture, we would expect to see the more dramatic decrease in $W_{e\text{-}k}$. Also in this study we found the more contribution of k_v parameter to the $t_{b\text{-}10}$ prediction, especially with the low $W_{e\text{-}k}$ vapor such as MEK and benzene.

The rate of mass transfer of the vapor in the binary mixture increases with v_L similar to the trend observed in single vapors, however the trend of k_v parameter does not follows the observation reported by Wood et al. Since we observed more than 15% the reduction in k_v parameter of low $W_{e\text{-}k}$ vapors such as MEK/BEN, BEN/MEK and BEN/MEK. The presence of covapor does not affect the rate of mass transfer of high $W_{e\text{-}k}$ vapor such as toluene and heptane that much, as we observed only slight reduction in k_v paramter in these vapor pairs. This suggested that the presence of covapor affects the rate of mass transfer onto mesoporous adsorbent material in some extent, especially with vapor with lower affinity to Carbopack X. The reduction in the rate of mass transfer in the presence of binary mixture combined with the reduction in $W_{e\text{-}k}$ contributes to the reduction in the dynamic adsorption capacity of the miniature preconcentrator. As described by Eq. (3.1).

Using the MPM to correct for $W_{e\text{-}k}$ in mixtures in combination with the correction factors proposed by Wood for respiratory cartridge is a poor combination for modeling. While the model follow general trend of the data, the deviations observed between experimental and model were large and demonstrated poor agreement between data and experiments. For this reasons, this method is not recommended for predicting the dynamic adsorption capacity of binary mixtures. Using single vapor breakthrough analysis to determine mixture breakthrough is not recommended. Since the simple treatment of mixtures based on data from single component testing may predict incorrect breakthrough times and support the need for laboratory

breakthrough testing to determine dynamic adsorption capacity of the miniature preconcentrator for targeted vapors and the potential interferences found in the field.

Table 3-1. Fitting parameter (m), exponent for linear velocity (n) and coefficient of determination (r^2) of power regression used to estimate k_v parameter

Vapor	m	n	r^2
MEK	25	0.62	0.79
BEN	32	0.86	0.91
TOL	27	0.92	0.93
HEP	33	0.94	0.90

Table 3-2. Experimentally determined and modeled equilibrium adsorption capacities of vapor as single and binary mixture.

Vapor	$W_{e\text{-}k1}$ [a] (µg/g)	$W_{e\text{-}k2}$ [b] (µg/g)	$W_{e\text{-}k1}/W_{e\text{-}k2}$	χ_i [c]	$W_{e\text{-}k2m}$ [d] (µg/g)
MEK/BEN	25	18	1.4	0.5	12
BEN/MEK	190	150	1.3	0.5	97
BEN/HEP	190	140	1.4	0.3	58
HEP/BEN	1800	1500	1.2	0.7	1200
HEP/TOL	1800	1100	1.6	0.4	710
TOL/HEP	1200	720	1.7	0.6	720

[a] from Eq. 1 for single vapor; [b] from Eq. 1 for binary mixture; [c] gas phase mole fraction, [d]MPM predicted $W_{e\text{-}k}$.

Table 3-3. Percent Error in $W_{e\text{-}k2m}$, k_v and $t_{b\text{-}10}$ estimation

Vapor	Error of $W_{e\text{-}k2m}$ [a] (%)	Error of Absolute k_v [b] (%)	Average error of $t_{b\text{-}10}$ [c] (%)	Error of $t_{b\text{-}10}$ [d]	
				Min(%)	Max(%)
MEK/BEN	-31	250	77	64	98
BEN/MEK	-34	113	42	26	54
BEN/HEP	-59	122	61	45	69
HEP/BEN	-17	44	16	-40	26
HEP/TOL	-36	53	27	11	43
TOL/HEP	-0.13	10	0.32	-9	21

[a] MPM prediction error ; [b] absolute error from Equations listed in Table 3-1 ; [c] the modified Wheeler model error, [d]range of $t_{b\text{-}10}$ error from the modified Wheeler model.

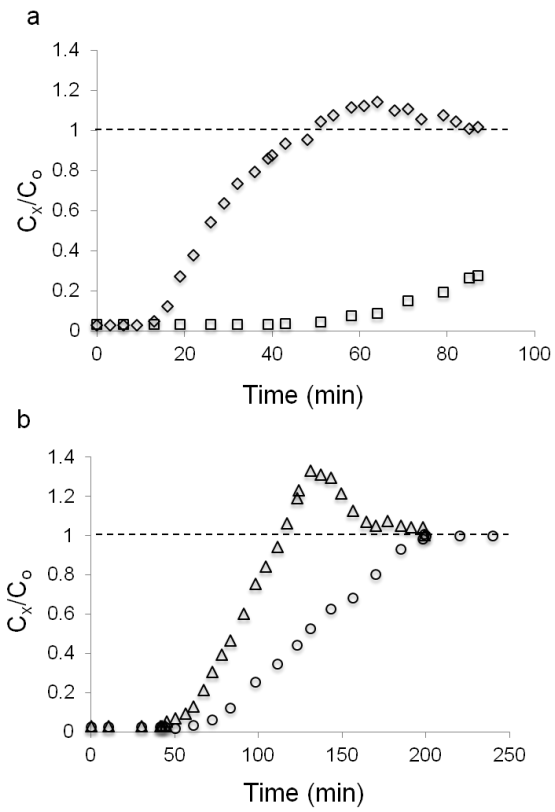

Figure 3-1. Example breakthrough curve of a) MEK and benzene at 10 ml/min sampling flow rate and b)heptane and toluene at 60 ml/min sampling flow rate. Dash line at Cx/Co=1 corresponds to 100 percent breakthrough.

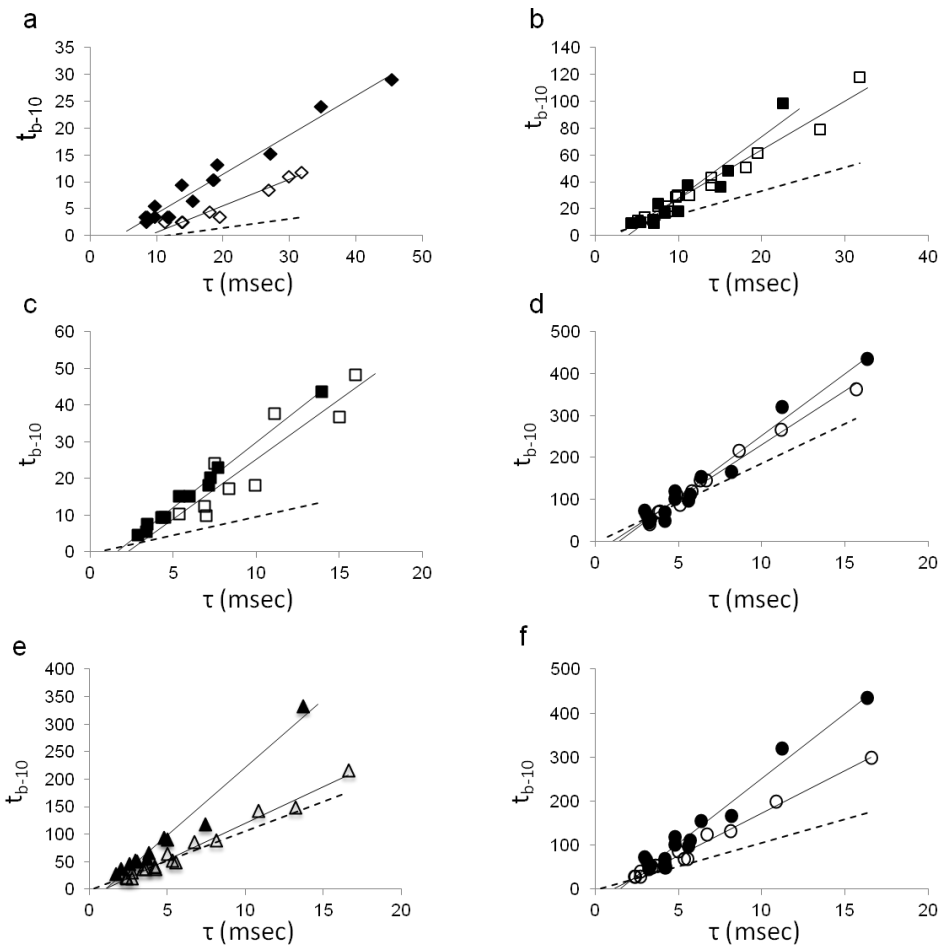

Figure 3-2. Comparison of t_{b-10} as a function of τ between single vapor (filled symbol) and binary mixture (open symbol) of MEK (diamonds), BEN (rectangles), TOL (triangles) and HEP (circles) Dash line represents the calculated t_{b-10} from the modified Wheeler equation; a) MEK/BEN; b) BEN/MEK; c) BEN/HEP; d) HEP/BEN; e) TOL/HEP and f) HEP/TOL (triangle).

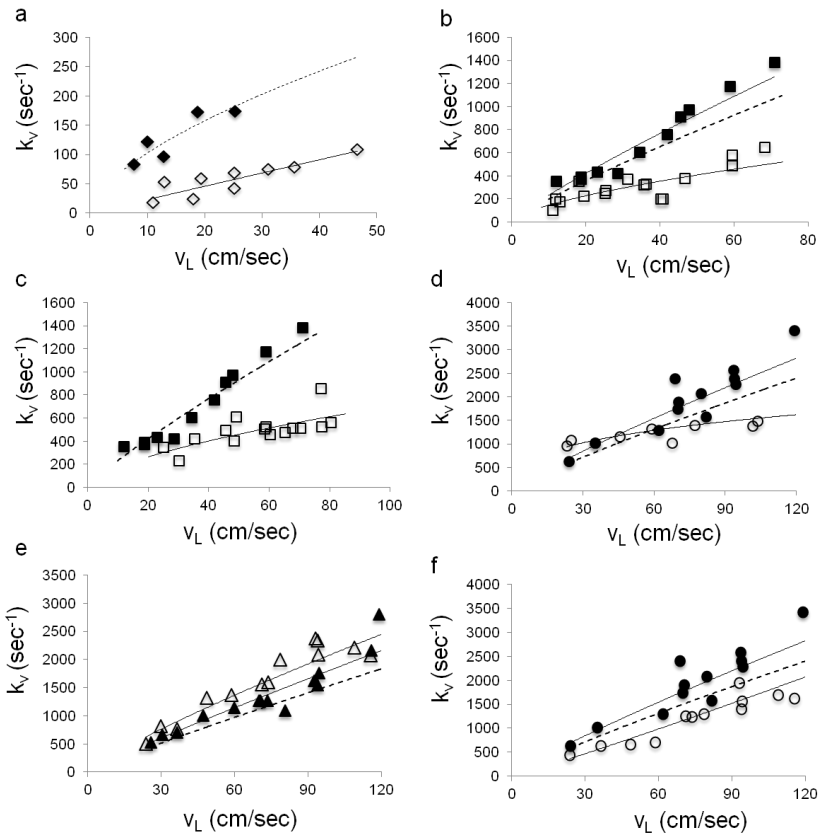

Figure 3-3. Comparison of k_v parameters between single vapor (filled symbol) and binary mixture (open symbol) of MEK (diamonds), BEN (rectangles), TOL (triangles) and HEP (circle). Dash line represents the calculated k_v using equations from Table 3-1 with correction factors ; a) MEK/BEN; b) BEN/MEK; c) BEN/HEP; d) HEP/BEN; e) TOL/HEP and f) HEP/TOL.

Reference

1. GasMet Technologies Inc., www.gasmet.com/na, accessed December 2012
2. Torion technologies Inc.,www.torion.com , accessed December 2012
3. INFICON HAPSITE chemical identification systems, www.inficonemergencyresponse.com/en/index.html, accessed December 2012
4. Defiant, Defiant gas chromatograph, http://www.defiant-tech.com/technology.php, accessed December 2012
5. Smiths Detection, www.smithsdetection.com, accessed December 2012
6. C. J. Lu, W. H. Steinecker, W. C. Tian, M. Agah, J. M. Potkay, M. C. Oborny, J. Nichols, H. Chan, J. Driscoll, R. D. Sacks, S. W. Pang, K. D. Wise, and E. T. Zellers, *Lab Chip*, 2005, 5, 1123.
7. S.K. Kim, H. Chang, and E.T. Zellers, *Anal. Chem*, 2011, 83, 7198.
8. P. R. Lewis, R. P. Manginell, D. R. Adkins, R. J. Kottenstette, D. R. Wheeler, S. S. Sokolowski, D. E. Trudell, J. E. Bymes, M. Okandan, J. M. Bauer, R.G. Manley, and G. C. Frye-Mason, *IEEE Sens. J.*, 2006, 6, 784.
9. S. Zampolli, I. Elmi, F. Mancarella, P. Betti, E. Dalcanale, G. C. Cardinali and M. Severi, *Sens. Actuator, B.*, 2009, 141, 322.
10. S. K. Kim, D. R. Burris, H. Chang, J. Bryant-Genevier, and E. T. Zellers, *Environ Sci Technol*, 2012, 46, 6065.
11. S. K. Kim, D. R. Burris, H. Chang, J. Bryant-Genevier, and E. T. Zellers, *Environ Sci Technol*, 2012, 46, 6073.
12. R. P. Manginell, J. M. Bauer, M. W. Moorman, L. J. Sanchez, J. M. Anderson, J. J. Whiting, D. A. Porter, D.A., D. Copic, and K. E. Achyuthan, *Sensors*, 2011, *11*, 6517.
13. J. Namieśnik, T. Górecki, B. Kozdroń-Zabiega, J. Łukasiak, *Build. Environ., 1992*, 27, 339.
14. M.E. O'Hara, T.H. Clutton-Brock, S. Green, S. O'Hehir, C. A. Mayhew, *Int. J. Mass spectrom.*, 2009, 281, 92.
15. M. Joshi, K. Rigsby, J.R. Almirall, *Forensic Sci. Int*., 2011, 208, 29.
16. T. Sukaew, H. Chang, G. Serrano and E.T. Zellers, *Analyst*, 2011, 136, 1664.
17. G. Serrano, T. Sukaew, E. T. Zellers, *J. Chromatogr. A*. accepted for publication, 2012.
18. C.J. Lu and E.T. Zellers, *Anal.Chem*., 2001, 73, 3449.
19. C.J. Lu and E.T. Zellers, *Analyst*., 2002, 127, 1061.
20. W. C. Tian, H. K. L. Chan, C. J. Lu, S. W. Pang, and E. T. Zellers, *J. Microelectromech. Sys.*, 2005, 14, 498.
21. W. C. Tian, S. W. Pang, C. J. Lu, and E. T. Zellers, *J. Microelectromech. Sys.*, 2003, 12, 264.
22. H.K.L. Chan, S.W. Pang, R.A. Veeneeman, E.T. Zellers, and M. Takei, *Proc. 2005*

Solid-State Sensor and Actuator Conf.-Transducers-05, Seoul, Korea, 2005, pp. 2901-2904.
23. A. B. A. Dow, W. Lang, *IEEE Sens. J.* , 2012, 12, 2528.
24. A.M. Ruiz, I. Gràcia, N. Sabaté, P. Ivanov, A. Sánchez, M. Duch, M. Gerbolés, A. Moreno, C. Cané, *Sens. Actuators, A.*, 2007, 135, 192.
25. I. Gràcia, P. Ivanov, F. Blanco, N. Sabaté, X. Vilanova, X. Correig, L. Fonseca, E. Figueras, J. Santander, C. Cané, *Sens. Actuators, B.*, 2008, 132, 149.
26. E.H.M. Camara, P. Breuil, D. Briand, L. Guillot, C. Pijolat, N.F. de Rooij, *Sens. Actuators, B.,* 2010, 148, 610.
27. A. Rydosz, W. Maziarz, T. Pisarkiewicz, K. Domański, P. Grabiec, *Microelectron. Reliab.*, 2012, 52, 2640.
28. R. P. Manginell, S. Radhakrishnan, M. Shariati, A. L. Robinson, J. A. Ellison, R. J. Simonson, *IEEE Sens. J.*, 2007, 7, 1032.
29. G. Grévillot, S. Marsteau, and C. Vallières, *J. Occup. Environ. Hyg*., 2011, 8, 279.
30. E.H.M. Camara, P. Breuil, C. Pijolat, Proc. Eurosensors XXIII, Lausanne, Switzerland, 2009, pp. 662-665.
31. W. A. Groves, E. T. Zellers, and G. C. Frye, *Analyt. Chim. Acta*, 1998, 371, 131.
32. L.A. Jonas and W.J. Svirbely, *J. Catal*., 1972, 24, 446.
33. N. Vahdat, *Carbon*, 1997, 35, 1545.
34. Y. H. Yoon, J. H. Nelson, J. Lara, C. Kamel and D. Fregeau, *Am. Ind. Hyg.Assoc. J*., 1991, 52, 65.
35. G.O. Wood, Report LA-UR-00-5268. Los Alamos, NM: Loas Alamos National Laboratory
36. L. A. Jonas, E. B. Sansone, and T. S. Farris, *Am. Ind. Hyg. Assoc. J.* , 1983, 44, 716.
37. G.O. Wood, *Carbon*, 2002, 40, 231.
38. C. A. Robbins and P. N. Breysse, *Am. Ind. Hyg. Assoc. J.*, 1996, 57, 717.
39. H. J. Cohen, D. E. Briggs, and R. P. Garrison, *Am. Ind. Hyg. Assoc. J.*, 1991, 52, 34.
40. G.O. Wood, *Carbon*, 2002, 40, 685.
41. G.O. Wood and P. Lodewyckyx, *Am. Ind. Hyg. Assoc. J*., 2003, 64, 646.

Chapter 4
Characterizing Carbon Nanotubes (CNTs) as an Adsorbent Materials for Microfabricated Preconcentrator/Focuser (μPCF)

4.1 Introduction

In order to develop a preconcentrator for use in a μGC, the nature and quantity of the adsorbent material are critical factors because of their influence on both the capacity and desorption efficiency/rate of target analytes. Thermal stability in air and hydrophobicity/hydrophilicity are important properties to consider as well, since sampling in humid air is commonplace. Since they exhibit many properties that are attractive in this context, carbon-based adsorbents are very popular as preconcentrator materials in environmental sampling [1,2].

Adsorbent materials for environmental sampling applications can be classified in three general categories; inorganic materials, carbon based adsorbents and organic polymers. Inorganic materials such as silica gel, zeolites, or alumina are excluded from the choice of materials for μPCF because their hydrophilicity leads to high water retention. Organic polymers generally provide lower adsorption capacity as compared to granular carbon adsorbent, and therefore are not suitable for μPCF that have been designed for exhaustive trapping [2]. Most carbon

adsorbent materials used in μPCF devices are commercially available and are used in conventional air sampling tubes that are thermally desorbed in a specialized desorption unit affixed to the front-end of a laboratory GC analyzer [3-9]. Among these materials, graphitized carbons Carbopack X and Carbopack B have been shown to have several desirable attributes: high capacity for VOCs within specific volatility ranges, efficient thermal desorption, thermal stability in air, commercial availability in a range of particle sizes, and low hydrophilicity [7-9]. Carbon molecular sieves are also common components of standard multi-bed preconcentrators [1-3]. Their high surface area and small pore sizes leads to high capacity for gases and highly volatile organic vapors, but they also have a high affinity for water vapor. Metal-organic frameworks (MOFs) have also been investigated but typically suffer significant degradation in performance in the presence of humidity [10, 11].

For use in a μGC, a balance must be struck between capacity and desorption rate/efficiency – an adsorbent should be used that has sufficient capacity for a given vapor but that also permits efficient thermal desorption upon heating such that the desorption band generated is not broadened significantly by strong vapor-adsorbent interactions that are not easily overcome by increased temperature. Striking that balance is a function of the chemical nature and volatility of the vapor analyte as well as the chemical nature, pore structure, surface area of the adsorbent material. Where mixtures of vapors are involved, it is often difficult to predict behavior, calling for empirical studies, such as those reported by Lu et al [7, 8] and Mitra et al [12, 13].

Carbon nanotubes (CNTs) also have a number of attractive features as μPCF adsorbents: high surface area, high thermal stability, and high thermal conductivity [14-18]. Conceptually, a nanotube is a micrometer-scale graphene sheet rolled into a cylinder of nanoscale diameter and

capped with a spherical fullerene, a cylinder consisting of a single graphene sheet is called a single-wall carbon nanotube (SWCNT), a stack of these sheets can roll up into a concentric cylinder to form a multiple-wall carbon nanotube (MWCNT) [14,16]. CNTs used in this study are made by chemical vapor deposition. In additional they can be grown directly on the substrate of a μPCF device. Some studies report higher adsorption capacity, easier and more efficient regeneration and stability at temperatures up to 600^{o}C with air carrier gas [15-17].

The adsorption properties of CNTs have been studied for removal of organic pollutants from air and water, and metals, fluoride, and radionuclides from water [17-23]. Mitra et al. reported a series of investigations of CNTs both packed in a miniature preconcentrator, as well as grown in a tube [24-28]. They found that the trapping and desorption characteristics of SWCNTs and MWCNTs to be comparable, or superior, to those of Carbopack B (100 m^2/g surface area). These studies are far from comprehensive; no study has yet investigated the effect of sampling flow rate on adsorption capacity of CNTs.

The research presented in this chapter has been done in collaboration with Professor A. John Hart. The primary goal of this project was to investigate the possibility of integration of CNTs in the μPCFs described in Chapter 2. The CNTs received from Prof. Hart's group were characterized by investigation of their dynamic retention capacity in the same manner as the C-X was characterized in Chapter 2.

We started by testing adsorbent material packed in capillary preconcentrator (cPCF), since this method allows retention capacity testing at different adsorbent masses. The knowledge obtained from the cPCF testing could then be used to inform μPCF design and fabrication [7, 8]. With similar mass and density of the material packed in both devices, the performance of two devices is assumed to be similar. The difference in packing density and bed geometry might

contribute to variation of the performance. In this study, there are two types of CNT samples obtained from the Hart group: one grown on a silicon wafer and the other grown inside the μPCF cavity directly. The former sample was packed inside a small diameter cPCF and tested against the cPCF packed with similar mass of Carbopack X; the latter was tested against the Carbopack X packed in similar μPCF size directly.

4.2 Experimental

4.2.1 Devices and Materials

The cPCF was constructed by packing a 5-cm-long section of thin-walled Inconel tubing (1.59-mm o.d., 1.35-mm i.d., cross sectional area = 0.0143 cm^2) with ~ 2 mg of CNTs. The process of cPCF packing is shown in Figure 4-1a and b. 1 mg of CNTs packed in glass tube with comparable diameter to the Inconel tubing is shown in Figure 4-1C in order to visualize the uniform packing of CNTs bed. First, the CNT forest was removed from the silicon wafer with a sharp blade, after which the forest was cut into small pieces and packed into the cPCF. Several attempts were made to pack the material into the tubes uniformly without creating too much pressure drop. Figure 4-2 shows the different packing density of 1 mg of CNTs in glass tube. CNTs can be compressed to different bed length and yielded different bed density. Too high packing density does not allow even a low flow to pass through, and too low packing density resulted in a large void space and non-uniform packing. For 2 mg of CNTs, the length that yielded uniform packing without overly high pressure drop is ~ 2.3 cm (which is equivalent to 0.033 ml bed volume).

A thin sleeve of polyimide (Microlumen, Tampa, FL) was placed around the packed section of the tube and a fine-wire K-type thermocouple was held snugly against the tube with

another thin polyimide sleeve. A section of varnished Cu wire, used to resistively heat the adsorbent bed following each test, was then coiled tightly around this assembly to create a heated length that extended beyond that of the adsorbent bed.

Figure 4-3 shows the CNT forest grown inside the μPCF cavity. Since the mass of CNTs grown in this cavity is not known, a small section of CNTs forest grown on silicon wafer was cut into a small section with surface area equivalent to the one grown inside μPCF chamber. With the assumption that the height of the CNTs forest on the silicon wafer is equivalent to the one grown inside the μPCF cavity. The estimated CNTs mass inside the μPCF cavity is 0.56 mg±0.048 (n=5, RSD= 8.5%).

Breakthrough testing was used to characterize both devices. The details of the method and vapor preparation are described in Chapter 2 and 3. The vapor choices are limited to those tested in Chapter 2; therefore, MEK and benzene were used to test CNTs in the cPCF. MEK and toluene were used to test CNTs in the μPCF.

4.3 Results and discussion

The lower density of the CNTs resulted in the different performance of the adsorbent bed compared to the device packed with Carbopack X. For Carbopack X, 2 mg of 212-250 μm size of this material resulted in ~ 0.005 ml adsorbent volume, while the same mass of CNTs resulted in 0.033 ml. This is almost 7 times higher in chamber volume, which leads to a higher bed residence time at constant flow rate. The same problem occurs with the μPCF device, the estimated mass of the CNTs grown in the μPCF chamber is ~ 4 times less than the similar device packed with Carbopack X, which would be ~ 2.2 mg. The very low mass of CNTs grown inside

the μPCF cavity does not allow the performance comparison between different adsorbent materials in this case.

4.3.1 Performance of the CNTs in cPCF

The comparison of the dynamic adsorption capacity of CNTs to Carbopack X is shown in Figure 4-4. We can see that, at constant sampling flow rate, the performance of MEK and benzene on two materials was comparable over the range of flow rates tested. The same breakthrough data was plotted against bed residence time shown in Figure 4-5, the data can be fitted to the linear form using the modified Wheeler equation. This plot illustrates clearly the difference in packing density of the two devices, by definition of the bed residence time described in Chapter 1. Assuming similar characteristic removal time, the longer bed residence time means increased possibility of vapor to be adsorbed, and this could increase the performance of the device packed with CNTs.

4.3.2 Performance of the CNTs Grown Inside the Cavity

Immediate breakthrough was found for MEK, however vapor adsorption is still occurred, as the ratio of breakthrough vapor to challenge vapor (C_x/C_o) is less than one. An additional test was performed with the higher molecular weight vapor, toluene, and even with a flow rate <10 mL/min immediate breakthrough was also observed. The results suggested channeling of vapor through the device. In this case, it is not possible to fit the data into the Wheeler equation.We still observed that for the vapors with lower vapor pressure, such as toluene as compared to

MEK, will take longer time to reach $C_x/C_o=1$. The adsorption period is longer for toluene compared to MEK.

The difference in bed geometry does not allow the comparison of CNTs to Carbopack X to be tested in this study. Based on the cPCF results, the performance of CNTs would be higher than Carbopack B and comparable to Carbopack X. This agrees with results from the literature. For example, the results from Mitra group suggested that the adsorption performance of CNT is better than Carbopack B in general [24]. The performance of CNTs is also reported to be higher than Tenax [29].

4.4 Conclusions

The performance of CNTs is comparable to Carbopack X at constant flow rate. It is, however, not possible to draw conclusions on performance based on this study because the adsorbent bed configuration is too different between the two devices. The results of vapor adsorption of MEK and benzene on CNTs still follow the Wheeler equation, and we can use the modified Wheeler as an alternative approach to compare the kinetic equilibrium adsorption capacity of different vapors on CNTs.

The results of the μPCF testing suggested that the preconcentration process occurred in the μPCF, since the device is not completely packed with adsorbent material, the device is operated as equilibrium preconcentrator, not an exhaustive device in this case.

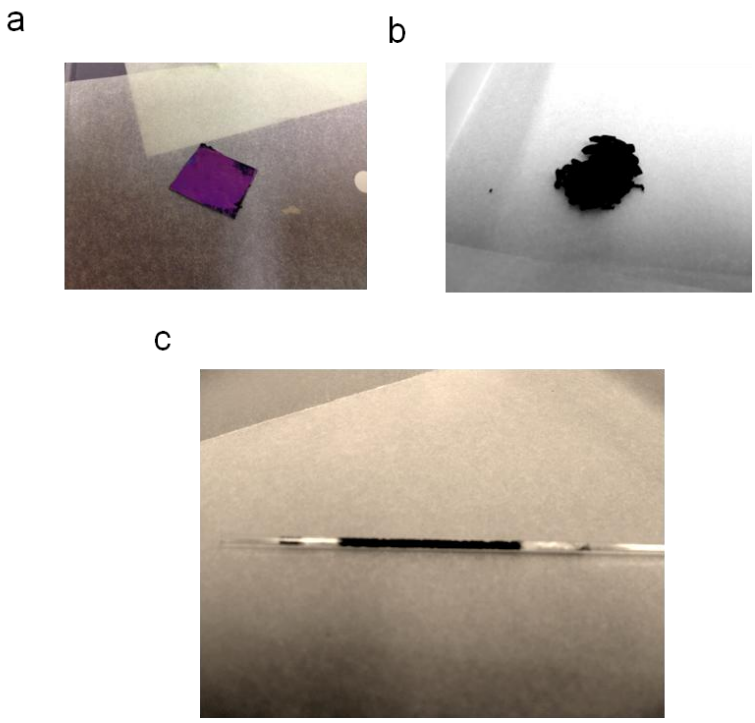

Figure 4-1. Pictures of CNTs forest removed from silicon wafer (a-b). CNTs packed in glass capillary tube and retained by wool and mesh (c).

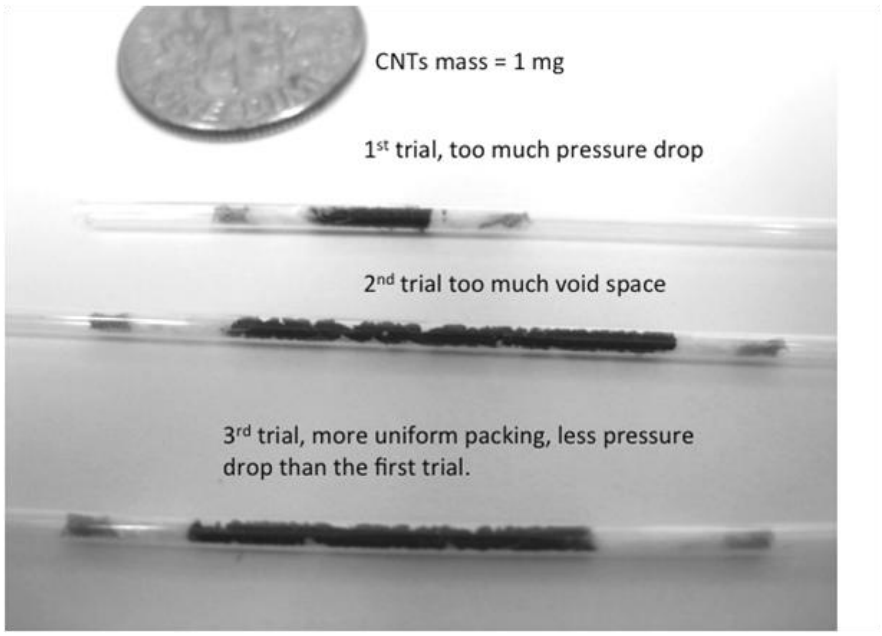

Figure 4-2. Capillary preconcentrator packed with 1 mg CNTs. Three cPCFs packed with similar mass shows different packing density and the effect of this parameter on the packing uniformity.

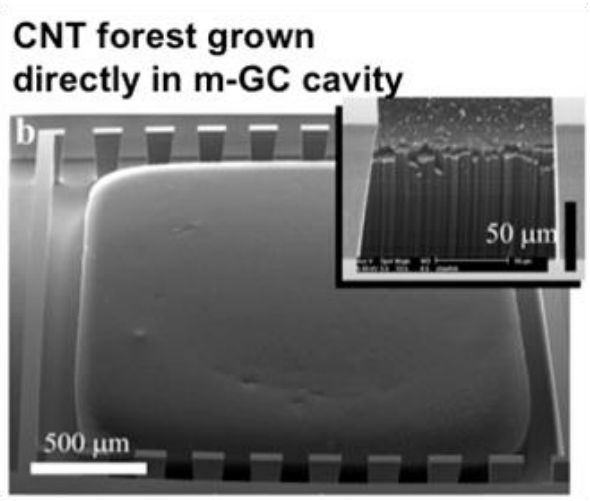

Figure 4-3. CNTs grown directly in the µPCF cavity (credit: Sameh Tawfick, Katharine Beach and A. John Hart)

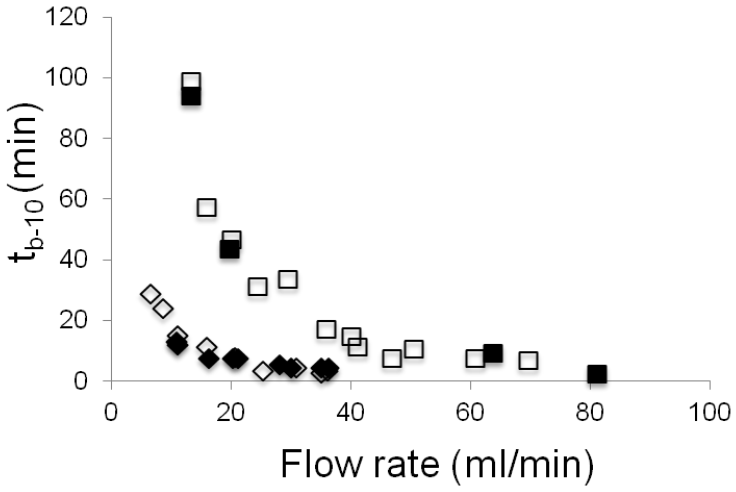

Figure 4-4. Plot comparing the t_{b-10} as a function of flow rate of MEK from CNTs (filled diamond) , benzene from CNTs (filled rectangle), MEK from Carbopack X (open diamond) and benzene from Carbopack X (open rectangle).

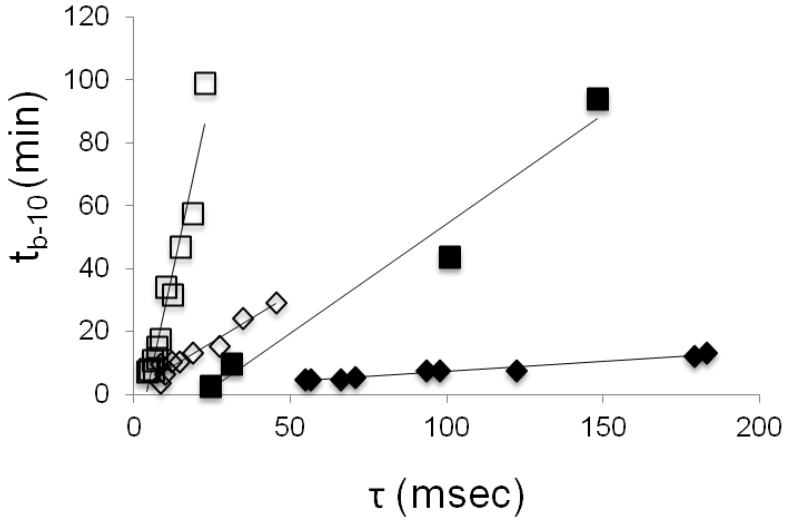

Figure 4-5. Linear plot of the t_{b-10} and τ of MEK (diamond) and benzene (rectangle) on CNTs (filled symbol) and Carbopack X (open symbol).

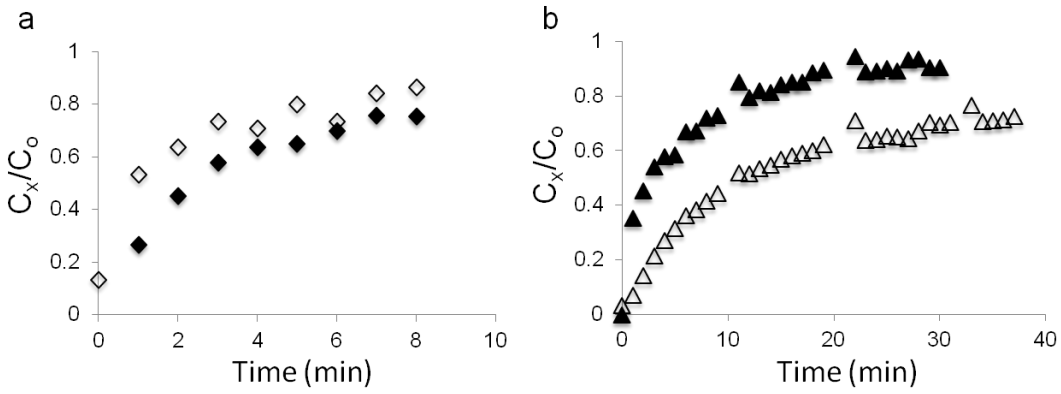

Figure 4-6. The breakthrough plot of a) MEK at 9.4 ml/min sampling flow rate ((filled diamond), and 12 ml/min sampling flow rate (open diamond). b) toluene at 7.6 ml/min sampling flow rate (filled triangle) and 25 ml/min sampling flow rate (open triangle)

References

1. J. Namiesnik, *Talanta*, 1988, 35, 567
2. K. Dettmer and W. Engewald, *Anal. Biochem*., 2002, 373, 490.
3. J. Brown and B. Shirey, Technical Report for Supelco, T402025, Bellefonte, PA, 2001.
4. A. B. A. Dow, and W. Lang, *IEEE Sens. J.*, 2012, 12, 2528.
5. I. Gràcia, P. Ivanov, F. Blanco, N. Sabaté, X. Vilanova, X. Correig, L. Fonseca, E. Figueras, J. Santander, and C. Cané, *Sens. Actuators, B,* 2008, 132, 149.
6. A. Rydosz, W. Maziarz, T. Pisarkiewicz, K. Domański, and P. Grabiec, *Microelectron. Reliab.,* 2012, 52, 2640.
7. C.J. Lu and E.T. Zellers, *Anal.Chem*., 2001, 73, 3449.
8. C.J. Lu and E.T. Zellers, *Analyst*., 2002, 127, 1061.
9. W.A. Groves, E.T. Zellers, and G.C. Frye, *Anal. Chim.A*., 1998, 371, 131.
10. Z. Ni, J.P. Jerrell, K.R. Cadwallader and R.I. Masel, *Anal. Chem*. , 2007, 79, 1290.
11. A.G. Wong-Foy, A.J. Matzger, and O. M. Yaghi, *J. Am.Chem.Soc*., 2006, 128, 3494.
12. C. Feng, S. Mitra, *J. Chromatogr. A*., 1998, 805, 169.
13. C. Feng, and S. Mitra, *J. Micro Sep*, 2000, 12, 267.
14. S. Iijima, *Nature*, 1991,354, 56.
15. E.R. Meshot, D. L. Plata, S. Tawfick, Y. Zhang, E.A. Verploegen, and A. J. Hart, *ACS Nano*, 2009, 3, 2477.
16. A. Merkoçi, *Microchim Acta*, 2006, 152, 157.
17. B. Pan and B. Xing, *Environ. Sci. Technol*, 2008, 42, 9007.
18. M.S. Mauter and M. Elimelech, *Environ. Sci. Technol*, 2008, 42, 5843.
19. M.R. Cuervo, E. Asedegbega-Nieto, E. DÎaz, A. Vega, S. OrdÓÑez, E. Castillejos-LÓpez and I. RodrÍguez-Ramos, *J. Chromatogr. A*, 2008, 1188, 264.
20. X. Peng, Y. Li, A. Luan, A. Di, H. Wang, B. Tian and Z. Jia, *Chem. Phys. Lett.*, 2003, 376, 154.
21. W. Chen, L. Duan and D. Zhu, *Environ. Sci. Technol*. 2007, 41, 8295.
22. C. Lu and H. Chiu, *Chem. Eng. Sci*. 2006, 61, 1138.
23. C. Lu, Y. Chung and K. Chang, *J. Hazard. Mater*. 2006, 138, 304.
24. C.M. Hussain, C. Saridara and S. Mitra, *Analyst*, 2008, 133, 1076.
25. C.M. Hussain, C. Saridara and S. Mitra, *J. Chromatogr. A*, 2008, 1185, 161.
26. C. Saridara, S. Ragunath, Y. Pu and S. Mitra, *Anal. Chim.Acta.*, 2010, 677, 50.
27. C. Saridara, R. Brukh, Z. Iqbal, and S. Mitra, *Anal. Chem*., 2005, 77, 1183.
28. C. Thammakhet, P. Thavarungkul, R. Brukh, S. Mitra, P. Kanatharana, *J. Chromatogr. A*, 2005, 1072, 243.
29. F. Zheng, D. L. Baldwin, L. S. Fifield, N. C. Anheier, Jr., C. L. Aardaht, and J. W. Grate, *Anal. Chem*., 2006, 78, 2442.

Chapter 5

Multi-Stage Preconcentrator/Focuser Module Designed to Enable Trace Level Determinations of Trichloroethylene in Indoor Air with a Microfabricated Gas Chromatograph

5.1 Introduction

Vapor intrusion (VI) is a term used to describe indoor air contamination arising from the migration of volatile organic compounds (VOC) into residences or office buildings from surrounding contaminated ground water or soil [1]. The problem is generally associated with improper waste disposal or leakage of storage tanks, and can take many years to develop. Due to its volatility, persistence, widespread use as a degreasing solvent, and indiscriminant disposal practices historically, trichloroethylene (TCE) is a common VI contaminant that has been identified in more than 1,500 hazardous waste sites around the U. S [2].

Prevalent indoor air concentrations of TCE arising from VI are in the sub-parts-per-billion (ppb) range [3,5]. Although exposure at these levels is considered to present very low risk of adverse health effects, proactive efforts to remediate locations impacted by VI are often triggered when TCE concentrations are found in this range [1]. This is also the concentration range within which many common indoor air contaminants are typically

encountered [6-8]. Thus, determining TCE in locations potentially affected by VI requires its separation from such co-contaminants.

The most common methods used to determine indoor air concentrations of TCE at these low levels are EPA Methods TO-15 [9] and TO-17 [10], which rely on sample collection using a canister or an adsorbent-packed tube, respectively, followed by laboratory analysis by GC-MS or GC-FID. These conventional methods are subject to errors associated with sample storage and transport, they are expensive and labor intensive, there is a delay in obtaining data, and they provide limited time resolution in the measured concentrations because samples are typically collected over 24-hr time period [11]. Use of mobile laboratories, such as the EPA trace atmospheric gas analyzer (TAGA) [12], can mitigate some, but not all, of these issues.

Of the relatively few commercial field-portable direct-reading instruments suitable for *in situ* determinations of TCE in the presence of co-contaminants at such low concentrations, the most promising appears to be the Hapsite® portable gas chromatograph with mass-spectrometer detector (GC-MS) [13]. With its on-board preconcentrator this instrument is capable of fairly rapid analyses of multiple VOCs at concentrations below 1 ppb, and reports have appeared demonstrating its utility for indoor-air monitoring (and emergency response) [13,14]. However, since this instrument is large, expensive and requires a trained operator, it is not ideally suited for application as a continuous monitor for assessing chronic VI contamination levels or the effectiveness of long-term VI remediation efforts. Thus, there remains a need for portable instruments that are capable of determining specific VOCs in complex mixtures, yet small, simple, and inexpensive enough to be used for routine monitoring.

Several years ago we described the first laboratory prototype microfabricated gas chromatograph (μGC) capable of determining the components of VOC mixtures at ppb

concentrations [15-17]. That μGC included a microfabricated preconcentrator/focuser (μPCF), which served as both a trap and an injector, a microfabricated separation column, and a detector consisting of an integrated array of chemiresistor microsensors that employed thiolate-monolayer-protected gold nanoparticles (MPN) as the interface layers. Combining the response pattern generated from the microsensor array with the corresponding chromatographic retention time facilitated the differentiation and identification of the components of VOC mixtures [15].

Since then, we have continued to improve the performance and expand the capabilities of the μGC components [18-28], and are now beginning to integrate them into robust, fieldable microsystems capable of autonomous analysis of VOCs for environmental monitoring, homeland security, and medical diagnostics [29-32]. Among the most recent design revisions are the inclusion of two series-coupled 3-m-long separation microcolumns [31-32] and ultra-miniature sensor arrays with patterned interface layers [26]. Recent reports of other μGC systems developed for chemical warfare agents [33] and environmental VOCs [34] by other groups are also noteworthy.

In considering the application of μGC to the assessment of TCE contamination from VI in homes, it became apparent that the air sample volume required to achieve the sub-ppb detection limits demanded by this application would exceed the capacity of the μPCF devices we have used in our previous μGC prototypes. In addition, any semi-volatile organic compounds (SVOCs) present in the air would tend to strongly adsorb to surfaces or only slowly desorb from the μPCF at normal desorption temperatures [28]. Thus, a high-volume sampler and a means of precluding SVOCs were required upstream from the μGC.

The most common approaches to preconcentration for field portable GC entail the collection of discrete air samples via solid-phase microextraction (SPME) [35-37] or

conventional single- or multi-adsorbent sampling tubes [38-41], followed by subsequent introduction to the GC column using a thermal desorber unit or a heated injector port. Several reports describe approaches to integrating the preconcentration function into the GC [14,15,18,19,33,34,41-48,50], but relatively few use selective preconcentration explicitly to reduce interferences [18,19,48], and none has focused specifically on analyzing ppt levels of TCE.

In response to the requirements specific to the application considered here, we have developed a multi-stage preconcentrator-focuser (PCF) module consisting of a pre-trap, sampler, and microfabricated focuser (μF) to (ultimately) interface with the μGC we are constructing in order to enable its use for TCE determinations in VI-impacted residences. Building on previous work by our group [15,18,19,42,43,49,50] and by others [41,44-48,51] concerned with integrated single- and multi-adsorbent VOC preconcentrators for fieldable GC analyzers, we have devised a means of selectively and quantitatively capturing, transferring, and injecting TCE vapor samples at low concentrations in the presence of common indoor air contaminants.

Figure 5-1 shows a block diagram of the essential analytical components and fluidic paths of the μGC prototype under development, including the PCF module. In operation, a commercial mini-pump (pump A) would draw an air sample through the pre-trap and sampler at a high flow rate. Then, valve A would be actuated and a second pump (pump B) would draw scrubbed air through the sampler as it is resistively heated and backflushed to desorb and transfer the captured VOCs (including TCE) to the μF at a low flow rate (note: valve B would be closed during this process to prevent VOCs from entering the column). Then, the flow from pump B would be reversed and air backflushed through the μF as it is heated rapidly to inject the

captured VOC mixture into the dual-microcolumn separation module for separation and identification/quantification by the array of nanoparticle-coated chemiresistor sensors.

In this Chapter we describe the design, development, optimization, and characterization of a PCF module for TCE. Although many of the critical design and operating parameters of the module are dictated by the microcolumns and microsensor array employed in the μGC, all testing reported here used conventional bench-scale GC instrumentation for the required analyses. Integration of the PCF with the μGC will be described in a separate report.

5.2 Experimental Design and Rationale

Several application-specific performance criteria were developed for the μGC which, in turn, led to the criteria we used to specify the design and operating features of the PCF-module components. Prioritizing these criteria, assessing the performance tradeoffs, and implementing the final specifications required a system-level approach for which we found no precedent in the literature. Therefore, we include the following rationale as a preface to the experimental methods employed.

Defining the detection limit (LOD) for TCE and the time limit for each determination was necessary at the outset in order to specify the maximum air-sample volume and the corresponding volumetric flow rate of the sampling step. A target LOD of 0.06 ppb was established on the basis of prior measurements indicating that prevalent TCE concentrations could be as low as this level, and in light of the fact that the mitigation action level (MAL) at the site where the μGC will be field tested is 2.3 ppb of TCE. This LOD would permit determinations of TCE at concentrations roughly 40 times lower than the MAL. Preliminary tests performed with the chemiresistor sensor array gave an LOD for TCE of ~1.2 ppb assuming a 1-L

air sample (i.e., “1.2 ppb-L,” or 6.2 ng). Thus, in order to achieve an LOD of 0.06 ppb, it would require a sample volume of 20 L. Higher concentrations would require smaller volumes.

Preliminary tests with the µGC separation module indicated that it would require ~3 min to separate TCE from the most critical co-contaminants, which are defined as those VOCs having chromatographic retention times similar to those of TCE. Since an analysis time of 15-30 minutes was considered acceptable for both short-term screening and long-term monitoring measurements, a sampling flow rate of 1 L/min was deemed sufficient.

Defining the nature and number of interferences was then necessary in order to specify the types and amounts of adsorbent materials to use in the PCF components, because the capacities, desorption efficiencies, and associated flow rates passing through these devices depend on these factors. The set of potential interferences (i.e., co-contaminants) considered in this study was determined from a set of field samples collected by one of our collaborators from VI-impacted homes prior to this study. These were then parsed into three subsets according to vapor pressure (p_v). Those with values of $p_v > 100$ torr were designated as sufficiently volatile as to not be of concern; by proper adsorbent selection, these interferences would be largely unretained by the sampler. Those with p_v values ranging from 3-100 torr and would be collected along with TCE in the sampler, transferred to the µF, and subsequently separated and detected. Those compounds with $p_v < 3$ torr would be captured by the upstream pre-trap. Since environments with high humidity might be encountered, it was necessary to account for this potential co-factor as well.

For the miniature diaphragm pumps to be used in the prototype, the flow rate achievable is a sensitive function of the resistance to flow in the sampling train [52]. Another design constraint to address, therefore, was the pressure drop presented by each component in the PCF

module. This generally dictated minimizing the masses of adsorbent materials. The size of the adsorbent granules was also a relevant variable, since packed beds of smaller granules lead to higher flow resistance. Minimizing the adsorbent masses would also reduce the power and time required for thermal desorption.

The pre-trap required a sufficient mass of a low-surface-area adsorbent to capture the less volatile co-contaminants while permitting the TCE to pass through unretained. Excluding such compounds from passing further downstream would prevent irreversible adsorption onto the higher-surface-area adsorbents in the sampler and μF and also would reduce the maximum temperature required for chromatographic separations and, thereby, the overall analytical cycle time. Experiments performed with this device focused on adjusting the mass of the selected adsorbent in order to optimize the tradeoff of low retention of TCE (p_v = 69 torr) and high retention of the less volatile interferences at the flow rate dictated by the sampler (see below), while also monitoring the pressure drop constraint imposed by the pump. It was also necessary to determine the capacity of the pre-trap for the less volatile co-contaminants to specify how often it would need to be thermally regenerated.

The sampler required a sufficient mass of a higher-surface-area adsorbent to capture TCE quantitatively in the presence of co-contaminants at relevant concentrations, and the flow rate through the sampler had to be high enough to keep the overall analytical cycle time under 30 min while capturing a sufficient mass of TCE to achieve the targeted LODs with the downstream detector. Rapid, quantitative transfer of the captured TCE from the sampler to the μF was also required. Experiments with this device focused on optimizing the tradeoff between adsorption capacity for TCE and the flow rate (and associated pressure drop), as well as documenting

sufficient capacity in the presence of co-contaminants and high humidity. The quantitative desorption of TCE at low flow rates also needed to be confirmed.

The μF was required to capture the TCE (quantitatively) and any accompanying co-contaminants desorbed from the upstream sampler, and then to thermally desorb them to provide a focused injection into the separation module. The narrower the injection band, the greater the chromatographic efficiency of any separation [51]. The microfabricated device used as the μF here is a refined version of devices used for both preconcentration and injection in our previous μGC prototypes [15, 18]. Experiments performed with this device focused on documenting its capacity for capturing quantitatively the TCE desorbed from the upstream sampler in the presence of co-contaminants as a function of flow rate, and then exploring the effect of flow rate on the injection bandwidth of TCE.

Following the series of experiments required to determine the nature and quantities of adsorbents to use in each of the three devices, the tolerable pressure drops, flow rate limitations, TCE dynamic adsorption capacity, humidity effects, desorption efficiencies and desorption bandwidths in the presence of anticipated co-contaminants, a final test series was necessary to demonstrate that the assembled multi-stage PCF provided quantitative capture, transfer, and injection of TCE.

5.3 Experimental Methods

5.3.1 VOCs and Adsorbent Materials

Table 5-1 lists the VOCs used in this study. They were culled from the set of 63 compounds detected in 12 air samples collected from residential field locations in canisters and analyzed by GC/MS according to EPA Method TO-15. Since those compounds with p_v values >

100 torr were eliminated from consideration (see above and below). Samples of all of the other compounds were purchased from Sigma-Aldrich/Fluka (Milwaulkee, WI) or Acros/Fisher (Pittsburgh, PA) in >95% (most > 99%) purity and were used as received.

A lower-surface-area commercial graphitized carbon, Carbopack B (C-B, specific surface area = 100 m^2/g), was chosen for use in the pre-trap to retain the low-p_v interferences [53]. Previous studies have demonstrated that small quantities of C-B can capture VOCs with p_v values up to ~28 torr from moderately large air volumes and release them efficiently by thermal desorption [42,43]. Another graphitized carbon, Carbopack X (C-X, specific surface area = 250 m^2/g) was chosen for use in the sampler, on the basis of evidence that it would be capable of capturing and efficiently desorbing VOCs with p_v values up to ~95 torr [42,43]. Interferences with higher vapor pressures were expected to pass through the sampler largely unretained. C-B and C-X (60/80 mesh) were obtained from Supelco (Bellefonte, PA). Samples of C-B and C-X were sieved and the fractions with nominal diameters in the range of 180-212 μm (for C-B only) and 212-250 μm (for C-B and C-X) were isolated and packed in the appropriate device.

5.3.2 Pre-trap, Sampler, and Microfocuser Construction

The pre-trap and sampler were constructed from thin-walled stainless-steel tubes (0.64-cm o.d., 0.54-cm i.d., 6 cm long, Figure 5-2) and were connected to upstream and downstream system components with Teflon Swagelok® fittings (H.E. Lennon, Farmington Hills, MI). The adsorbent materials were retained between plugs of silanized glass wool and micromesh stainless steel screening (42-6110, Ted Pella, Inc., Redding, CA), and a thin strip of stainless steel was bent and inserted in each end to prevent the bed from shifting over time. A heat-resistant thin polyimide tape (7648A713, McMaster Carr, Santa Fe Springs, CA) was wrapped around each

tube for electrical insulation. A fine-wire thermocouple (Type K, Omega, Stamford, CT) was positioned near the center of the packed bed and held in place with the coil of insulated Cu wire (100-μm o.d., EIS, Inc., Atlanta, GA) used to heat the devices during desorption. The heated length ranged from 1.3-2.8 cm for adsorbent bed masses of 50-200 mg. The Cu wire was held tightly around the tube by a second layer of polyimide tape.

The coil was heated open-loop by the application of a pre-set dc voltage. Using the heater coil, the packed sampler and pre-trap were subjected to a one-time preconditioning treatment consisting of heating under a flow of N_2 at 300 ^oC for 4-6 hours after initial preparation. Subsequently, these components were heated to 300 ^oC under N_2 for 30 minutes routinely between experiments to ensure removal of any residual contamination. For the sampler desorption experiments, maximum temperatures of 180 and 220 °C were tested: application of 7V resulted in heating to 170 °C within 1 min and to 180 °C within 2 min; application of 9V resulted in heating to 200 °C within 1 min and to 220 °C within 3 min. The maximum temperatures could be maintained for as long as required by a given experiment.

The μF devices (4.18 mm(w) × 9.76 mm(l) × 0.6 mm(h), Figure 5-2c) were fabricated from double-polished 4-inch Si wafers. Deep-reactive-ion etching (DRIE) was used to form a central chamber (internal volume = 4.3 mm^3) with opposing, tapered inlet and outlet sections, and a set of pillars (0.15 mm widths and spaces, 0.38 mm height) near the inlet and outlet ports for retaining the adsorbent granules. A third port etched on the side of the cavity was used for filling the chamber of the sealed device with the adsorbent. An additional flow channel etched into the chip forms a tee connection with one of the two main flow channels, which facilitated loading and backflushing of the VOC samples. All three fluidic ports on the μF chip have expansion sections that accept the fused-silica capillaries used for interconnections. A Ti/Pt

resistive temperature device (RTD) was evaporated onto the backside of the Si along with two large Ti/Pt contact pads for applying current to heat the device during desorption. The device was sealed with an anodically bonded Pyrex plate (0.1 mm thick). Capillaries (0.25-mm i.d., 0.32-mm o.d., deactivated fused silica, intermediate polarity, Supelco, Bellefonte, PA) were inserted in the three fluidic ports and secured with silicone adhesive (Duraseal® 1531, Cotronics, Brooklyn, N.Y). Electrical connections to a custom printed circuit board were made using Al wire-bonds.

To pack the μF with C-X, gentle suction was applied through the outlet port through the fill port at the side of the cavity, while the capillaries extending from the unused ports were temporarily blocked. The adsorbent is retained in the cavity with the pillars described above. After packing, the fill port was sealed with Duraseal®. The μF holds ~2.3 mg of C-X when fully packed, as determined gravimetrically.

5.3.3 Test Atmosphere Generation

Concentrations of TCE and co-contaminants found in the field samples were generally in the 0.01 - 10 ppb range. Therefore, testing was generally constrained to this concentration range. Test atmospheres were generated by injecting pre-determined volumes of liquid TCE (and interfering compounds, when necessary) into a Tedlar® bag (SKC, Inc. Eighty Four, PA) prefilled with a known volume of clean, dry air or N_2 from compressed gas cylinders. Serial dilutions were made to achieve the targeted concentrations. For compounds with vapor pressures above ~3 torr, we have found that the concentrations in the bag can be estimated accurately from the injection and dilution volumes. For less volatile compounds, some loss is expected from condensation and adsorption to the bag walls. For tests performed at high humidity, dilution air

was passed through a fritted bubbler filled with distilled water prior to filling the Tedlar® bag. An additional volume of 0.5 mL of distilled water was added to the bag by syringe to maintain 100% RH, since water vapor permeates through Tedlar® rapidly [54]. Little or no loss of test vapors to the liquid water was observed, however, breakthrough test fractions were normalized to the extant concentration in the bag, so this issue did not affect determinations of breakthrough volumes. All test atmospheres were used at ambient temperature.

5.3.4 Analytical Methods

Analyses were performed with a bench-scale GC (Model 6890, Agilent Technologies, Palo Alto, CA). Where separations were required, 15 m long, 320 μm i.d. capillary column with a 0.25 μm thick HP–1 stationary phase (19091Z-411, Agilent Technologies) was typically used with N_2 carrier gas. For the final tests of the assembled module a 6-m column was used instead, to mimic the microcolumn length used in the μGC. One of two types of detectors was employed, depending on the nature of the analysis being performed. An FID was used in pre-trap breakthrough tests and in some of the tests of the sampler, and an ECD was used to monitored TCE in those experiments where the concentrations of the co-contaminants did not need to be determined. Breakthrough fractions were determined by comparing the peak area of injected samples of the relevant compound from the challenge test atmosphere to that measured in the same injection volume downstream from the device under test (see below). For those tests requiring quantification of TCE, the ECD was calibrated by analyzing separate serially diluted test atmospheres prepared in Tedlar® bags that spanned the required range of injected mass.

5.3.5 Pressure Drop, Capacity, and Desorption Volume

The pressure drop across the coupled pre-trap and sampler devices was examined as a function of adsorbent mass over a range of flow rates using a differential pressure gauge (Magnehelic, Dwyer Instruments, Inc., Michigan City, IN) connected by a tee to the line connecting the pre-trap/sampler to the same type of diaphragm pump to be used in the field prototype μGC instruments (SN020, KNF Neuberger, Trenton, NJ). The two devices were connected by large-bore tubing that presented minimal additional pressure drop at 1 L/min.

The 25 most prevalent potentially interfering compounds with p_v values in the 3-95 torr range (out of 28) identified in the field samples were used in various combinations and subsets to assess the impact of co-contaminants on PCF performance. Four of these VOCs are chlorinated hydrocarbons (i.e., bromodichloromethane, 1,2-dichloropropane, tetrachloroethylene, and 1,1,2-trichloroethane), and the first two of these are difficult to resolve from TCE chromatographically. Therefore, in some of the breakthrough tests performed with a GC column downstream only 23 co-contaminants were included, and in those tests where the mixture was passed directly to an electron capture detector (ECD) without separation, only 21 of the co-contaminants were included in the test mixture.

Figure 5-3a shows the breakthrough test set-up. The test atmosphere was drawn through the sampler or pre-trap using pump A (UN86, KNF Neuberger) at 1 L/min and a fraction of the downstream air was drawn through a sampling loop (112-μL or 250-μL) by pump B (UN86, KNF Neuberger). At 1-min intervals, the six-port valve was actuated to inject the contents of the loop to the injector of the GC. The sample volume required for the concentration downstream from the adsorbent tube to reach 10% of the inlet concentration, $V_{b\text{-}10}$, was used as the metric of

the dynamic adsorption capacity of the devices. Breakthrough tests were run in duplicate to assess the reproducibility of the results.

The set-up shown in Figure 5-3b was used to test the flow rate and air volume required to desorb TCE from the sampler and transfer it to the μF, as well as to test the capacity of the μF. The sampler was spiked with a 10-mL aliquot from a test atmosphere containing 1 ppm of TCE (52 ng, 10 ppb-L) along with similar concentrations of all 25 co-contaminants by gas-tight syringe while drawing N_2 gas from a Tedlar® bag through the sampler at ~25 mL/min. The sampler was subsequently heated to different temperatures while backflushing with N_2 at different flow rates. TCE peak areas were monitored with the ECD detector to determine when desorption was complete.

To test the capacity of the μF for different sampler desorption conditions, the μF was placed in line between the sampler and the six-port valve (Valco, Houston, TX) (Figure 5-3b) and the breakthrough of TCE was monitored downstream from the μF. To assess the effect of flow rate on the desorption band width of TCE from the μF, the outlet port of the device was connected directly to the ECD via a section of deactivated fused silica capillary of the same diameter and similar length as that to be used in connections to the first microcolumn in the μGC. A 1-mL sample containing 1 ppm of TCE (5.2 ng, 1 ppb-L), alone or with a subset of co-contaminants at similar concentrations, was injected into the μF via the upstream capillary (i.e., through the tee branch on the μF chip) by gas tight syringe under a flow of 25 mL/min of N_2. The μF was then heated to 225°C in 0.6 sec with the integrated heater and the sample was thermally desorbed with backflushing directly into the ECD. Flow rates through the μF were measured with a bubble flow meter. The peak width at half height (PWHH) was measured at different flow rates. Chemstation software (Rev.B.01.01, Agilent Technologies), GRAMS32

(version 6.0. ThermoScientific, Pittsburg, PA) and Microsoft Excel were used for data acquisition and processing.

5.4 Results and Discussion

5.4.1 Pressure Drop and Sampling Flow Rate

To characterize the pressure drop constraint, initial range-finding tests were performed with 50 mg of the smaller-diameter fraction of C-B in the pre-trap (i.e., 180-212 μm) and 200 mg of C-X (212-250 μm) in the sampler. Although somewhat arbitrary, these adsorbent masses are consistent with those used in sampling tubes for EPA Method TO-17 [55]. The pressure drop increased linearly with flow rate (slope = 0.054 L/min/kPa) to a maximum of 18 kPa at 0.95 L/min, which was the highest flow rate the pump could provide. This pressure-flow relationship is consistent with data provided by the pump manufacturer [52]. Replacing the C-B with the same mass of the larger diameter C-B (i.e., 212-250 um) permitted the desired flow rate of 1 L/min to be reached at a pressure drop of 16 kPa. With 100 mg C-X (212-250 μm) and 50 mg C-B (212-250 μm) a flow rate of 1 L/min could be achieved with a pressure drop of only 11 kPa.

5.4.2 Pretrap Optimization

The first performance criterion for the pre-trap is that it not retain TCE to any significant extent. Breakthrough tests were performed at 1 L/min with pre-traps containing either 50 or 75 mg of C-B (212-250 μm) challenged with 1 ppb of TCE in air. A low TCE concentration was used in order to have the greatest sensitivity to small losses of vapor to the pre-trap adsorbent. Figure 5-4a shows that there is some retention of TCE over the first 1-2.5 min of exposure, but

that the amount retained with the smaller bed mass is significantly less. Experiments were run in duplicate, with essentially the same results as shown in Figure 5-4a.

Since the temporal resolution of these breakthrough measurements is limited it is difficult to precisely quantify the loss of TCE, but a conservative estimate can be made by integrating the area above the breakthrough curves. For the 50-mg C-B bed this yields 7.8 ng (1.5 ppb-L) and for the 75-mg bed it is 13 ng (2.5 ppb-L). For a 20-L sample, this would correspond to potential losses of 1.8 % and 6.2 % of the TCE in the sample stream for the 50 and 75 mg beds, respectively. For a 5-L sample, this amounts to losses of 7 and 25%, respectively. Note that in the presence of less-volatile co-contaminants, some displacement of TCE is likely to occur, reducing further the amount retained on the pre-trap. The losses of TCE to the 50-mg bed were considered acceptably small, and this mass of C-B was used in subsequent testing.

The second performance criterion for the pre-trap is its ability to retain/remove low-volatility interferences. On the basis of prior studies [42, 43], the pre-trap packed with C-B was expected to efficiently adsorb compounds with p_v < 8 torr. However, initial tests of a 50-mg bed of C-B with a mixture containing a subset of four vapors with p_v values ranging from 3.5-28 torr (i.e., 500 ppb each of toluene, PCE, m-xylene, and cumene; see Table 5-1), run in duplicate, gave V_{b10} values < 12 L (1 L/min) for all mixture components. Despite the high challenge concentrations used for this test, it was apparent that compounds with vapor pressures in this range would not be retained effectively, and that a lower 'cut-off' p_v value would need to be defined.

Toward this end, a mixture of each of the following less volatile co-contaminants was prepared, which spanned a range of p_v values from 0.5 to 3.4 torr: cumene, 4-ethyltoluene, d-limonene and 1,2,4-trichlorobenzene (Table 5-1). The nominal concentration of each component

was 500 ppb, although fractional losses to the bag walls are to be expected for all of these compounds. Since all $V_{b\text{-}10}$ determinations were referenced to the test-atmosphere peak areas, this factor did not preclude obtaining useful data.

Figure 5-4b shows that while cumene (p_v = 3.5 torr) gives a V_{b10} value of only 8 L, the remaining compounds give $V_{b\text{-}10}$ values ≥ 30 L. Thus, it appears as if this trap can effectively retain compounds with $p_v \leq 3$ torr. The 4-ethyltoluene showed 2% breakthrough at 28 L, suggesting that it would serve as a good 'sentinel' vapor for the capacity of the pre-trap, since all less volatile compounds should give larger breakthrough volumes. In duplicate testing cumene gave the same $V_{b\text{-}10}$ value and 4-ethyltoluene showed 2% breakthrough at 29 L.

A subsequent experiment was performed with a mixture of 4-ethyltoluene, d-limonene, 1,2,4-trichlorobenzene, and naphthalene (p_v range = 0.085 - 3.0 torr), which includes the least volatile compounds found in the field samples. The nominal concentration of each component was 40 ppb. To minimize losses to fluidic interconnections in the test system the pre-trap was connected directly to the Tedlar® bag containing the test atmosphere by a short section of tubing and a septum-capped tee fitting was inserted just downstream. The test atmosphere was drawn through the pre-trap and 1-ml samples were collected periodically by gas-tight syringe and injected into the GC-FID.

Although a low level of the sentinel compound 4-ethyltoluene was detected in early samples, the amount decreased over the first 30 L, and we attribute the initial amounts to contamination of the syringe, which had been used to sample the challenge test atmosphere initially. The downstream levels did not increase to > 10% of the challenge concentration until the sample volume was 110 L when the test was concluded. This test was not repeated, but

suggests that these compounds are retained effectively and that reconditioning of the pre-trap could be performed roughly every 5-6 operational cycles (assuming 20-L samples per cycle).

5.4.3 Sampler Optimization

To assess the dynamic capacity as a function of the mass of C-X packed in the sampler, a test atmosphere containing 500 ppb each of TCE, benzene, 2-butanone, and n-heptane (in air), was drawn through beds of 50, 100 and 200 mg at 1 L/min. The 200-mg bed gave a $V_{b\text{-}10} > 20$ L for all vapors, indicating more than enough capacity. With the 100-mg bed, $V_{b\text{-}10}$ for 2-butanone was about 8 L, but for TCE and all other mixture components $V_{b\text{-}10}$ was > 20 L. With the 50-mg bed of C-X, the TCE $V_{b\text{-}10}$ was ~8 L, indicating that this is an insufficient mass.

Subsequent testing was performed with 100 mg C-X beds using test atmospheres of 50 ppb of TCE in a mixture with similar concentrations of each of 23 interferences with $p_v > 3$ torr (Table 5-1, compounds 1-26, excluding 6 and 8). A $V_{b\text{-}10} > 30$ L was obtained for TCE. This test was repeated using a test atmosphere saturated with water vapor and there was no reduction in the dynamic capacity for TCE. All of these breakthrough experiments were repeated and yielded the same results. Thus, there appears to be ample capacity for TCE using the 100-mg C-X bed mass for the sampler.

Medium-term aging effects were explored by first running a breakthrough test with the same 50-ppb mixture ($V_{b\text{-}10} > 30$ L for TCE). Then a test atmosphere containing a mixture of 1 ppm each of TCE and 21 co-contaminants was prepared (excluding all chlorinated hydrocarbons) and a 10-mL aliquot (10 ppb-L) was spiked onto the sampler under a low flow of N_2. The sampler was then heated to 220 ºC and backflushed directly to the ECD at 20 mL/min. The peak measured by the ECD was due only to TCE. A set of 10 replicates of such spikes was analyzed.

Then another breakthrough test was performed (50 ppb of TCE with 23 interferences at 1 L/min), followed by another set of 20 replicate spiked analyses. This was followed by a final breakthrough test with the 50-ppb mixture.

The peak areas from the 30 desorbed spikes were averaged and the relative standard deviation was only 8.5%, demonstrating reproducible sampler desorption and no evidence of aging or accumulation of residual vapors that might affect TCE desorption. Values of $V_{b\text{-}10}$ for TCE in the 50-ppb samples, initially and after 10 and 20 spike replicates, were all >30 L, indicating no loss in capacity for TCE after repeated challenges and temperature excursions in the presence of co-contaminants.

5.4.4 Quantitative Transfer from Sampler to µF

Tests were then performed to assess the effect of temperature and flow rate on the desorption profile obtained from the sampler. Figure 5-6a compares the TCE desorption profiles for the most relevant subset of conditions with spiked samples corresponding to 10 ppb-L of TCE and each of the 25 interferences. At 180 °C and 20 mL/min it required between 4 and 5 min to completely desorb the TCE. By increasing the flow rate to 30 mL/min, TCE was completely desorbed in 3 min (note: at 180 °C and 10 mL/min it required > 8 min to completely desorb the TCE, data not shown). Increasing the maximum temperature to 220 °C, at 10 mL/min the TCE was desorbed within 5 minutes and at 20 mL/min it was desorbed in 2.5 min.

The µF TCE breakthrough profiles under these four sampler desorption conditions are shown in Figure 5-6b. At 180°C and 30 mL/min, TCE was detected at ~1% of the challenge concentration within 1 min, and by 3 min there was ~5% breakthrough. Although this extent of loss is not significant, raising the maximum temperature to 220 °C and lowering the flow rate to

20 mL/min resulted in only 0.7% breakthrough at 3 min. After desorbing the TCE from the μF and repeating this test, the 3-min breakthrough fraction was 0.8%. This combination of temperature and flow rate thus appears to be the most acceptable.

These results reveal that the capacity of the μF for TCE in complex mixtures is quite limited. In part, this is because the peak concentration generated from the sampler desorption profile is rather high; we estimate it to be on the order of 1-3 ppm for TCE (and all other co-contaminants). In any case, by including in the test mixture realistic concentrations of the co-contaminants likely to be present with TCE, we have a certain margin of safety built in to the conditions derived from these experiments.

5.4.5 μF Desorption Profile and Preconcentration Factor

Decreasing the injection band width leads to increased chromatographic resolution by virtue of the reduced band dispersion at the outset of the separation, and also to decreased LODs by virtue of the increased peak height. Thus, it is desirable to maximize the rate at which samples captured on the μF are desorbed and injected. In general, this calls for rapid heating and high flow rates through the μF [41-43,51].

As part of the μGC development effort we have developed control circuitry permitting the μF to be heated at a rate of ~375 ^{o}C/sec and then held at any set-point temperature. In light of the sampler tests, and the fact that field operation will entail performing desorptions in an air matrix, a decision was made to fix the maximum temperature of the μF at 225 °C and to examine the effect of flow rate on the width of the desorption band of TCE. The maximum separation efficiency (i.e., smallest theoretical plate height) for the microcolumns is achieved with a microcolumn flow rate of ~ 0.4 mL/min, but operation at up to three times that value is possible

for rapid separations [31,32]. Therefore, the tests spanned the range of 0.3 to 3.6 mL/min. As stated above, the diameter of the capillary connector used was the same, and the length was similar, to that to be used in connecting the μF to the first microcolumn in the μGC.

The μF was spiked with TCE (see Experimental Section) and then heated to thermally desorb the TCE and backflush it directly to the ECD. Tests were performed in duplicate both with TCE alone and then with TCE in a mixture with similar quantities of a representative subset of 9 co-contaminants at ~ 1 ppb-L each: benzene, ethylacetate, heptane, toluene, octane, ethyl benzene, o-xylene, a-pinene and cumene. Average values of the PWHH at each flow rate are shown in Figure 5-7. Relative standard deviations were < 5% for tests with TCE alone and < 13% for tests with the mixture. At the lowest flow rate, the PWHH is about 2.8 sec, and as the flow rate increases it asymptotically approaches a minimum value of ~1 sec. However, beyond about 2 mL/min there is only a slight reduction in the bandwidth. The peak height values show the corresponding inverse trend (data not shown). As shown, there is no significant effect on the desorption profile of TCE by the other mixture components.

If it is assumed that a 20-L sample of TCE was collected and quantitatively transferred to the μF, and that the same mass of TCE is contained in the peak ultimately injected into the GC, then for a peak width of 1.5 sec at 1 mL/min the TCE is contained in a volume of ~25 μL and the preconcentration factor for the multi-stage PCF is ~800,000.

5.4.6 Performance of Assembled Multi-Stage PCF

The PCF module components were then assembled in a manner similar to that shown in Figure 1 except that the downstream port of the μF was connected to a 6-m fused-silica capillary GC column with ECD detector. A test atmosphere containing 0.2 ppb of TCE and each of 27 co-

contaminants (i.e., 4 low-volatility compounds expected to be retained in the pre-trap, and 23 compounds expected to be captured on the sampler) in air was prepared. A low concentration of TCE was used to confirm the quantitative transfer of TCE under expected conditions in the field. The mixture was drawn through the pre-trap (50 mg C-B) and sampler (100 mg C-X) at 1 L/min. After 20 minutes, the sampler was backflushed with N_2 and the captured vapors were transferred from the sampler to the μF by heating to 220 °C at 20 ml/min for 3 min. The μF was then heated to 225°C and maintained at this temperature for 1 min as the mixture was backflushed and injected onto a 6-m capillary column at 1 mL/min. The TCE eluted within 1 min at room temperature and was detected with the ECD. This experiment was performed twice.

The recovered peak area of TCE was evaluated against a calibration curve generated prior to these experiments for the ECD under the conditions of analysis. For the 20.0-L and 20.4-L samples of 0.2 ppb of TCE collected, the expected masses are 21 and 22 ng, respectively. From the recovered peaks areas, the masses were 26 and 21 ng, respectively. The corresponding sample transfer efficiencies are 120% and 95%, which give an average of 107%. We estimate the overall error of the method to be between 5 and 10%. The positive error in the first determination is puzzling, and despite preconditioning of the module components, must be attributed to residual TCE in the system prior to the first test being run. Subsequent calibrations were performed and showed that TCE peak areas varied linearly for samples ranging from 4-80 ppb-L (20-430 ng).

5.5 Conclusions

Developing an effective multi-stage preconcentrator/focuser (PCF) module suitable for use with a μGC for quantitative determinations of VOCs at low concentrations in the presence of

common airborne co-contaminants requires numerous tradeoffs in design and operation. Among the variables that must be considered are the overall time of analysis, target-analyte detection limits, pressure drop through the sampling train, volumetric flow rates, dynamic adsorption capacities, heating rates, desorption efficiencies and rates, and the nature, physical properties, and number of co-contaminants present in the air. We have considered all of these variables and the associated tradeoffs in designing and specifying the operating conditions of a multi-stage PCF module intended to facilitate the detection of sub-ppb concentrations of TCE by a downstream μGC in homes potentially affected by vapor intrusion from underlying contaminated soil. It is hoped that the approach presented here might serve as a general model for efforts to develop field monitoring instrumentation that incorporates on-board preconcentration functions.

Selective preconcentration is critical to module performance because of limitations on chromatographic resolution inherent to μGC systems, which employ relatively short separation columns. Use of a limited quantity of a low-surface-area adsorbent in the pre-trap to exclude the less volatile co-contaminants serves to reduce the analytical duty cycle because such compounds would require long elution times. It also prevents the accumulation of less-tractable compounds on the surfaces of downstream components. The use of a medium-surface-area adsorbent in the sampler results in quantitative capture of the target analyte (TCE in this case) while allowing the more volatile co-contaminants to pass through largely unretained. This reduces congestion in the early part of the chromatograms and should permit faster analyses by allowing faster temperature programming of separations. Rejection of water vapor is also achieved in this approach by use of hydrophobic adsorbents of limited surface area.

Interfacing the macro-scale sampler with the micro-scale focuser is also a critical feature of the PCF module. Extremely large preconcentration factors are achievable by virtue of being

able to collect large air-sample volumes with the macro-device and then to focus the captured analyte mass into a small injection volume via the micro-device. This not only increases the target-analyte concentration to levels measurable by the downstream detector (microsensor array), but it also enables efficient chromatographic separations by minimizing band dispersion at the inlet to the microcolumn. Being able to sweep the mF device effectively at the low flow rates required for efficient microcolumn separations is also important. Although the chemiresistor sensors used in the μGC we are developing are quite sensitive, preconcentration factors approaching 10^6 are necessary to detect VOCs at the parts-per-trillion concentrations prevalent in many environmental remediation efforts, such as that considered in this study. Achieving such low detection limits using micro-scale preconcentration components alone would not be possible.

On-going work directed at integrating this PCF with our μGC has yielded promising results in our initial laboratory tests, including the selective determination of TCE at concentrations < 200 ppt [31,32]. A fieldable prototype that couples this μGC with the PCF module described here has been constructed and successfully field tested in VI-affected homes, the results of which were reported in the literature [57,58].

Table 5-1. Test compounds and their corresponding vapor pressures, p_v, at 25 ^{o}C [56].

No.	Compound	p_v/torr	No.	Compound	p_v/torr
1.	Benzene	95	17.	n-Butyl acetate	15
2.	Ethyl Acetate	94	18.	n-Octane	14
3.	2-Butanone	89	19.	Ethylbenzene	9.6
4.	Acetonitrile	73	20.	m-Xylene	8.3
5.	Trichloroethylene	69	21.	o-Xylene	6.6
6.	Bromodichloromethane	65	22.	Styrene	6.4
7.	Ethanol	60	23.	α-Pinene	4.8
8.	1,2-Dichloropropane	54	24.	n-Nonane	4.5
9.	n-Heptane	46	25.	Cumene	3.5
10.	2-Propanol	44	26.	1-Propylbenzene	3.4
11.	Methylmethacrylate	39			
12.	Toluene	28	27.	4-Ethyltoluene	3.0
13.	1,4-Dioxane	27	28.	1,3,5-Trimethylbenzene	2.5
14.	4-Methyl-2-pentanone	20	29.	d-Limonene	2.0
15.	Tetrachloroethylene	18	30.	1,2,4-Trichlorobenzene	0.5
16.	1,1,2-Trichloroethane	17	31.	Naphthalene	0.085

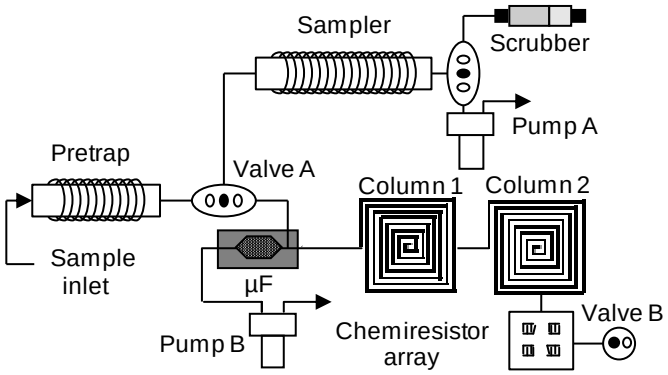

Figure 5-1. Diagram showing the key components of the µGC with multi-stage PCF module.

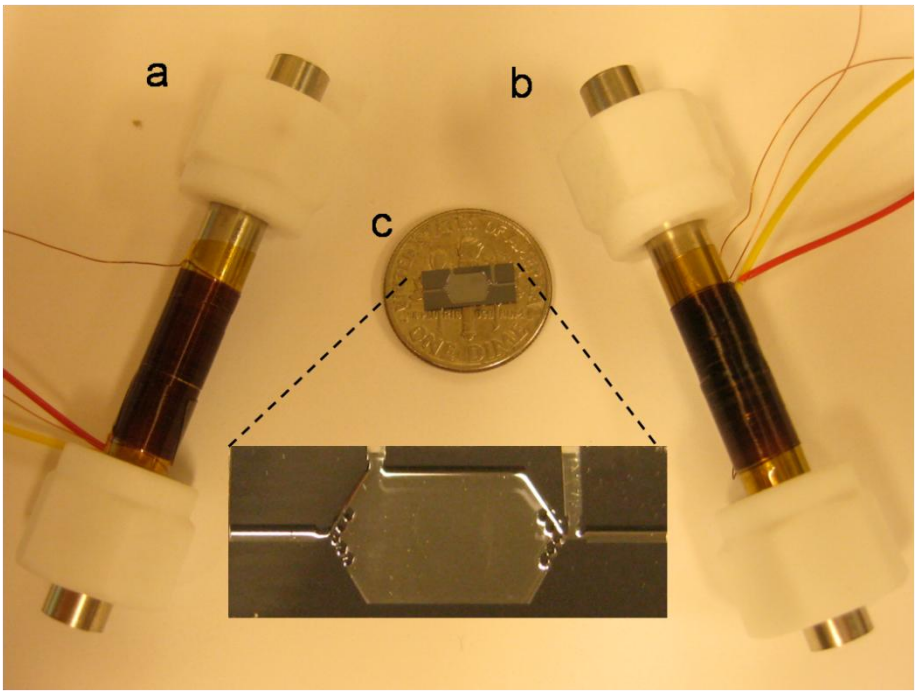

Figure 5-2. Components of the multi-stage PCF module: a) pre-trap packed with 50 mg of C-B; b) high-volume sampler packed with 100 mg of C-X, and; c) µF packed with 2.3 mg of C-X. Pre-trap and sampler are shown with Teflon connectors, resistive-coil heaters, and thermocouples. An enlarged image of the µF is shown to highlight the microfluidic features of the device.

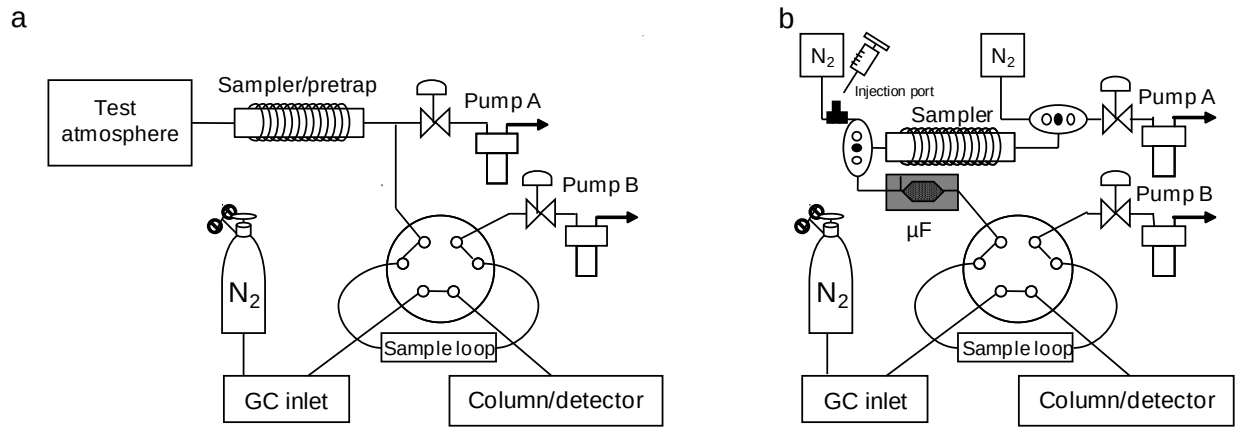

Figure 5-3. Configuration used for testing (a) breakthrough volume of sampler and pretrap and (b) sampler desorption volume and breakthrough volume of µF.

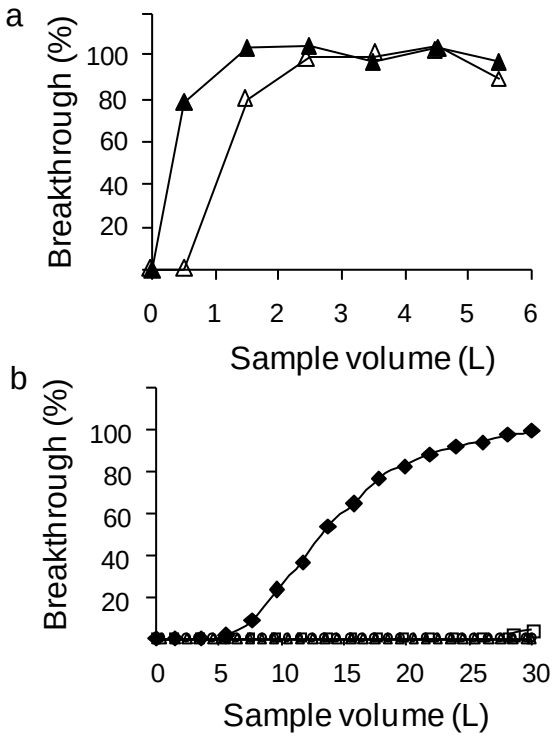

Figure 5-4. a) TCE breakthrough curves (1-ppb challenge concentration; 1 L/min) for pre-traps packed with 50 mg (filled triangles) and 75 mg (open triangles) of C-B showing minor degree of retention; b) breakthrough curves for the pre-trap packed with 50 mg of C-B challenged with a mixture of 500 ppb each of cumene (filled diamonds, p_v = 3.4 torr), 4-ethyltoluene (open squares, p_v = 3 torr), d-limonene (crosses, p_v = 1.9 torr), and 1,2,4- trichlorobenzene (open triangles, p_v = 0.5 torr) at 1 L/min, showing $V_{b\text{-}10}$ > 30 L for all compounds except cumene for which $V_{b\text{-}10}$ = 7 L.

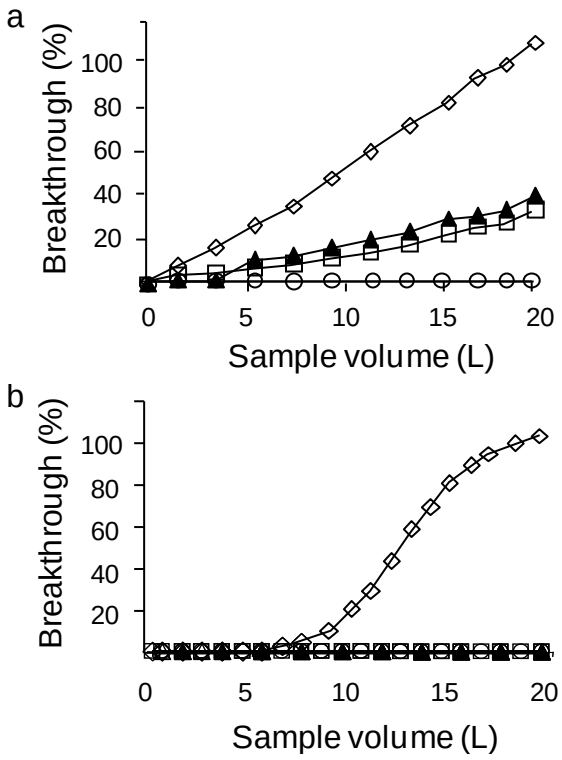

Figure 5-5. Breakthrough curves for the high-volume sampler packed with a) 50 mg and b) 100 mg of C-X challenged with a mixture of 500 ppb each of 2-butanone (open diamonds), benzene (open squares), TCE (filled triangles), and n-heptane (open circles) at 1 L/min. The 50-mg bed gives $V_{b\text{-}10}$ values < 10L for all compounds except n-heptane, while the 100-mg bed shows $V_{b\text{-}10}$ > 20 L for all vapors except 2-butanone.

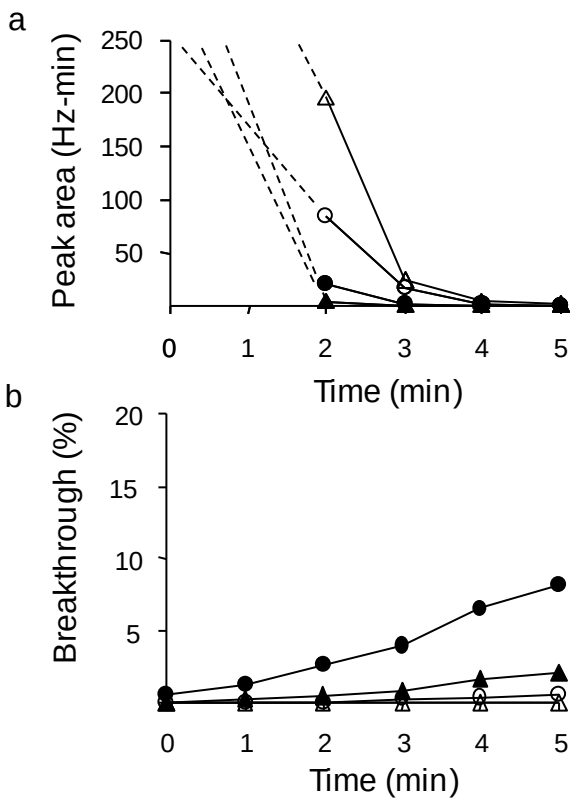

Figure 5-6. a) Desorption profiles of TCE (52-ng spikes) from the sampler at different maximum desorption temperatures and flow rates: 180 ºC/20 mL/min (open circles); 180 ºC/30 mL/min (filled circles); 225 ºC/10 mL/min (open triangles); and 225 ºC/20 mL/min (filled triangles); b) TCE breakthrough curves for the μF placed downstream from the sampler during desorption under the same conditions as described in a).

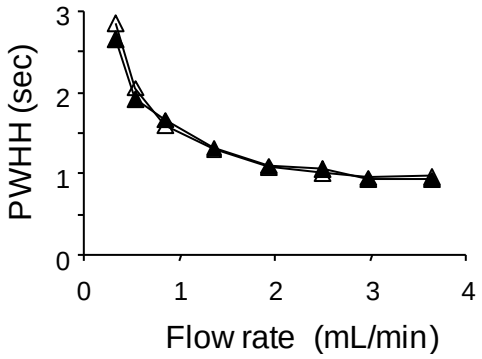

Figure 5-7. Effect of flow rate on desorption (injection) bandwidth of TCE from the µF for 5.2 ng spikes of TCE alone (open triangles) and as a component of a mixture with 9 co-contaminants (filled triangles). The µF was heated to 225 °C at 375 °C/sec in all cases. PWHH is the peak width at half height.

References

1. U. S. EPA, *Draft Guidance for Evaluating the Vapor Intrusion to Indoor Air Pathway from Groundwater and Soils.* Report No. EPA/540/1-89/002, U. S. EPA, Washington DC, 2002
2. A. C. Weihsueh, J. C. Caldwell, N. Keshava, and C. S. Scott, *Environ. Health Perspect*., 2006, 114, 1445.
3. N. A. Fitzpatrick and J. J. Fitzgerald, *Soil and Sediment Contam.*, 2002, 11, 603.
4. Agency for Toxic Substances and Disease Registry (ATSDR), *Public Health Assessment: Hill Air Force Base, Utah, Davis and Weber Counties, Utah*, Federal Facilities Assessment Branch, Division of Health Assessment and Consultation, ATSDR, 2003. Retrieved from http://www.atsdr.cdc.gov/hac/pha/pha.asp?docid=795&pg=0, accessed July, 2010.
5. D. Folkes , W. Wertz, J. Kurtz, and T. Kuehster, *Ground Water Monit. Remed*., 2009, 29, 70.
6. U. S. EPA., *Sources, Emission and Exposure for Trichloroethylene (TCE) and Related Chemicals*, Report No. EPA/600/R-00/099, National Center for Environmental Assessment, Office of Research and Development, U.S. EPA, Washington DC, 2001.
7. J. Kurtz and D. Folkes, *Proc. of the 9th International Conference on Indoor Air Quality and Climate,* Santa Cruz, California, 2002, pp. 920-925.
8. T. E. McHugh, J. A. Corner, and F. Ahmad, *Environ. Forensics*, 2004, 5, 33.
9. U. S. EPA, *TO-15, Compendium of Methods for the Determination of Toxic Organic Compounds in Ambient Air*, Report No. EPA/625/R-96/010b, US EPA, Washington DC, 2nd edn., 1999.
10. U. S. EPA, *TO-17, Compendium of Methods for the Determination of Toxic Organic Compounds in Ambient Air*, Report No. EPA/625/R-96/010b, U.S. EPA, Washington DC, 2nd edn., 1999.
11. N. Ochiai, A.Tsuji, N. Nakamura, S. Daishima and D. B. Cardin, *J. Environ. Monit*., 2002, 4, 879.
12. U.S. EPA website, http://www.epa.gov/region06/6lab/taga.htm, accessed July 2010.
13. Inficon website, http://www.inficonvocmonitoring.com/en/index.html, accessed July 2010.
14. J. D. Fair, W. F. Bailey, R. A. Felty, A. E. Gifford, B. Shultes, and L. H. Volles, *J. Environ. Sci. (China)*, 2009, 21, 1005.
15. C. J. Lu, W. H. Steinecker, W. C. Tian, M. Agah, J. M. Potkay, M. C. Oborny, J. Nichols, H. Chan, J. Driscoll, R. D. Sacks, S. W. Pang, K. D. Wise, and E. T. Zellers, *Lab Chip*, 2005, 5, 1123.
16. C. J. Lu, W. C. Tian, W. H. Steinecker, A. Guyon, M. Agah, M. C. Oborny, R. D. Sacks, K. D. Wise, S. W. Pang, and E. T. Zellers, *Proc. of the 7th International Conference on Miniaturized Systems for Chemistry and Life Sciences, mTAS '03,* Squaw Valley, CA, 2003, pp. 411-415.
17. E. T. Zellers, W. H. Steinecker, G. R. Lambertus, M. Agah, C. J. Lu, H. K. L Chan, J. A. Potkay, M. C. Oborny, J. M. Nichols, A. Astle, H. S. Kim, M. P. Rowe, J. Kim, L. W. DaSilva, J. Zheng, J. J. Whiting, R. D. Sacks, S. W. Pang, M. Kaviany, P. L. Bergstrom, A. J. Matzger, Ç. Kurdak, L. P. Bernal, K. Najafi, and K. D. Wise, *Proc. Solid-State Sensors, Actuators, and Microsystems Workshop*; Hilton Head, SC, 2004, pp. 61-66.

18. W. C. Tian, H. K. L. Chan, C. J. Lu, S. W. Pang, and E. T. Zellers, *J. Microelectromech. Sys.*, 2005, 14, 498.
19. Q. Zhong, W. H. Steinecker, and E. T. Zellers, *Analyst*, 2009, 134, 283.
20. E. T. Zellers, S. Reidy, R. A. Veeneman, R. Gordenker, W. H. Steinecker, G. R. Lambertus, H. Kim, J. A. Potkay, M. P. Rowe, Q. Zhong, C. Avery, H. K. L. Chan, R. D. Sacks, K. Najafi, and K. D. Wise, *Proc. 14th International Conf. on Solid-State Sensors, Actuators, & Microsystems; Transducers '07*, Lyon, FR, 2007, pp.1491-1496.
21. H. Kim, W. H. Steinecker, G. R. Lambertus, A. A. Astle, K. Najafi, E. T. Zellers, P. D. Washabaugh, L. P. Bernal, and K. D. Wise, *Proc. 14th International Conf. on Solid-State Sensors, Actuators, & Microsystems; Transducers '07,* Lyon, France,2007,pp.1505-1508.
22. F. I. Bohrer, E. Covington, Ç. Kurdak, and E. T. Zellers, *Proc. 15th International Conference on Solid-State Sensors, Actuators, and Microsystems; Transducers '09*, Denver, CO, 2009, pp. 148-151.
23. E. T. Zellers, S. K. Kim, G. Serrano, H. Chang, F. Bohrer, R. Veeneman, E. Covington, and C. Kurdak, *Transactions of the Electrochemical Society Symposium on "35 Years of Chemical Sensors in Honor of Jiri Janata,"* 2009, 19 (6), 315-325.
24. G. Serrano, S. Reidy, and E. T. Zellers, *Sens. Actuators, B*, 2009, 141, 217.
25. S.-J. Kim, S. M. Reidy, B. P. Block, K. D. Wise, E. T. Zellers, and K. Kurabayashi, *Lab Chip*, 2010, 10, 1647.
26. E. Covington, F. I. Bohrer, C. Xu, E. T. Zellers, and C. Kurdak, *Lab Chip*, 2010, 10, 3058.
27. F. I. Bohrer, E. Covington, C. Kurdak, and E. T. Zellers, *Analytical Chemistry*, in review.
28. Q. Zhong, R. A. Veeneman, W. H. Steinecker, C. Jia, S. A. Batterman and E. T. Zellers, *J. Environ. Monit.*, 2007, 9, 440.
29. S.K. Kim, H. Chang, E.T. Zellers, *Proc. 15th International Conference on Solid-State Sensors, Actuators, and Microsystems; Transducers '09*, Denver, CO, 2009, pp. 128-131.
30. G. Serrano, H. Chang, E. T. Zellers, *Proc. 15th International Conf. on Solid-State Sensors, Actuators, & Microsystems; Transducers '09*, Denver, CO, 2009, pp.1654-1657.
31. H. Chang, S. K. Kim, T. Sukaew, F. Bohrer, and E. T. Zellers, *Proc. Solid-State Sensors, Actuators, and Microsystems Workshop*, Hilton Head, South Carolina, 2010, pp. 278-281.
32. H. Chang, S. K. Kim, T. Sukaew, F. I. Bohrer, and E. T. Zellers, *Proc. Eurosensors XXIV*, Linz, Austria, 2010, *Procedia Engineering*, 5, 973-976.
33. P. R. Lewis, R. P. Manginell, D. R. Adkins, R. J. Kottenstette, D. R. Wheeler, S. S. Sokolowski, D. E. Trudell, J. E. Bymes, M. Okandan, J. M. Bauer, R.G. Manley, and G. C. Frye-Mason, *IEEE Sens. J.*, 2006, 6, 784.
34. S. Zampolli, I. Elmi, F. Mancarella, P. Betti, E. Dalcanale, G. C. Cardinali and M. Severi, *Sens. Actuator, B.*, 2009, 141, 322.
35. M. Jia, J. Koziel, and J. Pawliszyn, *Field Analytical Chem. and Technol.*, 2000, 4, 73.
36. G. L. Hook, G. L. Kimm, T. Hall, P. A. Smith, *Trends Anal. Chem*., 2002, 21, 534.
37. L. Müller, T. Górecki and J. Pawliszyn, *Fresenius J. Anal. Chem.*, 1999, 364, 610.
38. W. Frank and H. Frank, *Chromatographia*, 1990, 29, 571.
39. O. O. Kuntasal, D. Karman, D. Wang, S. G. Tuncel, G. Tuncel, *J. Chrom. A*, 2005, 1099, 43.
40. E. Staples, S. Viswanathan, *Ind. Eng. Chem. Res.*, 2008, 47, 8361.
41. J. M. Sanchez and R. D. Sacks, *Anal. Chem*. 2003, 75, 978.
42. C. J. Lu and E. T. Zellers, *Anal. Chem.*, 2001, 73, 3449.
43. C. J. Lu and E. T. Zellers, *Analyst*, 2002, 127, 1061.

44. C. Feng, and S. Mitra, *J. Microcolumn Separations*, 2000, 12, 267.
45. S. Mitra, Y. H. Xu, W. Chen, and A. Lai, *J. Chrom. A*, 1996, 727, 111.
46. C. Feng, and S. Mitra, *J. Chrom. A*, 1998, 805, 169.
47. P. Foley, N. Gonzalez-Flesca, I. Zdanevitch and J. Corish, *Environ. Sci. Technol*., 2001, 35, 1671.
48. C. Thammakhet, P. Thavarungkul, R. Brukh, S. Mitra and P. Kanatharana, *J. Chrom. A*, 2005, 1072, 243.
49. W. A. Groves, E. T. Zellers, and G. C. Frye, *Analyt. Chim. Acta*, 1998, 371, 131.
50. C. J. Lu, J. Whiting, R. D. Sacks, and E. T. Zellers, 2003, *Anal. Chem*. 75, 1400.
51. J. J. Whiting and R. D. Sacks, *J. Separation Sci.*, 2006, 29, 218.
52. KNF Neuberger, Inc. website, http://www. Knf.com/oemicro.htm
53. K. Dettmer and W. Engewald, *Anal. Bioanal. Chem.*, 2002, 373, 490.
54. W. A. Groves and E. T. Zellers, *Am. Ind. Hyg. Assoc. J.*, 1996, 57, 257.
55. SKC Inc. website, www.skcinc.com, accessed June, 2010.
56. P. H. Howard and W.M. Meylan, Eds., *Handbook of Physical Properties of Organic Chemicals*, CRC Press: Boca Raton, FL, 1997.
57. S. K. Kim, D. R. Burris, H. Chang, J. Bryant-Genevier, and E. T. Zellers, *Environ Sci Technol*, 2012, 46, 6065.
58. S. K. Kim, D. R. Burris, H. Chang, J. Bryant-Genevier, and E. T. Zellers, *Environ Sci Technol*, 2012, 46, 6073

Chapter 6

Conclusions and Future Work

In summary, the research described here was targeted at improving the design and operation of in-line preconcentrators used in field-portable gas chromatograhic instrumentation for the determination of toxic organic vapors at low concentrations encountered in residential and workplace environments. The primary focus was placed on characterizing microfabricated preconcentrators that were designed for integration with microfabricated GC (μGC) instruments for *in situ* environmental analysis. The research addresses the dearth of information on this topic in the literature. Devices suitable for use with μGC instrumentation were characterized in the context of known models to assess whether they adhere to performance predicted by such models for single-vapor challenges and binary-mixture challenges. Studies focused on commercially available graphitized carbons as well as carbon nanotubes, whose use in such applications has been the subject of surprisingly few reports. These fundamental studies were complemented by an applied study related to the development of a preconcentrator module (integrating conventional and microfabricated components) for specific μGC applications related to vapor intrusion of trichloroethylene into homes from contaminated soil.

Adsorbent-packed preconcentrators are essential elements of most microanalytical systems designed for monitoring airborne volatile organic compounds (VOC) at low concentrations. These devices also serve as thermal desorption injectors that transfer focused bands of captured VOCs to downstream separation and/or detection modules. Despite their importance, the factors affecting the capture efficiency of such devices have not been extensively or systematically studied. In Chapter 2, the dynamic retention capacities of four deep-reactive-ion-etched Si micropreconcentrator-focusers (μPCF) packed with a commercial graphitized carbon, Carbopack X (C-X), were characterized for several VOCs and compared to those of a reference capillary preconcentrator-focuser (cPCF). Devices were challenged with ~100 parts-per-billion of benzene, 2-butanone, toluene, or n-heptane in dry N_2 over a range of volumetric flow rates, Q.

The relationships between the bed residence time, τ, and the 10% breakthrough volume and breakthrough time ($V_{b\text{-}10}$ and $t_{b\text{-}10}$, respectively) were evaluated in the context of the modified Wheeler Model. The values of the parameters in the large scale activated carbon bed, such as bed mass, challenge concentration, and flow rate are ~ 10^3-10^4 fold higher than conditions applicable to the microscale-adsorbent bed. Furthermore the bed residence time tested in this study is on the order of miliseconds, which means that the time the vapor stays in the bed is more than 1000 times shorter than reported in the literature for large scale adsorbent bed. Therefore, the present studies started by evaluting the applicability of the modified Wheeler model to these vastly smaller adsorbent beds.

This study has confirmed that the modified Wheeler Model provides a useful framework for assessing the effect of flow rate on the performance of miniaturized and microfabricated PCF devices designed to provide exhaustive trapping of VOCs. The results from several parts of this study reflect the importance of sampling flow rate on the performance of the miniature

preconcentrator. The results show an increased critical flow rate with higher equilibrium adsorption capacity. Both $V_{b\text{-}10}$ and $t_{b\text{-}10}$ decrease monotonically with decreasing τ, in accordance with the model. The performance of the largest μPCF packed with 2.3 mg of C-X, was comparable to that of the reference cPCF packed with a similar quantity of C-X. The critical flow rates, $Q_{c\text{-}10}$, corresponding to immediate breakthrough, ranged from 70-290 mL/min and varied inversely with the affinity of the vapor for the adsorbent. It was shown that the critical bed residence time varies inversely with the vapor adsorption capacity of the adsorbent (i.e., $W_{e\text{-}k}$). The VOCs examined here spanned the range of $W_{e\text{-}k}$ values for which the adsorbent examined here (i.e., C-X) would be recommended.

Bed residence time must be maintained above a critical value to avoid immediate breakthrough, which would negatively bias any subsequent quantitative analysis. This has direct implications for the sizes and operating flow rates of such devices. As a practical operating guideline, it is recommended that flow rates be limited to $< 0.4Q_c$ for reliable performance of any μPCF used for quantitative analysis.

This study demonstrates clearly the tradeoff between Q and $t_{b\text{-}10}$. The higher Q leads to the shorter instrumental cycle times, however there is a limit to the maximum allowable sampling flow rate for each device. As shown by the modified Wheeler Model, aside from an influence of the $W_{e\text{-}k}$ parameter, the maximum allowable sampling flow rate depends on device characteristics such as the bed mass, bed density and vapor characteristics such as challenge concentration that reflect $W_{e\text{-}k}$ for each condition. This Q_c reflects a limit to μPCF miniaturization, below which it is not possible to operate the device at reasonable flow rates without suffering early breakthrough. To be able to shorten instrumental cycle time, additional adsorbent mass is required and this additional bed mass would broaden the injection band. Broad

injection bands lead to decreased efficiency in the separation column. In addition, higher power consumption is required for thermal desorption of the larger bed mass.

A major limitation of the Wheeler Model was shown in this study. Despite its utility for interpreting performance and guiding design and operating conditions, it is not possible to use this model in a predictive manner for untested vapors. This is because the $W_{e\text{-}k}$ and k_v parameters need to be independently determined for $t_{b\text{-}10}$ prediction. While we have shown an ability to model k_v with acceptable accuracy, however the inability to independently model $W_{e\text{-}k}$ leads to the loss of prediction power of the model.

In Chapter 3, the effect of a covapor on the dynamic adsorption capacity of the targeted vapor in miniature preconcentrators was investigated. The study presented a series of data which investigated the effect of covapor on the $t_{b\text{-}10}$ of different vapor on Carbopack X. Breakthrough time of binary mixtures was determined in the context of the modified Wheeler Model over a range of bed residence times.

We found a reduction of $t_{b\text{-}10}$ for vapors in binary mixtures in all cases. With the linearized Wheeler model approach, we found a reduction in $W_{e\text{-}k}$ for all vapors tested; the magnitude of the $W_{e\text{-}k}$ reduction varies with its affinity to Carbopack X when comparing the covapors in binary mixtures. The rate of mass transfer of the vapor in the binary mixture increases with v_L, similar to the trend observed in single vapors. With the exception of toluene, which exhibits a similar k_v parameter as single vapor, we found the reduction in k_v parameter for all vapors tested with the magnitude of the diffence increaseing with higher v_L.

As described by the modified Wheeler Model, the reduction in $W_{e\text{-}k}$ and k_v parameter in a binary mixture, contributes to the reduction of the dynamic adsorption capacity of the adsorbent bed. The vapor in a binary mixture with smaller $W_{e\text{-}k}$ as compared to the covapor, was affected

more than its vapor pair. This result supports the findings in Chapter 2 regarding the importance of the $W_{e\text{-}k}$ parameter in the performance of miniature preconcentrator. The vapor with high affinity to the adsorbent material can tolerate higher sampling flow rate, and its capacity is not depleted much in the presence of covapor.

The modified Wheeler equation was used to predict $t_{b\text{-}10}$ of vapors in binary mixtures. The Molar Proportionality Model (MPM), which assumes that the $W_{e\text{-}k}$ of each vapor in the binary mixture is proportional to its mole fraction in the binary mixture, was used to determine $W_{e\text{-}k}$ of vapors in binary mixtures. The k_v prediction equation developed in Chapter 2 for single vapors, was used to calculate the k_v of each vapor in binary mixtures. These calculated values were corrected by the correction factor published by Wood et al. to obtain k_v parameter for each vapor in the vapor pair.

Using the MPM to correct for $W_{e\text{-}k}$ in mixtures in combination with the correction factors is a poor combination for modeling. We have found that the MPM underestimates the $W_{e\text{-}k}$ values of all vapors in binary mixture. For this reason, this method is not recommended for predicting the dynamic adsorption capacity of binary mixtures. From this study, we found the modified Wheeler model to be descriptive, rather than predictive, model. The model is still a useful guide for μPCF design and operation in various application, however. The concentration of the binary mixtures examined in this study resulted in the mole fraction of ~ 50%, in the more complex mixture, we would expect to see a more dramatic decrease in $W_{e\text{-}k}$. The simple treatment of mixtures based on data from single component testing may predict incorrect breakthrough times and which supports the need for laboratory breakthrough testing to determine dynamic adsorption capacity of the miniature preconcentrator for targeted vapors and the potential interferences found in the field.

The results from the first two chapters demonstrated the importance of the $W_{e\text{-}k}$ parameter on the performance of the miniature preconcentrator. These results imply that the material selection process is the critical step in the μPCF development. In Chapter 4 of this dissertation we have investigated the performance of a new adsorbent material for use in μPCF. Carbon nanotubes (CNTs) have been chosen due to its reported high capacity to VOCs, efficient desorption for vapors with wide volatility range and its ability to be deposited directly in the μPCF.

In chapter 4, we performed preliminary testing to investigate the dynamic retention capacity of the carbon nanotubes (CNTs). This material was tested as the adsorbent packed in a capillary preconcentrator and as adsorbent material grown *in-situ* in a microfabricated preconcentrator (μPCF). A problem regarding the packing density of the two materials was recognized in the beginning of the study. The PACKED-BED density of CNTs is much lower than Carboapck X, and this discrepancy leads to a problem in packing CNTs in both devices. A similar mass (2 mg) of CNTs yielded ~ 6.5 times larger bed volume than for the Carbopack X bed. As a result, for the μPCF in which the adsorbent bed volume is fixed, the mass of CNTs is ~ 4 time lower than the mass of Carboapck X in the same μPCF. With these packing density problems in both devices, it is not possible to make a solid conclusion on the performance these adsorbent material based on this study. The significantly larger bed volume of the CNT bed leads to the longer bed residence times at constant flow rate which contributed to a higher possibility of vapor adsorption. Breakthrough experiments revealed similar $t_{b\text{-}10}$ of MEK and benzene between the two adsorbent materials at similar challenge concentration and flow rate. The longer time that vapors can stay in the CNTs bed makes it difficult to draw conclusion regarding the performance of CNTs. The packing density problem hinders performance

comparison of CNTs in μPCF; the difference in adsorbent material mass packed in the μPCF does not allow the performance comparison between the adsorbent materials.

Even though the performance of this material was not as high as we expected (just comparable to Carbopack X), the results need to be confirmed with a wider range of vapor volatility. The desorption characteristics of this material are required before the further conclusions regarding the performance of this material can be made. In addition, the ability of the CNTs to be functionalized by various functional groups to change its polar properties, this can change its adsorption properties with organic compounds that warrants further investigation of this adsorbent material.

When considering μPCF performance, one missing piece in this study is the investigation of the desorption performance. We have demonstrated the characterization of the adsorption performance of μPCF without the tradeoff of the desorption performance of the device. As stated earlier, an increase in bed mass/bed length would degrade the chromatographic resolution of the column. A selection of adsorbent material would have to consider the tradeoff between these two important functions of the devices. The higher $W_{e\text{-}k}$ is preferred for adsorption capacity and maximum allowable flow rate, however too high affinity leads to a higher temperature required for thermal desorption and thereby higher power consumption of the systems, and the too high affinity adsorbent might lead to incomplete desorption which results in a carryover problem for subsequent analysis. We have demonstrated different bed efficiency from different vapor-adsorbent affinity and how this affinity would affect the flow rate tolerable of each vapor. We cannot base the adsorbent material selection on the basis of adsorption capacity alone. It would be interesting to further investigate the tradeoff between the bed efficiency and desorption

performance (desorption bandwidth) of the μPCF and come up with another guideline that considers both the adsorption/desorption aspects of the μPCF.

In considering the adaptation and deployment of a μGC for the assessment of TCE contamination from VI in homes, it became apparent that the air sample volume required to achieve the sub-ppb detection limits demanded by this application would exceed the capacity of the μPCF devices we have used in previous μGC prototypes. Thus, a high-volume sampler was required upstream from the μGC. It was also apparent from samples collected and analyzed by standard methods at some of the anticipated field-testing sites under consideration that a number of semi-volatile organic compounds (SVOCs) were present in the air, which would tend to adsorb to surfaces or only partially desorb from the μPCF at normal desorption temperatures. Thus, a means of precluding such compounds from entering the system was needed.

In response to these requirements, we have developed a multi-stage preconcentrator-focuser (PCF) module consisting of a pre-trap, sampler, and microfabricated focuser (μF) to facilitate the deployment of one of our μGC prototypes for TCE determinations in VI-impacted residences. In Chapter 5, we have developed an effective multi-stage preconcentrator/focuser (PCF) module for use with a μGC for quantitative determinations of VOCs at ppt- level concentrations in the presence of common airborne co-contaminants requires numerous tradeoffs in design and operation. Among the variables that must be considered are the overall time of analysis, target-analyte detection limits, pressure drop through the sampling train, volumetric flow rates, dynamic adsorption capacities, heating rates, desorption efficiencies and rates, and the nature, physical properties, and number of co-contaminants present in the air. We have considered all of these variables and the associated tradeoffs in designing and specifying the operating conditions of a multi-stage PCF module intended to facilitate the detection of sub-ppb

concentrations of TCE by a downstream μGC in homes potentially affected by vapor intrusion from underlying contaminated soil.

The results from previous chapters indicate the limited capacity of WIMS2 μPCF, especially at high flow rates. In addition to the flow rate effect, the presence of interferences decreases the capacity of the miniature devices. We have realized that that to design the preconcentration unit to work in the real environment where there is a complex mixture of interferences, selective preconcentration is critical to module performance This is not only because of the limited capacity of μPCF, but also because of limitations on chromatographic resolution inherent to μGC systems, which employ relatively short separation columns. With these problems, we realized that μPCF does not have enough capacity for this application. It is critical to integrate the macro-scale sampler with the micro-scale focuser, in order to operate the instrument at sampling flow rate that is high enough to reach the targeted analytical time at 30 minutes without the risk of breakthrough. In this study the use of a limited quantity of a low-surface-area adsorbent in the pre-trap to exclude the less volatile co-contaminants serves to reduce the analytical duty cycle because such compounds would require long elution times. It also prevents the accumulation of less-tractable compounds on the surfaces of downstream components. The use of a medium-surface-area adsorbent in the sampler results in quantitative capture of the target analyte (TCE in this case) while allowing the more volatile co-contaminants to pass through largely unretained. This reduces congestion in the early part of the chromatograms and should permit faster analyses by allowing faster temperature programming of separations. Rejection of water vapor is also achieved in this approach by use of hydrophobic adsorbents of limited surface area.

Extremely large preconcentration factors are achievable by virtue of being able to collect large air-sample volumes with the macro-device and then to focus the captured analyte mass into a small injection volume via the micro-device. This not only increases the target-analyte concentration to levels measurable by the downstream detector (microsensor array), but it also enables efficient chromatographic separations by minimizing band dispersion at the inlet to the microcolumn. Being able to sweep the μF device effectively at the low flow rates required for efficient microcolumn separations is also important. Although the chemiresistor sensors used in the μGC we are developing are quite sensitive, preconcentration factors approaching 10^6 are necessary to detect VOCs at the parts-per-trillion concentrations prevalent in many environmental remediation efforts, such as that considered in this study. Achieving such low detection limits using micro-scale preconcentration components alone would not be possible. The performance of this well characterized multi-stage preconcentrator has been proven in the field study. It is hoped that the approach presented here might serve as a general model for efforts to develop field monitoring instrumentation that incorporates on-board preconcentration functions.

Due to the growing interest in monitoring individual VOCs in the presence of complex mixtures, it is possible to adapt this approach in PCF development for other VOCs monitoring application, such as breath/saliva biomarker or explosive marker monitoring, as the PCF unit can be tailored to have specific affinity for target analytes with different volatility. It is important to point out that in an industrial setting application, where there are high concentrations of targeted VOCs and the targeted sample volume is not high, we can still benefit from the selective preconcentration approach.

Appendix: Supporting Information for Chapter 2

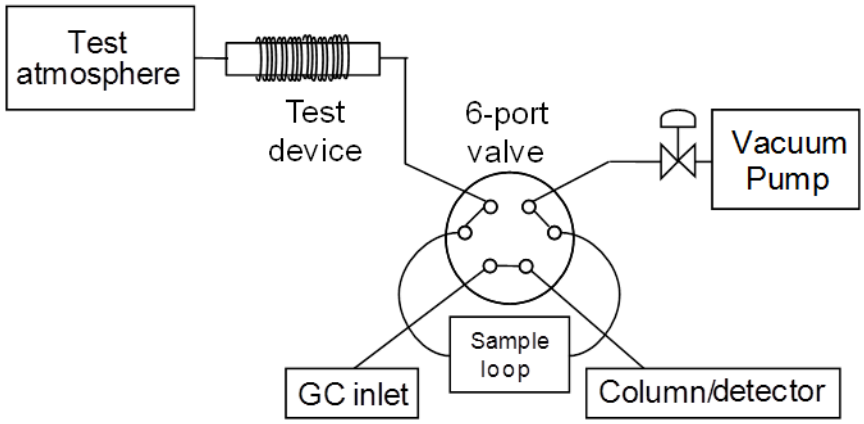

Figure A-1. Experimental set-up used to measure breakthrough for cPCF and µPCF devices. The sample is drawn through the device and the sample loop using the vacuum pump. At 1-min intervals the contents of the sample loop are then injected to the head of the GC column, rapidly passed through the column, and detected by the FID.

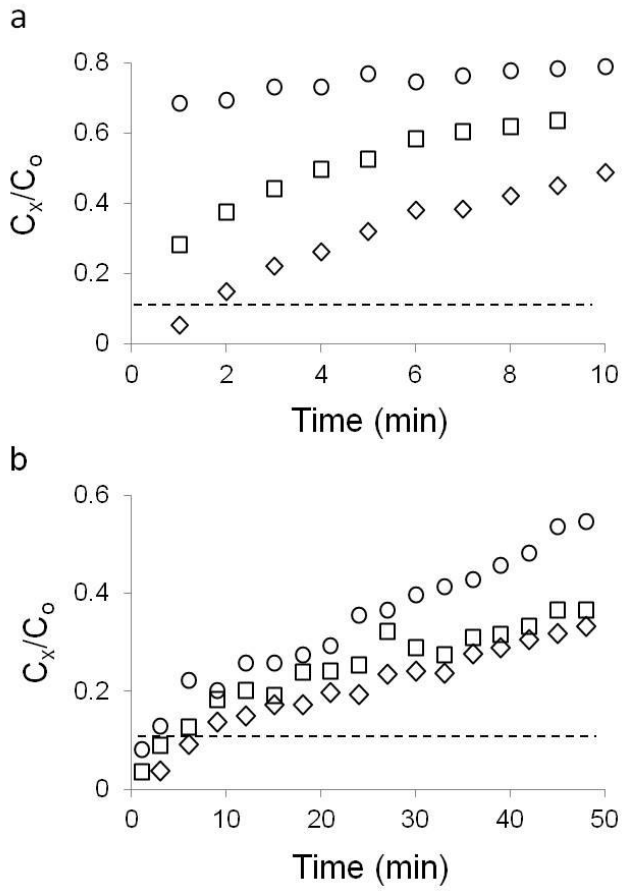

Figure A-2. Breakthrough curves for benzene (100 ppb challenge concentration) with a) the Type A μPCF at 5 (diamonds), 10 (rectangles) and 25 mL/min (circles); and b) the Type C μPCF at 10 (diamonds), 20 (rectangles), and 30 mL/min (circles). Dashed lines designate $t_{b\text{-}10}$.

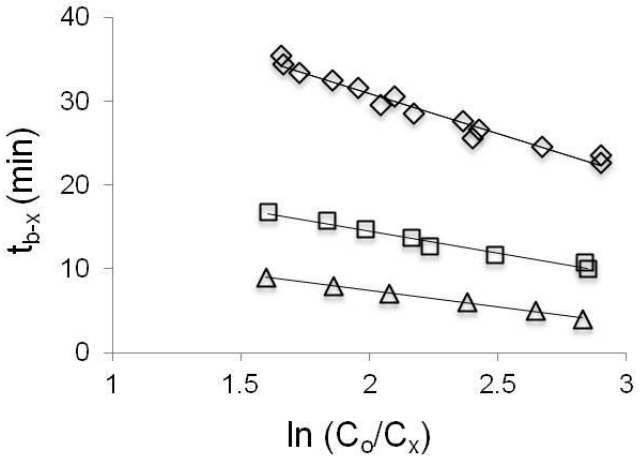

Figure A-3. Representative breakthrough data illustrating how k_v estimates are determined for all vapor-device combinations. Values of k_v are obtained from the slopes of these plots (via Eq. (2.2)) for x values in the range of 0.05-0.20. Plots shown are for benzene with the cPCF for challenge flow rates of 10 (diamonds), 30 (rectangles) and 60 mL/min (triangles). In all cases (including data not shown) linear regressions yielded r^2 values > 0.97, except for MEK at moderate flow rates, where r^2 values were as low as 0.94.